Polymerization Kinetics of Ethylene/1-Hexene Copolymers Made with Two Metallocene Catalysts

by

Sahar Saadat

A thesis submitted in partial fulfillment of the requirements for the degree of

Master of Science

in

Chemical Engineering

Department of Chemical and Materials Engineering

University of Alberta

Abstract

Polyolefins account for the largest portion of the world's plastics production. Increasing demands on the performance of polyolefin products require that we keep advancing our understanding of these ubiquitous plastics. Polymerization conditions and catalyst types have a marked influence on polyolefin microstructure which, in turn, determines their final application properties. The polyolefin industry is starting to use two metallocene catalysts to make polyolefins with controlled microstructures for advanced applications. Having a detailed knowledge of the polymerization kinetics of each individual catalyst is essential to control the microstructures of polymers made with these dual catalysts systems. An important question that needs to be answered is: if we know how each catalyst work alone, can we predict their behaviour in a binary mixture?

In this research project, the solution polymerization kinetics of ethylene and 1-hexene with two metallocenes, constrained geometry catalyst (**CGC-Ti**) and bis(cyclopentadienyl)-zirconium (IV) dichloride (**Cp_2ZrCl_2**), were investigated in a semi-batch reactor. The factors studied were: 1) ethylene/1-hexene ratio, 2) hydrogen/ethylene ratio, 3) methylaluminoxane (MAO) concentration, 4) catalyst concentration, and 5) MAO/catalyst ratio. Mathematical models to describe the polymerization kinetics with each catalyst were developed using experimental polymerization and polymer characterization results.

These models were then used to predict the behaviour of binary mixtures of the individual catalysts. The polymerization kinetics of the binary system could be described as a linear combination of the individual polymerization kinetics of CGC-Ti and Cp_2ZrCl_2. The molecular weight distribution (**MWD**) and short chain branch distribution (**SCBD**) of the copolymers made

with the dual catalyst could also be predicted from the equivalent distributions for copolymers made with the individual catalysts. The proposed approach allows us to predict the properties of polyethylenes made with dual catalysts, which is an important requirement when developing polyolefins for advanced applications.

Acknowledgements

I would like to express my gratitude to my thesis supervisor Prof. João B.P. Soares for his consistent guidance, support, and endless encouragement.

I would like to thank Prof. Phillip Choi for his support through the first year of my studies.

Thanks to Chevron Phillips company and Dr. Paul DesLauriers for providing financial support.

I would like to acknowledge my colleagues in the group of applied macromolecular engineering for their support and inspiration. Special thanks to Dr. Saeid Mehdiabadi for analyzing my samples with gel permeation chromatography, and his insight and support throughout my project.

My deepest gratitude goes to my parents and my sister for their endless love and encouragement. Without them, this achievement would not have been possible.

Table of Contents

List of Figures

List of Tables

Nomenclature

Acronyms

^{13}C NMR	Carbon-13 nuclear magnetic resonance
CGC	Constrained geometry catalyst
CSLD	Comonomer sequence length distribution
DSC	Differential scanning calorimetry
GPC	Gel permeation chromatography
HDPE	High-density polyethylene
LCB	Long chain branch
LDPE	Low-density polyethylene
LLDPE	Linear low-density polyethylene
MAO	Methylaluminoxane
MWD	Molecular weight distribution
PDI	Polydispersity index
PSO	Particle swarm optimization
SCB	Short chain branch
SCBD	Short chain branch distribution
TIBA	Triisobutylaluminum

Symbols

$\emptyset_i$	Molar fraction of living polymer chain terminated in monomer i
C_d	Deactivated active site
C^*	Active site
Di	Dead polymer chain
f_i	Molar fraction of monomer i in liquid phase
F_i	Molar fraction of monomer i in copolymer
F	Ethylene flow rate
k_{pij}	Propagation rate constant when polymer j reacts with a polymer chain terminated in monomer i
k_i	Initiation rate constant
k_a	Activation rate constant
k_d	Deactivation rate constant
k_{dth}	Thermal deactivation rate constant
k_{tHi}	Rate constant of transfer to hydrogen
$k_{t\beta i}$	β-hydride elimination rate constant
k_{ti}	Rate constant of chain transfer to monomer

k_{tAli}	Rate constant of chain transfer to cocatalyst
M_n	Number average molecular weight
M_w	Weight average molecular weight
P_E	Ethylene pressure
r_i	Reactivity ratio of monomer i
r_n	Number average chain length
V_R	Reaction medium volume
V_s	Solvent volume

Chapter 1 : Introduction

1.1 Motivation and Objectives

Polyolefins are a class of polymers that comprise polyethylene and polypropylene. They play an essential role in industrial societies nowadays because the demand for polyolefins is continuously growing: according to Plastics Europe (Association of Plastic Manufacturers), the production of polymers has increased to 322 million tonnes in 2015,[1] and it has been reported that more than 55% of these plastics are polyolefins.[2] Commodity polyolefins are used in applications such as automotive parts, pipes, processing equipment, injection moulding, medical equipment, household containers, and many others due to their wide range of properties as well as their low production cost.[3]

The properties of polyethylenes are determined by their distributions of molecular weight, chemical composition (also called short chain branching), and long chain branching. Polyethylenes have been historically classified according to their densities, which depend strongly on their short chain branching frequencies, and slightly on their molecular weights. This classification is inadequate, since polyolefins with the same density may have different physical properties, yet it is still widely used in the industry. The three major types of polyethylenes are high-density polyethylene (**HDPE**), low-density polyethylene (**LDPE**), and linear low-density polyethylene (**LLDPE**). Coordination polymerization is needed to produce HDPE and LLDPE, while free radical polymerization is required to make LDPE.

A catalyst precursor, catalyst activator (also called initiator), ethylene, and in most cases an α-olefin commoner are the primary ingredients to make HDPE and LLDPE. Catalyst type, α-olefin /ethylene ratio, H_2/ethylene ratio, and polymerization temperature are the main factors affecting the microstructure of polyethylenes and, consequently, their end-use applications.

Mathematical modeling is needed to quantify the behaviour of ethylene/α-olefin copolymerizations, predict polyolefin microstructures and properties, and help design, scale-up, and optimize polymerization reactors. Mathematical models have had a long tradition in the

polyolefin industry because its practitioners realize that they can be used to design products with better properties and higher profit margins.

The main objectives of this thesis are: 1) to estimate the kinetic constants for ethylene/1-hexene copolymerization with two metallocene catalysts, CGC-Ti and Cp_2ZrCl_2, individually and in combination, and 2) to use these models to predict the microstructure of ethylene/1-hexene copolymers made with these catalysts under different polymerization conditions.

1.2 Thesis Outline

This thesis is divided in seven chapters:

Chapter 1: Brief overview of the research project.

Chapter 2: Literature on ethylene/α-olefin copolymerization, catalyst types, polymerization processes, polymerization mechanisms, and polyolefin microstructures.

Chapter 3: Description of polymerization procedures and characterization techniques.

Chapter 4: Discussion of experimental results, development of mathematical models for the polymerization with CGC-Ti, and estimation of model parameters.

Chapter 5: Investigation of the polymerization kinetics and estimation of model parameters for polymerizations catalyzed with Cp_2ZrCl_2.

Chapter 6: Comparison of the polymerization kinetics with binary catalysts with those for the individual metallocene catalysts, and also with the properties of the resulting polymers.

Chapter 7: Summary of the key results, and recommendations for future work.

Chapter 2 : Literature Review

2.1 Introduction

Polyethylene is one of the most commonly used polymers in everyday life due to its low production cost and wide range of properties. Figure 2.1.[4] shows that more than 50% of the world polymer market is constituted of polypropylene and the three major types of polyethylene, high-density polyethylene (**HDPE**), low-density polyethylene (**LDPE**), and linear low-density polyethylene (**LLDPE**).

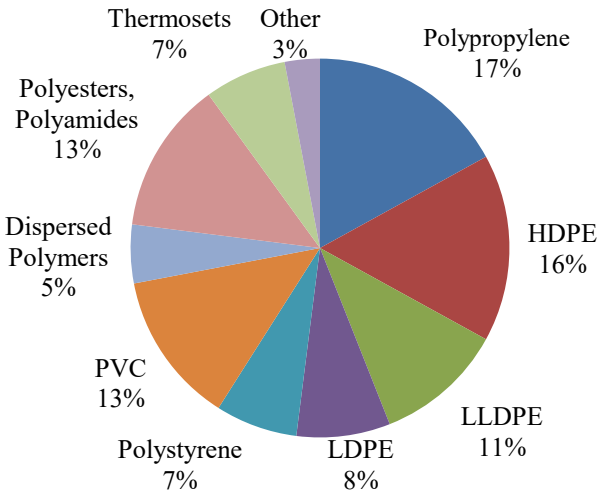

Figure 2.1 World polymer market.

This literature review will focus on polymerization mechanisms, polymerization processes, and properties of polyethylenes, which are the main topic of this thesis.

2.2 Polyethylene Types

Polyethylenes are historically categorized according to their density ranges. Low-density polyethylene (LDPE), the oldest type of commercial polyolefin, is produced by free radical polymerization, and typically has 40 to 150 short chain branches (**SCB**) for every 1000 ethylene units. The SCBs in LDPE are formed through backbiting reactions, while long chain branches (**LCB**), containing hundreds of carbon atoms, are produced by chain transfer to polymer.[5] LCBs are present in LDPE in a frequency of about 1 LCB per 10 SCB.[6] High pressures of 15,000-50,000 psi and temperatures up to 350 $^{\circ}$C are required to produce LDPE. The density of LDPE varies from 0.915 to 0.94 g/cm^3, but this range may differ slightly among different sources.[6,3,7]

High-density polyethylene (HDPE) is made through coordination polymerization using organometallic catalysts. Relatively low temperatures (70-110 $^{\circ}$C) and low pressures of (150-700 psi) are needed to make HDPE. The copolymerization of small amounts of α-olefin with ethylene forms SCBs in HDPE. HDPE has less than 15 SCB per 1000 ethylene units, and a density of 0.945-0.97 g/cm^3. The low SCB frequency is responsible for the higher crystallinity (up to 90%)[6], and increased hardness, stiffness, chemical resistance, and tensile strength of HDPE. Chains with few SCB pack more efficiently into the crystal lattice (Figure 2.2).

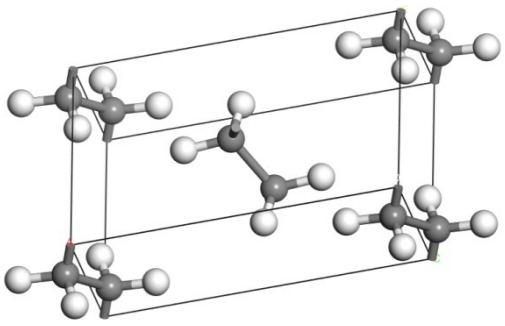

Figure 2.2 Polyethylene crystal structure.

Linear low-density polyethylene (LLDPE) is also made through coordination polymerization at low temperatures and pressures. LLDPE has densities between 0.915 and 0.94 g/cm^3. The copolymerization of ethylene and α-olefin such as 1-octene, 1-hexene, and 1-butene, leads to the production of LLDPE with different densities – the higher the α-olefin fraction, the lower the density. Since LLDPE is tough, transparent, and flexible, it has a large application in the film industry.[6]

2.3 Olefin Polymerization Catalysts

The catalyst is the most important factor in the production of polyolefins by coordination polymerization. Different catalyst types make polyolefins with distinct microstructures.

The development of coordination catalysts for olefin polymerization started in the 1950s with the joint discovery of coordination catalysts for ethylene polymerization by Karl Ziegler and Giullio Natta.[8] Ziegler-Natta catalysts are mostly used for the production of the commercial grades of HDPE and LLDPE. They are also widely used to make polypropylene. Phillips catalysts, also discovered in the 1950s by Hogan and Banks, play an important role in HDPE production. More recently, metallocene and late transition metal catalysts (often called post-metallocenes) have increased their contribution in the commercial polyethylene market. Each of these catalyst types is briefly described below.

2.3.1 Ziegler-Natta Catalysts

In 1953, Ziegler introduced a type of organometallic complex that nowadays we call Ziegler-Natta catalyst, to produce polyethylene at low pressures. In 1954, Natta modified Ziegler's complexes to allow them to manufacture isotactic polypropylene.[9,10] The contributions of these two researchers to polymer science was so significant that both received the Nobel Prize in Chemistry in 1963.

Ziegler-Natta catalysts can polymerize ethylene, propylene, and higher α-olefin at lower pressures (8 to 30 atm) and temperatures (60 – 80 °C)[11] than free radical polymerization, which

makes them economically attractive. Ziegler-Natta catalysts can also control SCB and LCB frequencies in polyethylene much better than free radical polymerization, and therefore can tailor the properties of the final product more effectively.

Ziegler-Natta catalysts are divided into two groups, heterogeneous or homogeneous, depending on whether or not they are soluble in the polymerization medium. Heterogeneous Ziegler-Natta catalysts have multiple active site type. The polymers made with these catalysts have non-uniform microstructures with broad (and sometimes bimodal) MWDs and SCBD.

Heterogeneous Ziegler-Natta catalysts are used to make most commercial LLDPE resins and have a high share of the HPDE market (together with Phillips catalysts). The majority of commercial Ziegler-Natta catalysts are titanium-based complexes such as $TiCl_4$ or $TiCl_3$ supported on $MgCl_2$ or SiO_2. The catalyst (most correctly called a pre-catalyst or catalyst precursor) is activated using an organoaluminum compound such as triethylaluminum.[11]

Homogeneous Ziegler-Natta catalysts are usually based on vanadium chlorides or oxychlorides. They have important commercial applications in the manufacture of ethylene-propylene-diene (EPDM) elastomers since they produce terpolymers with the low crystallinity required for elastomer applications. This class of catalysts generally makes polymers with narrow MWD and SCBD.[3]

2.3.2 Phillips Catalysts

Phillips catalysts are one of the most difficult ethylene polymerization systems to study in academia. The exact structure of their active sites and their polymerization mechanism are still not completely understood, despite their commercial importance in the HDPE market. These catalysts are based on chromium oxide supported on silica and/or alumina. Phillips catalysts have more than one active site type, similarly to heterogeneous Ziegler-Natta catalysts. Thermal activation is required for the production of the active sites before polymerization. Phillips catalysts are used in both gas-phase and slurry polymerization processes. Polyethylene made with Philips catalysts have very broad MWDs, with polydispersities ranging from 12.0 and 24.0.[12,13]

2.3.3 Metallocene Catalysts

Metallocene/methylaluminoxane systems were discovered by Hansjorg Sinn and Walter Kaminsky in 1980 in Hamburg.[14] Even though metallocenes had been used since the fifties in fundamental polymerization studies, their commercial potential was only realized when methylaluminoxane (**MAO**) was used as a cocatalyst. Alkylaluminums, the cocatalysts used with Ziegler-Natta catalysts, cannot activate metallocenes adequately because the resulting active site is unstable. It is no exaggeration to say that the discovery that MAO could activate and stabilize metallocenes revolutionized the polyolefin industry. Later, it was discovered that bulky Lewis acids, such as trispentafluorophenylborane ($B(C_6F_5)_3$), were also excellent cocatalysts for metallocenes.[15]

Metallocenes are known as sandwich compounds, in which a transition metal lies between two cyclopentadienyl rings (Figure 2.3).[3] The catalyst behavior depends on the type of the transition metal, and on the structure of the ligands (shape, geometry, and chemical structure).

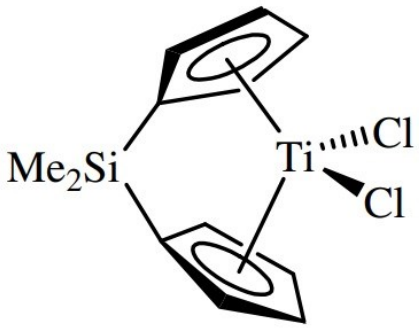

Figure 2.3 A metallocene catalyst.

Most metallocenes have only one type of active site, which classifies them as single-site catalysts. Therefore, they produce polymers with uniform microstructures that can be predicted using fundamental polymerization models.[16] Metallocenes are molecular catalysts that are soluble in the polymerization medium, and therefore are classified as homogeneous catalysts, but they can also be easily supported on SiO_2 and other inorganic carriers to act as heterogeneous

catalysts.[17] This is important because most olefin polymerization processes were developed for heterogeneous catalysts.

A half-sandwich complex is another sort of metallocene composed of only one cyclopentadienyl ring coordinated to the transition metal (Figure 2.4). They are also called constrained geometry catalysts (**CGC**). Comparing to other metallocenes, these complexes are more stable at higher temperatures and are well suited for solution polymerization processes. The absence of one cyclopentadienyl ring decreases steric hindrance around the active site, making CGCs more reactive towards the incorporation of α-olefins in ethylene/α-olefin copolymerizations.[18]

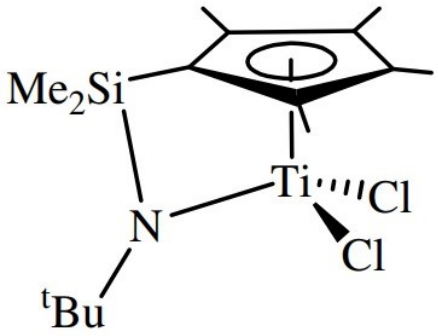

Figure 2.4 Half-sandwich metallocene catalyst.

2.3.4 Late Transition Metal Catalysts

Transition metals from groups 8, 9, and 10 of the periodic table of elements form the core of late transition metal catalysts. These catalysts are sometimes called post-metallocenes, since they were discovered in the 1990s, about a decade after metallocenes. These compounds have a higher tolerance towards polar comonomers and impurities, which allow them to copolymerize ethylene with vinyl alcohols, acrylates, or other functional vinyl monomers. Using post-metallocenes, ethylene may be even polymerized as an emulsion in water.[19] The polar functional groups in these polyolefins increase their hydrophilicity and enhance some their properties including dyeability, adhesion, and compatibility with other polar polymers. Examples of late transition metal catalysts for ethylene and α-olefin polymerization include bidentate diamine

[N,N] nickel and palladium complexes, tridentate 2,6 bis(imino)pyridyl [N,N,N] iron and cobalt complexes, and bidentate salicyl imine [N,O] nickel complexes.[20]

2.4 Olefin Polymerization Processes

All commercial olefin polymerizations reactors are operated continuously. A brief description of these processes is given below.

2.4.1 Solution Polymerization

In solution polymerization, all reagents, catalysts, and polymers are soluble in the reaction medium. The process is performed in autoclave, tubular, and loop reactors[12] at high temperatures (typically above 140 ºC) to ensure the polymer is dissolved in the reaction medium (generally aliphatic solvents). Since the polymer is dissolved in the solvent, the solvent recovery process increases production costs. On the other hand, the presence of the solvent eliminates intraparticle mass and/or heat transfer limitations that may be present in processes that use heterogeneous catalysts.[15] Since average reactor residence times are short in solution processes (typically a few minutes), they are used to make lower-volume specialty or differentiated commodity polyolefins that require frequent changes between grades.

2.4.2 Slurry Polymerization

Slurry polymerizations are classified into diluent (aliphatic solvent) and bulk (liquid propylene) processes. Autoclaves and loop reactors are used for slurry processes. Slurry polymerization requires a liquid diluent, while gaseous or liquid monomers are fed to the reactor. The catalyst is dispersed in the continuous medium, and the polymer is formed as a solid around the catalyst particles.[4] In the bulk process, liquefied propylene is fed to the reactor; therefore, it is only used to make polypropylene.[12]

2.4.3 Gas-Phase Polymerization

Gas-phase polymerization is one of the most common processes for polyethylene production.[21] Gas-phase reactors are classified as fluidized bed or stirred bed. The polymer is formed around the catalyst particles, since the catalyst is suspended (via fluidization or stirring) in the gaseous monomer. In terms of energy and economic efficiency, this process is very attractive, especially for the production of large-volume commodity polyolefins. One of the advantages of gas phase processes is the absence of solvent or diluent: solid polymer particles are ready for packaging as they leave the reactor. Unfortunately, intraparticle heat transfer limitations may be significant, since the polymerization is exothermic and the gas phase medium has a low heat capacity.

2.5 Ethylene/α-Olefin Solution Copolymerization with Metallocenes

Ethylene solution polymerization is promoted by a catalyst that results from the combination of a catalyst precursor and a cocatalyst. A few different cocatalysts may be used with metallocenes, but MAO is the most common type. The metallocene complex itself should be strictly called a catalyst precursor, since before activation it cannot catalyze olefin polymerization. However, it is common to call these complexes *catalysts* even before activation with the cocatalyst. We adopted this less rigorous, but more convenient convention, in this thesis.

Since cocatalysts play a key role in the polymerization with metallocenes, Mehdiabadi et al.[22] investigated the effect of cocatalyst type on polymerization kinetics, catalyst activity, and polymer molecular weight. They compared MAO and tetrakis(pentafluorophenyl) borate dimethylanilinium salt ($[B(C_6F_5)_4]^-[Me_2NHPh]^+$) (referred to as borate in the rest of this paragraph) for ethylene polymerization with rac-dimethylsilyl-bis(indenyl)hafnium dimethyl catalyst. They showed that polymer yield with MAO was higher than with borate. One of the interesting findings in this study was MAO made ethylene/1-octene copolymers with bimodal SCBD, while those made with borate were unimodal. This is attributed to the presence of more than one active site type with MAO.

MAO (which is used as the cocatalyst in this thesis) forms active sites by alkylating and reducing the metallocene catalyst, and it also prevents bimetallic deactivation of the formed active sites.[23]

MAO also acts as an impurity scavenger by reacting with chemical compounds that may deactivate the catalyst. It is formed by the reaction of trimethylaluminium with small amounts of water under controlled conditions. Many structural models have been proposed for MAO in the literature,[14,24,25] but its structure is still not fully understood. The general chemical formula of MAO is: $(Al(CH_3)_xO_Y)_n$. Figure 2.5 shows a proposed cage structure for MAO, which is one of the most accepted structures for this compound.

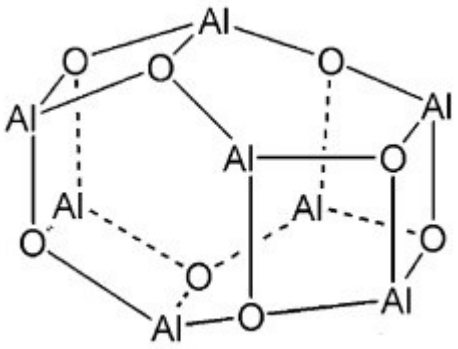

Figure 2.5 MAO cage structure.[23]

After the active site is formed by reacting the catalyst precursor and the cocatalyst, it starts reacting with monomer molecules to form a polymer chain. The polymer chain keeps propagating until a chain transfer reaction takes place, forming a dead polymer chain.

In copolymerization, the Bernoullian and the terminal models are the most commonly used models to describe ethylene/α-olefin copolymerization with metallocene catalysts. The Bernoullian model assumes that only the coordinating monomer species influences propagation, while the terminal model assumes that propagation depends not only on the coordinating monomer but also the last monomer attached to the growing chain.

2.6 Polymerization Kinetics Model

A polymerization kinetics model is essential to predict the yield and microstructure of polyolefins made under different polymerization conditions. Despite many previous investigations, there is no general model that can describe the polymerization of olefins with all coordination catalyst types, even though some steps are common to most models.[26]

2.6.1 Estimation of Polymerization Kinetic Parameters

Touloupidis reported that keeping track of all living (reactive) and dead (non reactive) species is essential to model polymerization kinetics.[27] It is possible to derive a set of differential or algebraic equations for different species such as monomers, living polymer chains, and dead polymer chains in the reaction medium.

For a given polymerization mechanism, the values of the kinetic constants depend on the temperature and types of catalyst, cocatalyst, monomer, comonomer, and sometimes on other parameters such as H_2 concentration, electron donors, etc. With so many variables at play, the values reported for kinetic constants in the literature can only be used with confidence under the same, or very similar conditions, for which they were estimated.[27,28]

Embiruçu et al.[29] estimated the kinetic parameters from ethylene polymerization industrial data, using a methodology for data reconciliation. The parameters were estimated using a nonlinear optimization procedure. Their approach led to good predictions of process data under different conditions.[29]

Sirohi and Choi[30] developed an on-line parameter estimation method to reduce the time and cost of off-line estimation procedures. They used a catalyst as a reference, and extend the information on the reference catalyst to estimate parameters for other catalysts under similar polymerization conditions. Only the key parameters that had the most influence on production rate, polymer density, and molecular weight were selected to simplify the estimation process (propagation, deactivation, and chain transfer to H_2 rate constants were considered as the dominant parameters). Two methods based on extended Kalman filter and nonlinear dynamic parameter estimation were developed for the online estimation of these three parameters. The simulation results for both methods were considered acceptable by the authors.[30]

A mathematical model for ethylene homopolymerization and ethylene/1-hexene copolymerization using a metallocene supported on silica was developed by Kou et al.[31,32] The first step in fitting the mathematical model to experimental data was to assess the parameter estimability to determine whether or not the parameters could be estimated.[33] Using GREG, one of the most powerful FORTRAN subroutines for nonlinear parameter estimation, the parameters

of the multivariate nonlinear regression model were estimated.[34] Kou et al.[31] showed that a single-site model could not fit the complete polymerization rate curve, polymer average molecular weights, and polydispersity index. They found that a two-site model was more adequate to describe their system, likely because when the catalyst was supported on silica more than one effective active site was created, either by chemical or physical interactions with the support.

Mehdiabadi et al.[35] proposed a novel mathematical model based on the trigger mechanism for ethylene homopolymerization with CGC/MAO. Proposing reversible deactivation and activation steps with MAO, they explained how polymerization time, monomer and catalyst concentration affected the rate of polymerizations.

Khare et al.[36,37] developed steady-state and dynamic models for HDPE and polypropylene production processes. They proposed an iterative method to estimate the model parameters. The initial values of kinetic parameters were obtained from literature, and then manually adjusted to match the plant data.

Zhang et al.[38] developed a novel parameter estimation methodology for HDPE based on its MWD. In their study, the sensitivity between output variables and kinetic parameters was assessed to determine the estimability of the model parameters. They transformed an ill-conditioned parameter estimation problem into well-conditioned sub-problems by proposing a multistep methodology.[39] The methodology consisted of MWD deconvolution, kinetic parameter estimation by fitting the regressed MWD parameters, followed by a re-estimation step.

In a set of experiments for ethylene/1-octene copolymerization, Mehdiabadi et al.[40] combined reactivity ratio estimations with ethylene flow rates to estimate the propagation rate constants and their joint confidence regions. They showed that the confidence intervals estimated through asymptotic regression were narrower than that covered by the joint confidence regions, and that even using a rigorous statistical analysis, variation in constant estimations is inevitable.

2.6.2 Reactivity Ratio Estimation

For the case of binary copolymerizations of ethylene and an α-olefin, chain propagation becomes a competitive step between the monomer (ethylene) and comonomer (α-olefin). Reactivity ratios are needed to calculate copolymer composition from the molar fractions of monomer and comonomer in the reactor at a given polymerization time. In its simplest implementation, the reactivity ratio estimation procedure involves performing multiple copolymerizations at various monomer/comonomer ratios, and then fitting the experimental data to the Mayo-Lewis equation.

Equation (2.1) is the Mayo-Lewis equation, which calculates copolymer composition as a function of feed composition[41]

$$F_A = \frac{r_A f_A^2 + f_A f_B}{r_A f_A^2 + 2 f_A f_B + r_B f_B^2} \tag{2.1}$$

where F_A is the fraction of monomer type A in the copolymer, f_A is fraction of monomer type A in the reactor, and r_A and r_B are the reactivity ratios

$$r_A = \frac{k_{pAA}}{k_{pAB}} \tag{2.2}$$

Figure 2.7 shows how the fraction of comonomer in the copolymer (F_A) depends on the fraction of comonomer in the reactor (f_A) for different reactivity ratios, according to the Mayo-Lewis equation.

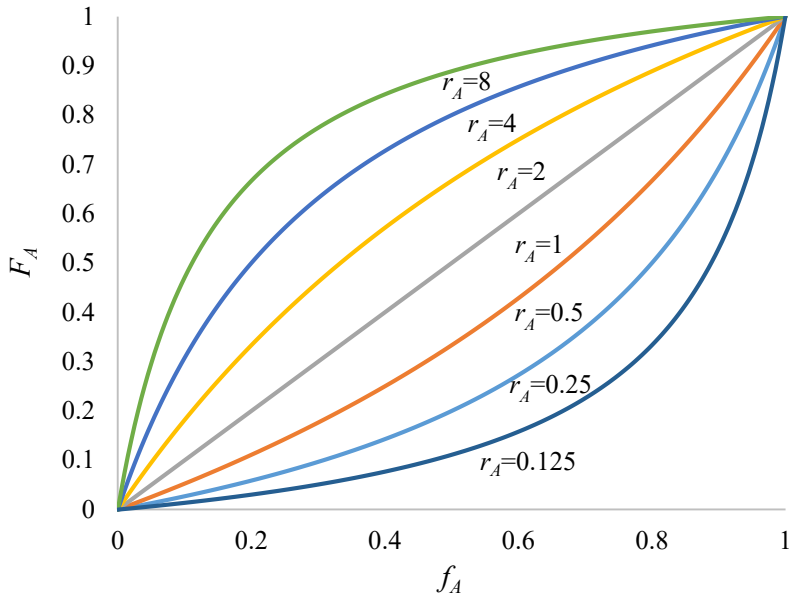

Figure 2.6 Comonomer fraction in copolymer versus fraction of comonomer in the reactor for different values of r_A when $r_A r_B = 1$.

In 1950, Fineman and Ross[42] developed a method to linearize the Mayo-Lewis equation, as shown below[43]

$$\frac{f_A(1-2F_A)}{F_A(1-f_A)} = r_A\left[\frac{f_A^2(F_A-1)}{F_A(1-f_A)^2}\right] + r_B \tag{2.3}$$

Based on Equation (2.3), plotting $\frac{f_A(1-2F_A)}{F_A(1-f_A)}$ versus $\frac{f_A^2(F_A-1)}{F_A(1-f_A)^2}$ yields a straight line with slope of r_A and intercept of r_B. Mueller et al.[41], however, noted that reactivity ratios should be estimated via nonlinear optimization algorithms instead of linear methods such as the Fineman-Ross method, but the latter is often used as a first approximation because it is easy to implement, and often leads to relatively accurate point estimates for r_A and r_B.

Galland et al.[44] estimated the reactivity ratios for the copolymerization of ethylene and several α-olefins (1-hexene, 1-octene, 1-decene) with $C_2H_4(Ind)_2ZrCl_2$. They used ^{13}C NMR comonomer sequence data and the Fineman-Ross method to estimate the reactivity ratios. Calculating reactivity ratios from ^{13}C NMR was previously done by Uozumi et al.[44]

Habibi et al.[43] believed that linearization methods were uncertain from the statistical point view, since the independent variables have errors and the dependent variable does not have constant variance.

Al-Saleh et al.[45] developed a new methodology to estimate the reactivity ratios of multiple site catalysts by combining MWD deconvolution and analysis of comonomer sequence length distribution (**CSLD**). First, the number of site types was determined by deconvoluting the MWD data into Flory's distribution. Second, the information obtained from the first step was combined with CSLD data (triad or tetrad) to estimate the reactivity ratio for each site.

Chapter 3 : Polymer Synthesis and Analysis Methods

This chapter describes the materials used in the polymerizations, sample preparation procedures, and characterization methods for ethylene/1-hexene copolymers.

3.1 Materials

The materials used for the synthesis of the ethylene/1-hexene copolymers were toluene, ethylene, 1-hexene, methylaluminoxane (**MAO**), nitrogen, triisobuylaluminum (**TIBA**), hydrogen, and two metallocenes: bis(cyclopentadienyl)zirconium(IV) dichloride (**Cp_2ZrCl_2**) and methyl(6-t-butoxyhexyl)silyl(η5-tetramethylcyclopentadienyl)(t-butylamido)titanium dichloride (**CGC-Ti**) (Figure 3.1).

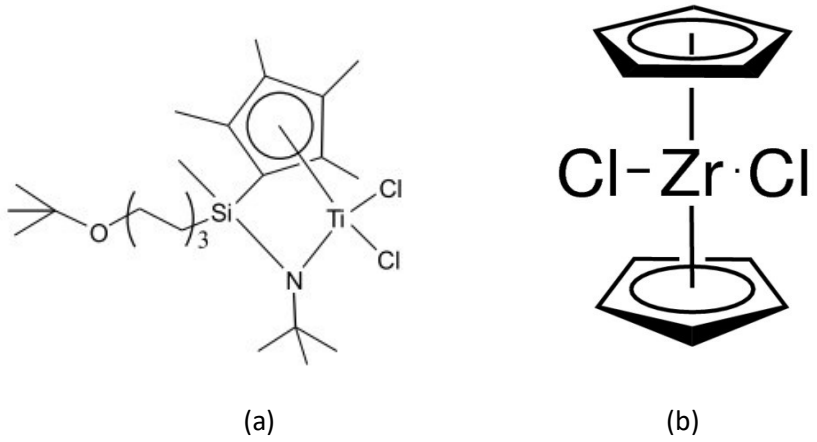

Figure 3.1 a) methyl(6-t-butoxyhexyl)silyl(η5-tetramethylcyclopentadienyl)(t-butylamido) titanium dichloride, b) bis(cyclopentadienyl)zirconium(IV) dichloride.

Ethylene (99%, Praxair) was purified by passing it through columns packed with molecular sieves (3A/4A mixture) and copper(II) oxide to remove polar impurities that may poison the catalysts. MAO (10 wt% in toluene) was purchased from Albemarle and used without further purification. Cp_2ZrCl_2 was purchased as a powder from Sigma-Aldrich and dissolved in distilled toluene to make solutions with desired concentration. CGC-Ti was donated by LG Chem (US 7294600, 2007) and dissolved in toluene. 1-Hexene was purified by storing it over 4-Å dry

molecular sieves to absorb residual impurities. Hydrogen (99.95%) and nitrogen (99.998%) were supplied by Praxair. TIBA (25 wt% in toluene) was purchased from Sigma-Aldrich and used as received. The solvent used to make metallocene solutions and as the polymerization medium, toluene (for HPLC, 99.9%; Sigma-Aldrich), was distilled over n-butyllithium/styrene/sodium system for 24 hours, and then purged with nitrogen in order to remove polar impurities, including water and oxygen. All air-sensitive materials were kept inside the glove box.

The catalyst, cocatalyst, and 1-hexene used in the experiments were always prepared under nitrogen pressure inside the glove box to avoid contamination with polar impurities. Twenty milliliter vials and corning Pasteur pipettes were also stored in the glove box and used to sample air-sensitive compounds. After weighing the needed amount of solution, the vials were sealed using rubber stoppers and open center metal seals to avoid contamination when the vials were taken out of glove box.

3.2 Polymerization Procedure

All polymerizations were performed in a 300 ml Parr autoclave reactor operated in semi-batch mode. Prior to starting the polymerization, the reactor was subjected to 7 cycles of nitrogen pressurization and evacuation to reduce the amount of oxygen and polar impurities. Then, the reactor was filled with 150 ml of toluene, 0.25 g of TIBA as a scavenger, heated up to 130 $^{\circ}$C, and kept at this temperature for 15 min. The reactor contents were then blown out under nitrogen pressure, and the reactor temperature was lowered to 30 $^{\circ}$C.

After reactor purification, solvent, cocatalyst, and 1-hexene were injected in the reactor by differential pressure using a transfer needle, and the temperature was raised to the desired set point under a stirring rate of 1000 rpm. After the set point temperature was reached, ethylene was supplied on demand until the set point pressure was reached, and the on-line flow meter measured no net flow of ethylene to the reactor. At this point, the reactor was ready for catalyst injection.

To start the polymerization, the catalyst was injected by pressure differential into the reactor. Upon catalyst injection, a 1-2 $^{\circ}$C temperature increase was observed because polymerization

reactions are exothermic, but the control loop quickly restored the temperature to 120 ± 0.1 °C throughout the polymerization. After about 11-15 min of polymerization, the ethylene feed flow valve was closed to stop the polymerization, and the reactor contents were blown out into a beaker filled with ethanol to precipitate the polymer. The polymer slurry was filtered through a grade 417 filter paper and allowed to dry overnight in the fume hood. Finally, the polymer was transferred to an oven (T = 70 °C) to evaporate the residual solvent.

Figure 3.2 shows the schematic diagram of the reactor setup.

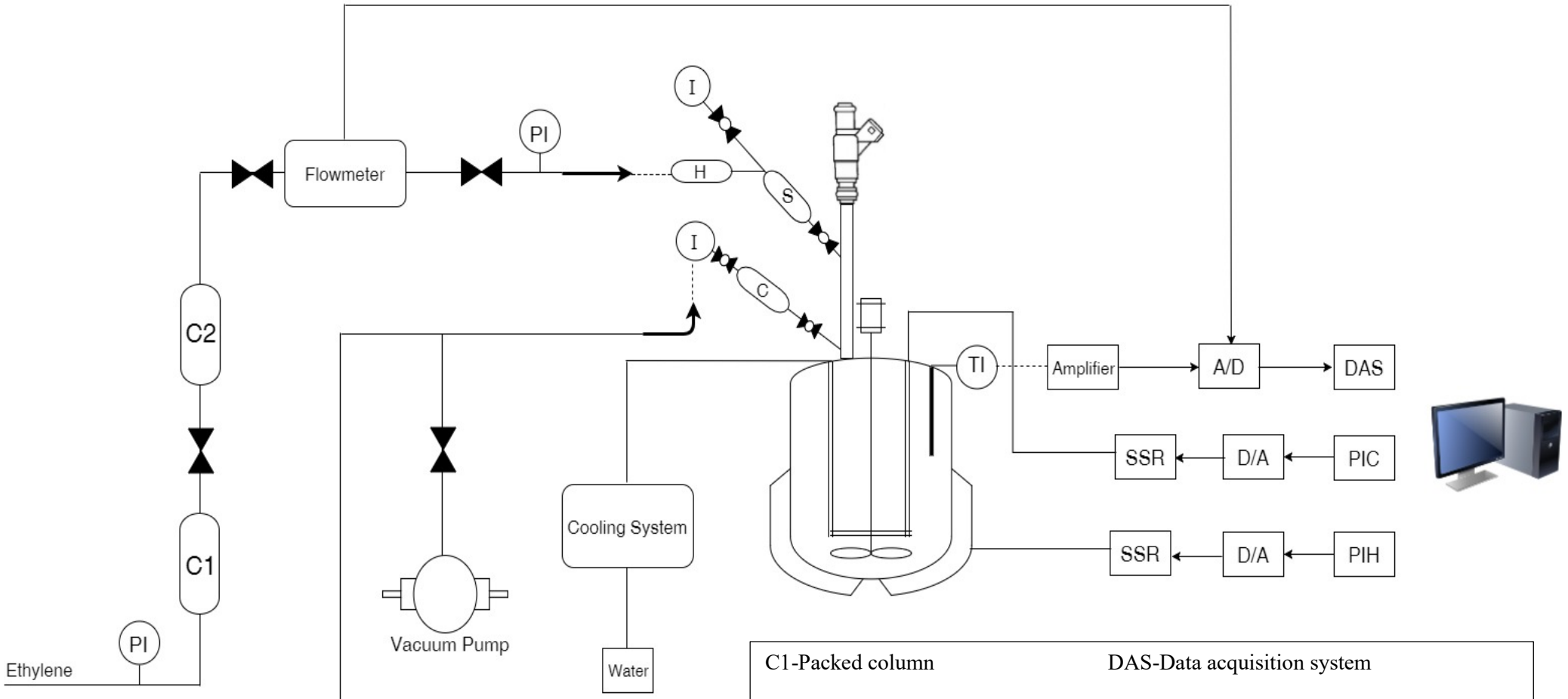

C1-Packed column	DAS-Data acquisition system
C2-Packed column	PIC-Proportional integral loop for cooling
PI-Pressure indicator	PIH-Proportional integral loop for heating
I-Injection port	SSR-Solid state relay
H- Hydrogen injection system	TI- Temperature indicator
S-Solvent	D/A-Digital to analog conversion board
C-Catalyst	A/D-Analog to digital conversion board

Figure 3.2 Schematic diagram of the reactor.

3.3 Polymer Characterization

3.3.1 Molecular Weight Distribution

Gel permeation chromatography (**GPC**) is an analytical method widely used to measure the molecular weight distribution (**MWD**) of polymers. GPC relies on the separation of polymer chains according to their hydrodynamic volumes. For the particular case of polyethylenes, high-temperature GPC (Polymer Char) was used, since polyethylene does not dissolve in any solvents at room temperature. The GPC was equipped with three linear columns (Agilent PLgel Olexis, 7.5×300 mm, 13μm particles) and three detectors: infrared, light scattering, and differential viscometer. Polystyrene narrow standards were used to calibrate the GPC columns using the universal calibration curve procedure. The analyses were performed at 145 °C using trichlorobenzene (TCB) as the continuous phase at a flow rate of 1 ml/min. The polymer sample solution was injected into the solvent flow passing through columns packed with crosslinked polydivinyl benzene particles. The elution time for small molecules is longer than from larger chains, since smaller chains penetrate in more pores in the column packing material. The calibration curve correlates elution time to polymer molecular weight.

3.3.1.1 Short Chain Branch Distribution

Besides molecular weight, short chain branching is one of the most important factors that influence the morphology and properties of a polyolefin.[46]

The short chain branching distribution (**SCBD**) across the molecular weight was measured using a dual-channel IR detector coupled with the GPC. The IR signals due to the presence of methyl and methylene groups in the polymer chain were used to measure SCBD. These measurements are carried out in TCB eluent, and relied on C-H stretching bands found between 3000 and 2800 cm^{-1}.[47,48]

A previously developed IR calibration curve was used to determine the SCBD. Nine ethylene/1-hexene copolymer samples of known butyl branch content made with CGC were used to build the calibration curve. Three ethylene homopolymers produced with CGC and two linear

polyethylene standards were used as reference point for zero SCB frequency. The average SCB frequency of the IR calibration standards was measured by ^{13}C NMR.[49] From the plot of SCB frequency across the MWD, it is possible to calculate the average SCB frequency for the whole polymer.

3.3.2 Carbon-13 Nuclear Magnetic Resonance (^{13}C NMR)

Five ethylene/1-hexene copolymers were analyzed with ^{13}C NMR previously in our group[49] and they were used to make a calibration curve for the differential scanning calorimeter method described in the next section.

A Bruker 500 MHz high-resolution spectrometer was used to quantify the number of SCBs per 1000 carbon atoms in these ethylene/1-hexene copolymers. The solutions were prepared in 5-mm tubes by dissolving 100 mg of copolymer sample in 1,2-dichlorobenzene-d4. The solutions were heated up on a heating plate up to 130 $^{\circ}C$ and kept at this temperature for 6 hours. The ^{13}C NMR operation conditions were: 14-microsecond 90° pulse, inverse gated proton decoupling, 10 s delay time between pulses, and 10000 scans for data averaging. All spectra were referenced by setting the main polyethylene chain peak to 30.00 ppm.[49] The method for calculating commoner content in the copolymer was obtained based on ASTM D5017-96 proposed by De Pooter et al.[50,51] Table 3.1 listed the spectrum regions of ethylene/1-hexene integration limits.

Table 3.1 Integration limits for ethylene/1-hexene copolymers.[50]

Area	Region (ppm)
A	41.5 to 40.5
B	40.5 to 39.5
C	39.5 to 37.0
D	Peak at 35.8
D+E	36.8 to 33.2
F+G	33.2 to 25.5
G	28.5 to 26.5
H	24.9 to 24.1

Integrating the areas under these spectral regions, and using Equations (3.1) to (3.5), allows us to calculate the copolymer composition.[50]

1-Hexene moles:

$$H_1 = \frac{[A+2C+2D]}{2} \tag{3.1}$$

$$H_2 = \frac{[1.5A+2B+(D+E)-D]}{3} \tag{3.2}$$

$$H' = \frac{H_1+H_2}{2} \tag{3.3}$$

Ethylene moles:

$$E' = \frac{[(F+G)-3A-3B-G-H]}{2} + H' \tag{3.4}$$

$$1 - Hexene\ mole\% = 100\% \times \frac{H'}{E'+H'} \tag{3.5}$$

3.3.3 Differential Scanning Calorimetry

In addition to measuring heat of transitions, differential scanning calorimetry (DSC) may also be used to determine the percentage of 1-hexene incorporated in ethylene/1-hexene copolymers, provided that a calibration curve is available.

A Mettler Toledo DSC was used to acquire the thermograms of the copolymer samples. The procedure involved weighing 5-10 mg of the dry sample and placing it in a 40 µl hermetic aluminum pan. The sealed sample and reference pan were placed on the heaters, and the thermogram was obtained from -20 °C to 160 °C. To make sure the history of the sample was erased, the samples were heated up to 160 ºC, cooled down to -20 ºC, then heated up again to 160 ºC. Only the second melting scan was used to estimate the melting temperature, which was correlated with the 1-hexene content in the sample. The heating rate was 10 °C/min and the temperature was kept at 160 °C for five min before cooling.

Chapter 4 : Ethylene/1-Hexene Copolymerization Kinetics with CGC-Ti

4.1 Introduction

Several polymerizations were performed under different conditions to evaluate the effect of varying ethylene/1-hexene, ethylene/hydrogen, and catalyst/cocatalyst ratios on the polymerization kinetics and properties of ethylene/1-hexene copolymers made with CGC-Ti in a semi-batch solution reactor. The experimental data was used to develop mathematical models to describe the copolymerization of ethylene and 1-hexene with CGC-Ti.

4.2 Copolymerization with CGC-Ti

4.2.1 Effect of Ethylene/1-Hexene Ratio

Eleven copolymers with different 1-hexene fractions were made to investigate the effect of 1-hexene concentration on the kinetics of copolymerization with CGC-Ti. Each polymerization was replicated at least once to assure reproducibility.

Figure 4.1 compares ethylene consumption rates for ethylene/1-hexene polymerizations, with 1-hexene concentration varying from 0 to 0.965 $mol.L^{-1}$. The ethylene uptake rate (which is proportional to the polymerization rate) decreases with increasing 1-hexene concentration in the reactor. Figure 4.1 shows that the ethylene uptake curves were reproducible over the complete 1-hexene concentration range. It also shows that the rate of ethylene uptake decreases monotonically as the concentration of 1-hexene in the reactor increases. This behaviour is expected, since the propagation rate for ethylene is expected to be much higher than for 1-hexene.

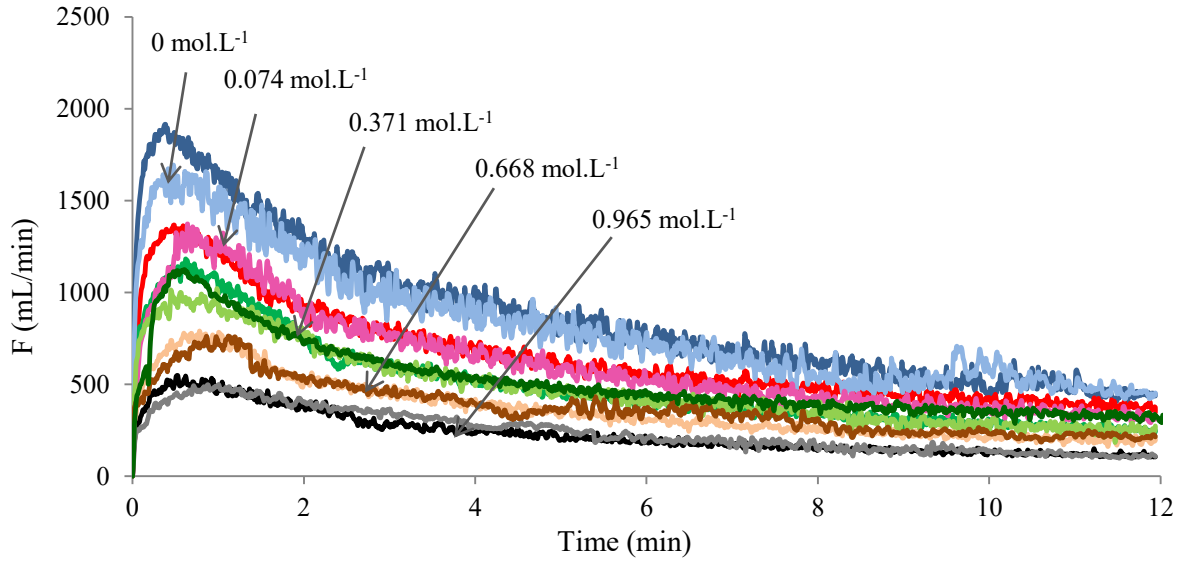

Figure 4.1 Ethylene consumption rates for different 1-hexene concentrations for copolymerization with CGC-Ti. The legends are the concentrations of 1-hexene injected in the reactor.

Table 4.1 lists the number average molecular weight (M_n), weight average molecular weight (M_w), polydispersity index (**PDI**), and the composition of ethylene/1-hexene copolymers made at different 1-hexene concentrations. The 1-hexene concentrations listed in Table 4.1 were calculated based on the number of moles fed into the reactor at room temperature, and shall not to be mistaken by the concentrations of 1-hexene at the equilibrium.

Table 4.1 M_n, M_w, PDI, SCB frequencies, and 1-hexene fraction of ethylene/1-hexene copolymers made with CGC-Ti at different 1-hexene concentrations.

Run	1-hexene (mol.L^{-1})	M_w	M_n	PDI	SCB/1000C	1-hexene in copolymer (mol %)
E/H-0A	0	65 000	19 000	3.4	0	0
E/H-0B	0	61 000	19 000	3.2	0	0
E/H-1A	0.074	41 000	14 000	2.8	9.66	2.01
E/H-1B	0.074	41 000	15 000	2.7	9.15	1.9
E/H-5A	0.371	36 000	11 000	3.3	32.7	7.52
E/H-5B	0.371	39 000	12 000	3.2	31.66	7.25
E/H-5C	0.371	39 000	12 000	3.2	31.7	7.26
E/H-9A	0.668	32 000	10 000	3.1	48.39	12.00
E/H-9B	0.668	27 000	9800	2.8	49.3	12.28
E/H-13A	0.965	27 000	9900	2.8	60.9	16.1
E/H-13B	0.965	26 000	8100	3.2	60.32	15.9

P_E = 120 psig, T = 120 °C, V_S = 160 mL, H_2 = 0.8 mmol, [Al]/[Ti] = 28 700.

Copolymer samples were characterized by GPC-IR in order to obtain their MWD and their SCB frequencies. The method for the calculation of SCBD using GPC-IR has been described in Chapter 3. Equation (4.1)[51] was used to calculate the mole percentage of 1-hexene in the copolymer from the number of short chain branches per 1000 carbons (SCB/1000C).

$$\frac{SCB}{1000C} = \frac{1000*(1-hexene\ mole\ percentage)}{2*(Ethylene\ mole\ percentage)+6*(1-hexene\ mole\ percentage)} \quad (4.1)$$

Most coordination catalysts deactivate during the polymerization following deactivation profiles that depend on catalyst type and polymerization conditions. Considering the most common first-order deactivation mechanism, the rate of ethylene uptake can be expressed as

$$\ln\frac{F}{V_R} = \ln\left(k_p[M][C_0]\right) - k_d t \tag{4.2}$$

where F is the ethylene molar flow rate, V_R is the volume of the reaction medium, k_p is the propagation rate constant, k_d is the deactivation rate constant, and t is the polymerization time. Equation (4.2) is derived in Appendix A.

Therefore, the $\ln(\frac{F}{V_R}) \times t$ plot should be linear if CGC-Ti follows a first order deactivation profile. Figure 4.2 shows that such a model does not describe the polymerization kinetics for this system.

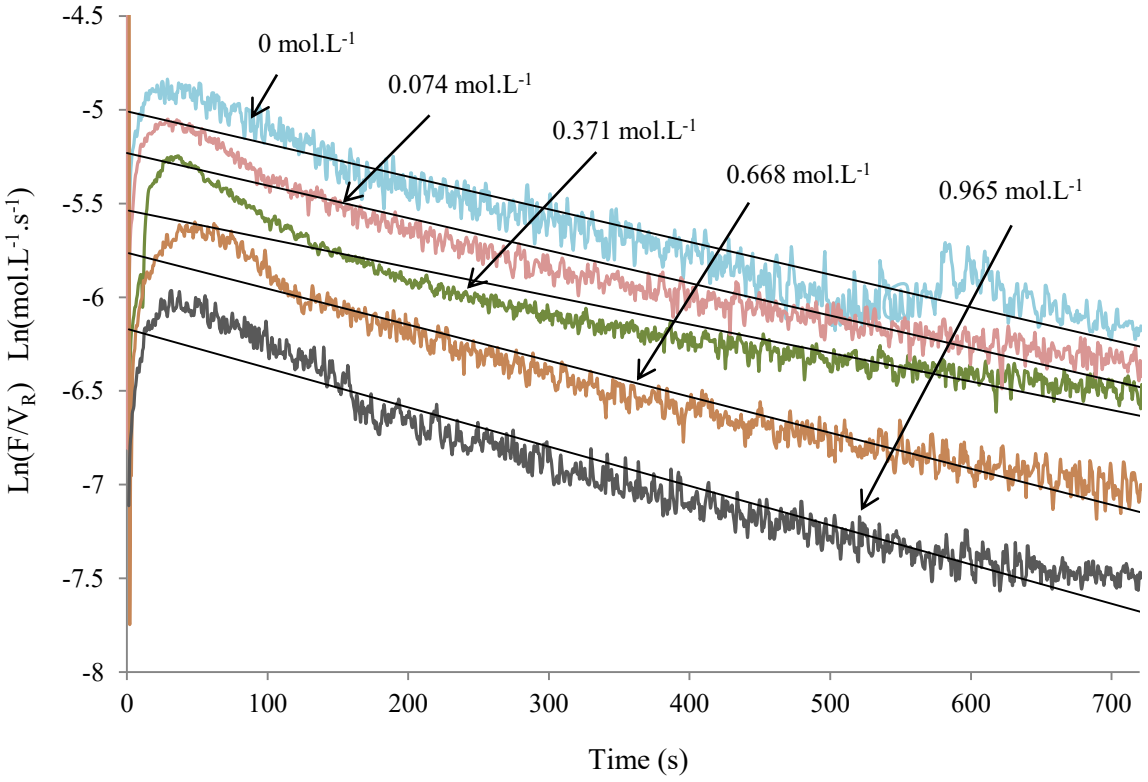

Figure 4.2 First order catalyst decay plot for ethylene/1-hexene copolymerization with CGC-Ti. The legends are the concentrations of 1-hexene injected into the reactor.

Since a first-order deactivation model cannot fit the monomer uptake data with CGC-Ti, we must propose an alternative model. In a previous publication from our group,[9] the polymerization kinetics for ethylene with CGC-Ti (without 1-hexene) was well described with a model that included a reversible catalyst activation/deactivation step with MAO, in addition to purely first-order thermal deactivation. Therefore, this seems to be an adequate first choice to describe the copolymerization behavior of ethylene/1-hexene with CGC-Ti.

Since we are now dealing with a binary copolymerization system (ethylene and 1-hexene), we need to extend the homopolymerization model to account for the presence of the comonomer 1-hexene. In the terminal model, reaction rates depend on the type of monomer taking place in the reaction *and* on the type of monomer attached to the end of the reacting polymer chain.

Table 4.2 summarizes the mechanism used to model the copolymerization of ethylene and 1-hexene with CGC-Ti/MAO. The MAO deactivation/reactivation mechanism is included as one of the elementary steps in Table 4.2, Equations (4.12) to (4.14). A thermal deactivation step was not needed to model the results of these copolymerizations.

Table 4.2 Copolymerization mechanism with CGC-Ti.

Activation	$C + MAO \xrightarrow{k_a} C^*$	(4.3)
Initiation	$C^* + A \xrightarrow{k_{iA}} P_1^A$	(4.4)
	$C^* + B \xrightarrow{k_{iB}} P_1^B$	(4.5)
Propagation	$P_i^A + A \xrightarrow{k_{pAA}} P_{i+1}^A$	(4.6)
	$P_i^A + B \xrightarrow{k_{pAB}} P_{i+1}^B$	(4.7)
	$P_i^B + A \xrightarrow{k_{pBA}} P_{i+1}^A$	(4.8)
	$P_i^B + B \xrightarrow{k_{pBB}} P_{i+1}^B$	(4.9)
Deactivation	$P_i^A \xrightarrow{k_{dth}} C_d + D_i$	(4.10)
	$P_i^B \xrightarrow{k_{dth}} C_d + D_i$	(4.11)
	$P_i^A + MAO \xrightarrow{k_d} C_d + D_i$	(4.12)
	$P_i^B + MAO \xrightarrow{k_d} C_d + D_i$	(4.13)
	$C_d + MAO \xrightarrow{k_a} C^*$	(4.14)

C^*: Active Site, A: Ethylene, B: 1-Hexene, P: Living Polymer Chain, D: Dead Polymer Chain, C_d: Dead Site.

The first step in this mechanism is catalyst (precursor) activation. When the catalyst reacts with the cocatalyst, an active site (C^*) is formed. In this step, one chlorine atom in the metallocene catalyst is exchanged with an alkyl group from cocatalyst, and another chlorine atom is abstracted by the cocatalyst creating a coordination vacancy where the monomer can coordinate and insert (initiation step) into the growing polymer chain (even though this 'step' in reality

involve two elementary reactions, they are very fast and always modelled as a single 'elementary' reaction).

After the first monomer is inserted in the initiation step, the polymer chain begins to grow (propagation) with successive insertions of ethylene or 1-hexene. P_i is the living polymer chain with length *i*; monomer addition (A or B) makes its length increase to *i*+1. The superscript in P_i indicate the type of monomer last inserted into the living polymer chain. Propagation continues until a chain transfer reaction happens (not shown in Table 4.3), or the site deactivates (the former is infinitely more common for stable coordination catalysts).

The model in Table 4.2 assumes that catalyst activation (reaction between the catalyst precursor and the cocatalyst) is instantaneous. The reversible activation and deactivation with MAO is assumed to be the dominant reaction (thermal deactivation was neglected), and independent of the type of monomer last inserted into the active site. Therefore, a single k_d value could be used for the MAO deactivation reactions in Equations (4.12) and (4.13). These assumptions were made to simplify the parameter estimation procedure.

The molar balance of ethylene concentration in the reactor is

$$\frac{\mathrm{d}[A]}{\mathrm{d}t} = \frac{F}{V_R} - \left(k_{pAA}[P_A] + k_{pBA}[P_B]\right)[A] \tag{4.15}$$

where F is the ethylene flow rate and V_R is the reaction medium volume. $[P_A]$ and $[P_B]$ are the concentration of living polymer chains terminated in monomer *A* (ethylene) and *B* (1-hexene), respectively. Since the concentration of ethylene is kept constant during semi-batch polymerizations, $\frac{\mathrm{d}[A]}{\mathrm{d}t} = 0$, and the ethylene flow rate can be written as

$$F = \left(k_{pAA}\emptyset_A + k_{pBA}\emptyset_B\right)[P][A]V_R \tag{4.16}$$

where $\emptyset_A$ and $\emptyset_B = 1 - \emptyset_A$ are the molar fractions of living polymer chains terminated in monomers *A* and *B*, respectively. The long chain approximation[3,40] can be used to calculate these variables from the knowledge of the mole fraction of monomers in the reaction medium and the cross-propagation constants

$$\emptyset_B = \frac{k_{pAB}f_B}{k_{pBA}(1-f_B)+k_{pAB}f_B} \tag{4.17}$$

By substituting Equation (4.17) and the equation for living polymer chains [P] (please see derivation details in Appendix B) into Equation (4.16), we obtain an expression that describes the rate of ethylene uptake during the copolymerization

$$F = \left(k_{pAA} \left(1 - \frac{k_{pAB} f_B}{k_{pBA}(1 - f_B) + k_{pAB} f_B} \right) + k_{pBA} \left(\frac{k_{pAB} f_B}{k_{pBA}(1 - f_B) + k_{pAB} f_B} \right) \right) \times$$

$$\left(k_i'[M] C_0^* \left[\frac{k_a'}{S_1 S_2} \left(\frac{S_1 + k_a'}{S_1(S_1 - S_2)} \right) e^{S_1 t} + \left(\frac{S_2 + k_a'}{S_2(S_2 - S_1)} \right) e^{S_2 t} \right] \right) \times [A] \times V_R \quad (4.18)$$

where

$$S_1 = \frac{-A - \sqrt{A^2 - 4B}}{2} \quad (4.19)$$

$$S_2 = \frac{-A + \sqrt{A^2 - 4B}}{2} \quad (4.20)$$

$$A = k_i'[M] + k_a' + k_d' \quad (4.21)$$

$$B = k_i'[M] k_d' + k_i'[M] k_a' + k_a' k_d' \quad (4.22)$$

Equation (4.18) includes 6 unknown parameters ($k_{pAA}, k_{pAB}, k_{pBA}, k_a', k_d'$ and k_i') that are difficult to estimate accurately, so we need to reduce the number of parameters as much as possible.

By performing a sensitivity analysis, it is evident that k_i' does not influence ethylene uptake appreciably. Assuming reasonable initial guesses for the other 5 unknown parameters, ethylene flow rates were calculated for three different values of k_i', varying from 1 to 10^8 L·mol^{-1}·s^{-1}. Figure 4.3 shows that varying k_i' over 8 orders of magnitude has no effect on ethylene flow rate. It is only when k_i' approaches zero that it starts influencing the rate of ethylene uptake. In this case, the active sites do not get initiated by ethylene to start forming polymer chains (Figure 4.3). This is, evidently, not a reasonable assumption for our active catalyst system.

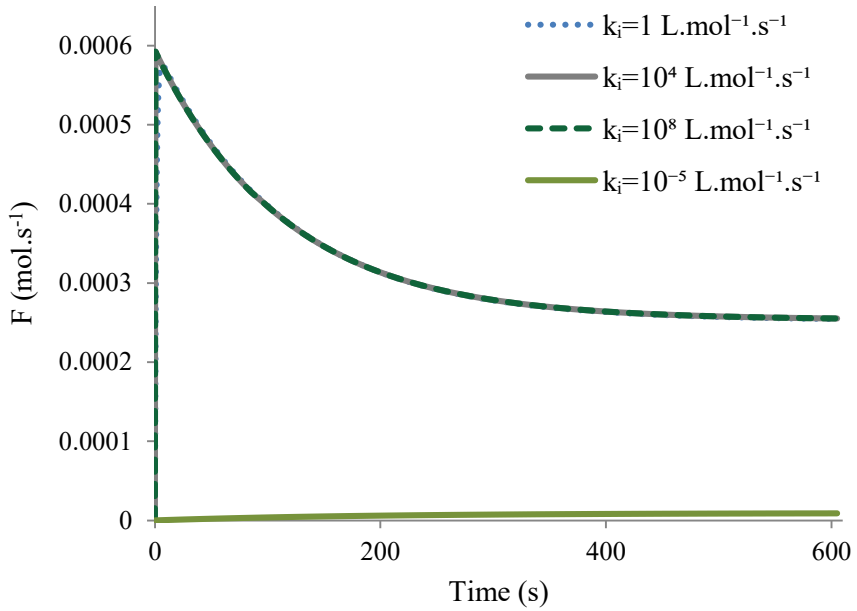

Figure 4.3 Sensitivity analysis for different k_i values ($k_d^{'}$ = 0.005 s^{-1}, $k_a^{'}$ = 0.0037 s^{-1}, k_{pAA} = 20050 $L \cdot mol^{-1} \cdot s^{-1}$, k_{pBA} = 9000 $L \cdot mol^{-1} \cdot s^{-1}$).

To simplify the final equation, the value of k_i' was set to 1 $L \cdot mol^{-1} \cdot s^{-1}$ (Figure 4.3 shows that practically any other value would predict the same ethylene uptake curve), reducing the number of parameters that must be estimated to 5. Since this is still a large number of parameters, we will show in the next section how to further reduce them to 4 using reactivity ratios.

4.2.1.1 Reactivity Ratio Estimation

The Mayo-Lewis equation, also known as the copolymer equation, relates the mole fraction of monomer in the copolymer, F_A, to the monomer mole fraction in the reactor, f_A

$$F_A = \frac{r_A f_A^2 + f_A(1-f_A)}{r_A f_A^2 + 2 f_A(1-f_A) + r_B(1-f_A)^2} \tag{4.23}$$

Reactivity ratios are defined as

$$r_A = \frac{k_{pAA}}{k_{pAB}} \tag{4.24}$$

$$r_B = \frac{k_{pBB}}{k_{pBA}} \tag{4.25}$$

The Mayo-Lewis equation was used to estimate the reactivity ratios for ethylene and 1-hexene with CGC-Ti and reduce the number of parameters that needed to be estimated in Equation (4.18) for the ethylene uptake rate.

To use the Mayo-Lewis equation, one needs to calculate the concentrations of ethylene and 1-hexene in the polymerization medium. In this investigation, these concentrations were estimated using the Peng-Robinson equation available in Aspen Hysys. Figure 4.4 shows that the mass of 1-hexene fed to the reactor and the concentration of 1-hexene in toluene at the polymerization conditions follow a linear relationship.

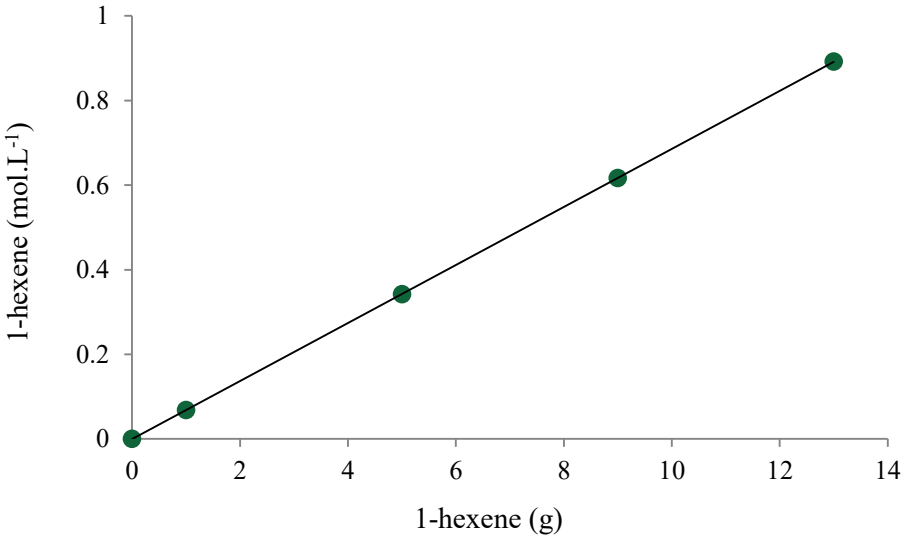

Figure 4.4 Concentration of 1-hexene in the liquid phase versus the amount of 1-hexene fed to the reactor at 120 °C.

Peng-Robinson equation available in Aspen Hysys was also used to estimate the concentration of ethylene in toluene at 120 °C and 120 psig. Under the mentioned conditions, the concentration of ethylene in toluene is estimated to be approximately 0.49 $mol.L^{-1}$.

Table 4.3 lists the mole fraction of ethylene in the copolymer, F_A, obtained from GPC-IR, and the mole fraction of ethylene in the liquid phase, f_A, calculated from Peng-Robinson equation in Aspen Hysys. Using these data, we fitted the Mayo-Lewis equation, Equation (4.23), to the experimental data to estimate the values of r_A and r_B.

Table 4.3 Feed and copolymer composition for samples made with CGC-Ti.

Run	1-hexene in copolymer (mol %)	F_B	f_A	F_A
E/H-0A	0	0	1	1
E/H-0B	0	0	1	1
E/H-1A	2.01	0.0201	0.8785	0.9799
E/H-1B	1.9	0.019	0.8785	0.981
E/H-5A	7.52	0.0752	0.5957	0.9248
E/H-5B	7.25	0.0725	0.5957	0.9275
E/H-5C	7.26	0.0726	0.5957	0.9274
E/H-9A	12.00	0.12	0.4555	0.88
E/H-9B	12.28	0.1228	0.4555	0.8772
E/H-13A	16.1	0.161	0.3717	0.839
E/H-13B	15.9	0.159	0.3717	0.841

MATLAB was used to fit the $f_A \times F_A$ data using the Levenberg-Marquardt algorithm to minimize the sum of the squares of the residuals, *s*, between model predictions and experimental data[52]

$$r_i = F_{Ai} - F'_{Ai} \tag{4.26}$$

$$s = \sum_{i=1}^{n} r_i^2 = \sum_{i=1}^{n} (F_{Ai} - F'_{Ai})^2 \quad (4.27)$$

where F_A is the observed response and F'_A is the fitted response.

Table 4.4 reports reactivity ratio estimations, the sum of the squared errors, and R^2.

Table 4.4 Reactivity ratios for ethylene/1-hexene copolymerization with CGC-Ti.

Parameter	Value	95% confidence interval
$\boldsymbol{r_A}$	8.1	(7.7,8.6)
$\boldsymbol{r_B}$	0.063	(0.024,0.10)
$SSE: 3.144 \times 10^{-5}$, $R^2: 0.9991$		

Figure 4.5 shows that the Mayo-Lewis equation fits the f_A x F_A plot well with this set of reactivity ratio estimates.

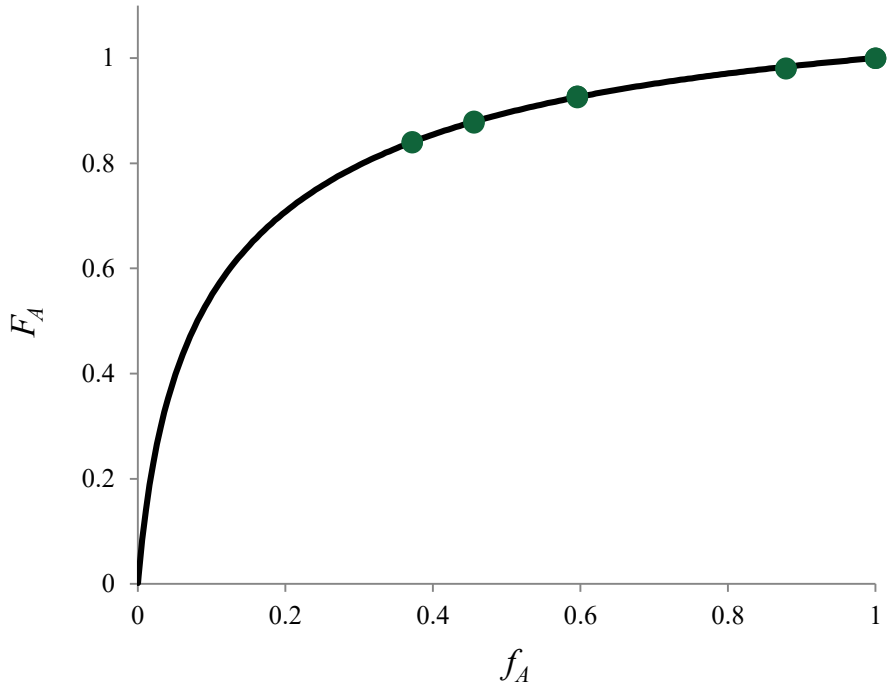

Figure 4.5 Mayo-Lewis curve fitting for ethylene/1-hexene copolymers made with CGC-Ti.

The estimate for r_A (obtained within a tight confidence interval, see Table 4.4) can be substituted in Equation (4.18) to eliminate the value of k_{AB} and reduce the number of unknown parameters from 5 to 4

$$\emptyset_B = \frac{(\frac{k_{pAA}}{r_A})f_B}{k_{pBA}(1-f_B)+(\frac{k_{pAA}}{r_A})f_B} \tag{4.28}$$

Therefore, the final equation used to fit the ethylene uptake rates contain only 4 adjustable $(k_{pAA}, k_{pBA}, k'_a, k'_d)$ parameters, is given by the expression

$$F = \left(k_{pAA} - \left(k_{pAA} - k_{pBA}\right)\left(\frac{\frac{k_{pAA}}{r_A}f_B}{k_{pBA}(1-f_B)+\frac{k_{pAA}}{r_A}f_B}\right)\right) \times$$

$$\left([M]C_0^*\left(\frac{k'_a}{s_1 s_2} + \frac{s_1+k'_a}{s_1(s_1-s_2)} \times e^{s_1 t} + \frac{s_2+k'_a}{s_2(s_2-s_1)} \times e^{s_2 t}\right)\right) \times [A] \times V_R \tag{4.29}$$

The optimization method called particle swarm was used to fit Equation (4.29) to the experimental ethylene uptake rate data and estimate the remaining 4 parameters. This procedure will be discussed in the next section.

4.2.1.2 Parameter Estimation Using Particle Swarm Optimization

An evolutionary global optimization algorithm, particle swarm optimization (PSO) was developed by Eberhart and Kennedy to optimize nonlinear functions.[53] In this method, some initial candidate solutions are randomly generated and then placed in the function search space. The individual solutions are assigned a velocity vector which determines their next displacement and they iteratively evolve in a swarm.[54]

The potential solution, called particle, keeps track of its location and value locally and globally. The concept of particle swarm optimization includes the accelerating of particles toward the best ever value and best ever location that it has achieved.[53]

The detailed PSO algorithm represents the position and velocity of *i*-th particle as below[55]

$$x_i = x_{i-1} + v_i \tag{4.30}$$

$$v_i = wv_{i-1} + C_1 r_1 \otimes (x_i^* - x_{i-1}) + C_2 r_2 \otimes (f - x_{i-1}) \tag{4.31}$$

where x represents the particle's position and v is the velocity which determines the particle's movement. C_1 and C_2 are the acceleration constants, and w is the inertia weight that shows the influence of previous velocity vectors. The random vectors r_1 and r_2 contain the dimensionality of the search space, x_i^* and f are the particle's and swarm's best-ever position, respectively, and $\otimes$ stands for the multiplication vector.

Boundary constraints are required to avoid particles moving outside of the practical boundary. To get the best performance with PSO, we have put the bounds on the values of the estimated parameters to be greater than zero.

4.2.1.2.1 Kinetic Parameter Estimation

Eleven sets of data obtained from the experiments in Section 4.2.1 were divided into two groups. Eight of them were used to estimate model parameters, and the others (E/H-1A, E/H-5B, E/H-9B) were randomly chosen and used to validate the model. The 4 parameters were estimated simultaneously by minimizing the sum square error (SSE) using the PSO method. Figure 4.6 shows that the proposed model fits the ethylene uptake profiles adequately.

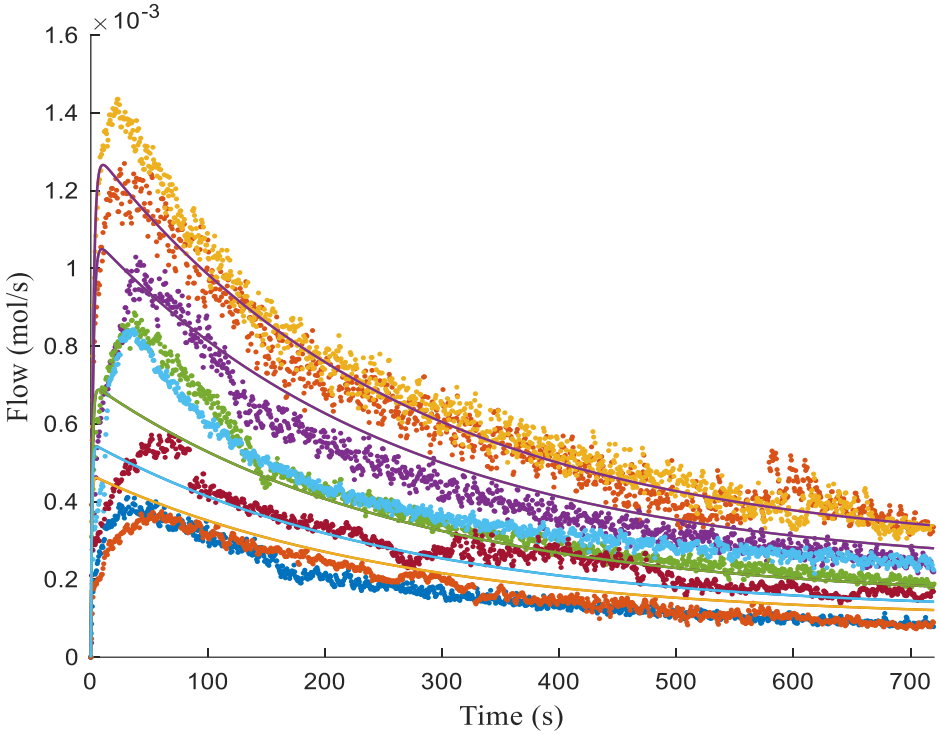

Figure 4.6 Experimental data versus model predictions for ethylene/1-hexene copolymerizations with CGC-Ti at different 1-hexene concentrations.

Larger deviations are only observed during the first 100 s of polymerization, which can be attributed to instabilities in ethylene flow and polymerization temperature right after catalyst injection at $t = 0$. During the first few seconds after catalyst injection, the reactor temperature increases by a couple of degrees until the reactor temperature control system can correct for the sudden heat release due to polymerization. Figure 4.7 illustrates the temperature profile of a typical polymerization experiment. Polymerization data during these first few seconds is less reliable, since the polymerization rate constants follow the Arrhenius law and are exponential functions of the temperature.

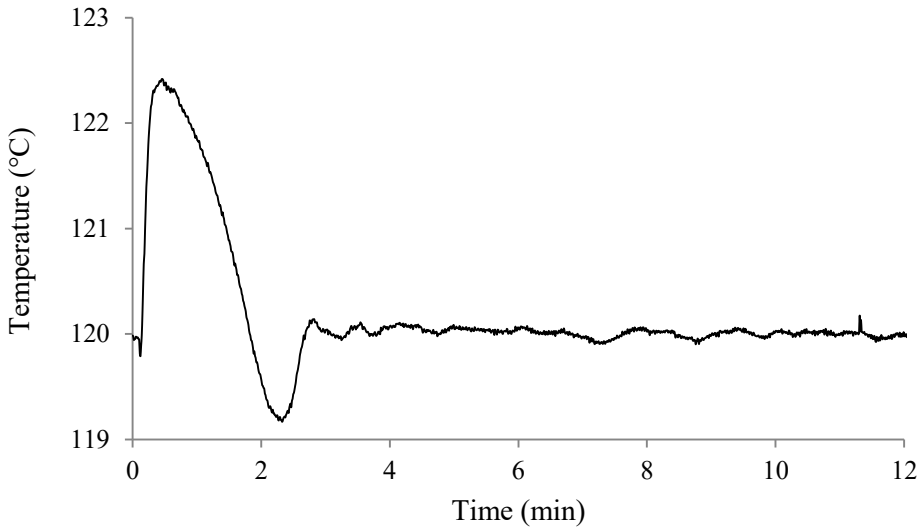

Figure 4.7 Temperature profile for experiment E/H-5A.

Table 4.5 lists the values estimated for the polymerization rate constants.

Table 4.5 Estimated polymerization rate constants for the copolymerization of ethylene and 1-hexene with CGC-Ti.

Parameter	Estimated Value
$\boldsymbol{k_{pAA}}$ ($L \cdot mol^{-1} \cdot s^{-1}$)	4.4×10^{4}
$\boldsymbol{k_{pBA}}$ ($L \cdot mol^{-1} \cdot s^{-1}$)	3.4×10^{3}
$\boldsymbol{k'_a}$ (s^{-1})	8.3×10^{-4}
$\boldsymbol{k'_d}$ (s^{-1})	3.1×10^{-3}
$\boldsymbol{k_{pAB}}$ ($L \cdot mol^{-1} \cdot s^{-1}$)	5.4×10^{3}
$\boldsymbol{k_{pBB}}$ ($L \cdot mol^{-1} \cdot s^{-1}$)	2.2×10^{2}
SSE: 0.006	

The values of k_{pAA} and k_{pBA} estimated from PSO, were substituted in Equation (4.24) and Equation (4.25) to calculate the values of k_{pAB} and k_{pBB} reported in Table 4.5.

The values estimated for the propagation constants agree with our expectations for this copolymerization. Considering that ethylene (monomer *A*) in more active than 1-hexene (monomer *B*), the expected order for the propagation constants is $k_{pAA} > k_{pAB} \approx k_{pBA} > k_{pBB}$ which agrees with the values estimated for these parameters.

4.2.1.2.2 Model Validation

Validating the model against experimental data is essential. In this regard, three copolymerizations done with different 1-hexene concentrations (0.074, 0.371 and 0.668 mol.L^{-1}), were used to validate the developed model (Figure 4.8).

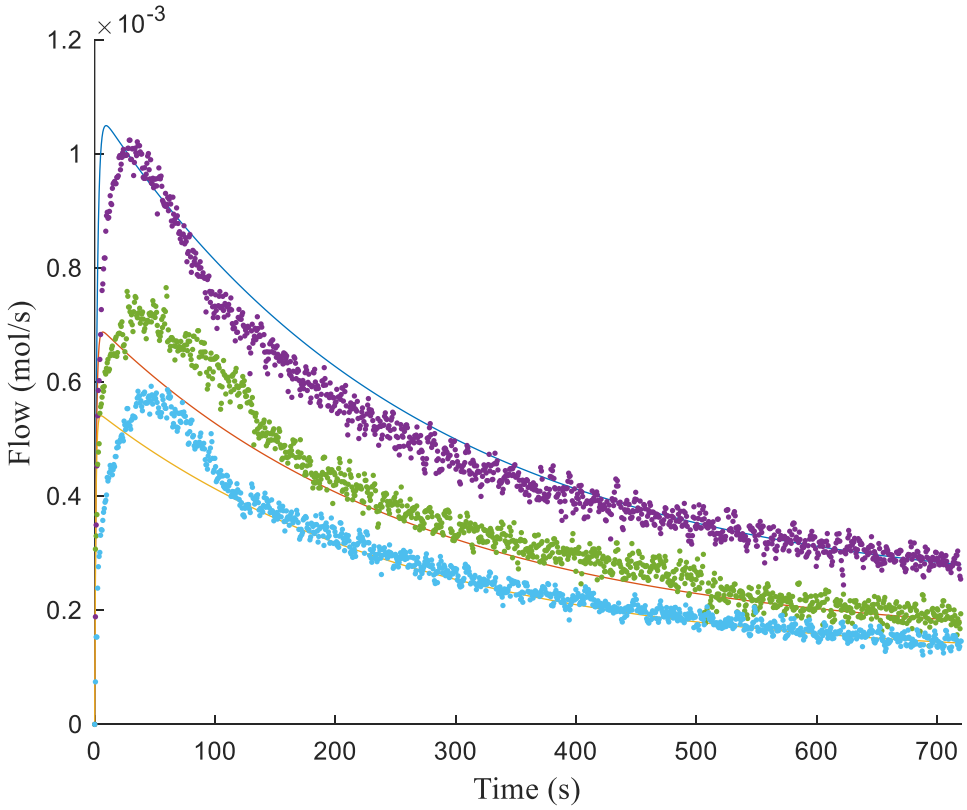

Figure 4.8 Validation of the model for the copolymerization of ethylene and 1-hexene with CGC-Ti.

Figure 4.8 shows that the proposed model describes well these 3 validation copolymerizations, confirming that the model is valid for the copolymerization of ethylene and 1-hexene using CGC-Ti under the range of conditions investigates herein.

4.2.2 Effect of Cocatalyst Concentration

Seven copolymerization runs were performed to investigate the effect of cocatalyst/catalyst ratio on polymerization rate and copolymers microstructure. Polymerization temperature, ethylene pressure, concentrations of 1-hexene, H_2, and catalyst were kept constant for all experiments; the [Al]/[Ti] ratio was changed by varying only MAO concentration in the reactor. It should be noted that the values of kinetic constants estimated in Section 4.2.1.2.1 are valid under the conditions that the experiments were performed. Estimation of kinetic constants under different conditions (cocatalyst/catalyst ratio) requires new sets of experiments.

Figure 4.9 shows that the ethylene consumption rates increase as the [Al]/[Ti] ratio increases.

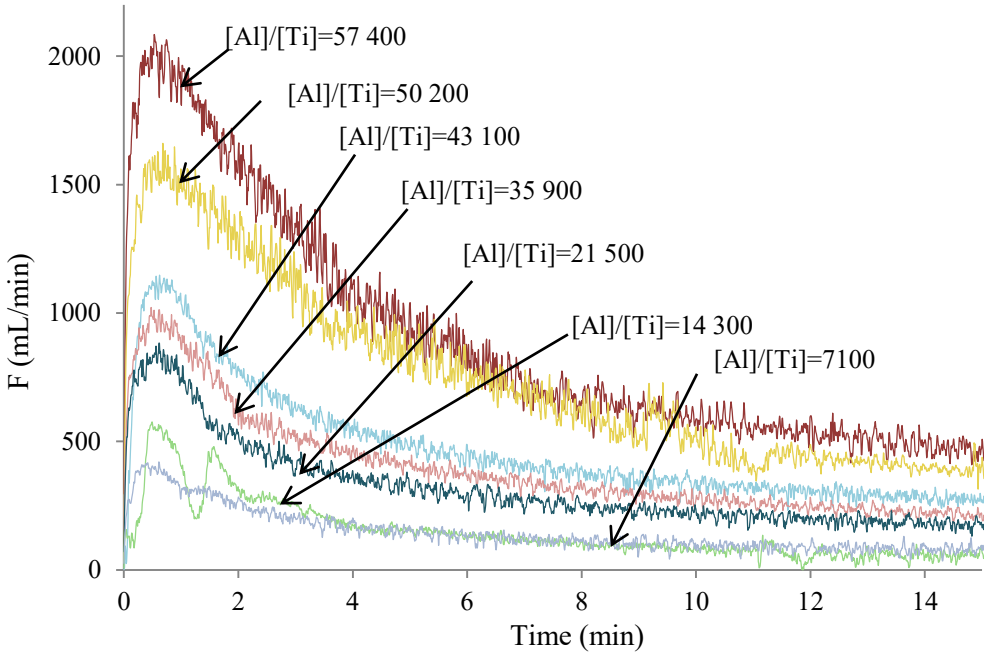

Figure 4.9 Ethylene uptake rates for different [Al]/[Ti] ratios for copolymerization with CGC-Ti.

Table 4.6 summarizes the polymerization conditions and copolymer properties for this set of experiments.

Table 4.6 M_n, M_w, PDI and copolymerization condition for different [Al]/[Ti] ratios.

Run	[Al]/[Ti]	M_w	M_n	PDI
C/C-1	57 400	49 000	12 000	3.9
C/C-2	50 200	49 000	12 000	3.9
C/C-3	43 100	40 000	11 000	3.8
C/C-4	35 900	36 000	11 000	3.4
C/C-6	21 500	34 000	11 000	3.2
C/C-7	14 300	28 000	9000	3.1
C/C-8	7100	26 000	8600	3.0

P_E = 120 psig, T = 120 °C, V_S = 160 mL, [1-*H*] = 0.148 mol.L^{-1}, H_2 = 0.8 mmol, [C] = 0.38 µmol.L^{-1}.

Figure 4.10 shows how M_n, M_w, and PDI of copolymers vary by changing the [Al]/[Ti] ratio from 7100 to 57400. M_n and M_w increase slightly with increasing [Al]/[Ti] ratio, and their distributions broaden, as shown by the higher PDI values. The broadening of these distributions is also clear from inspection of Figure 4.11.

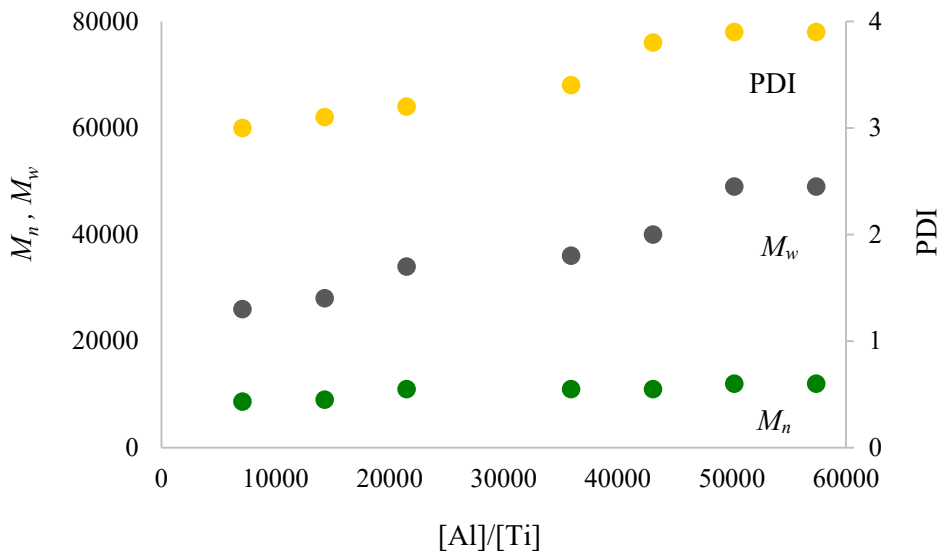

Figure 4.10 M_n, M_w, and PDI for ethylene/1-hexene copolymers made at different [Al]/[Ti] ratios.

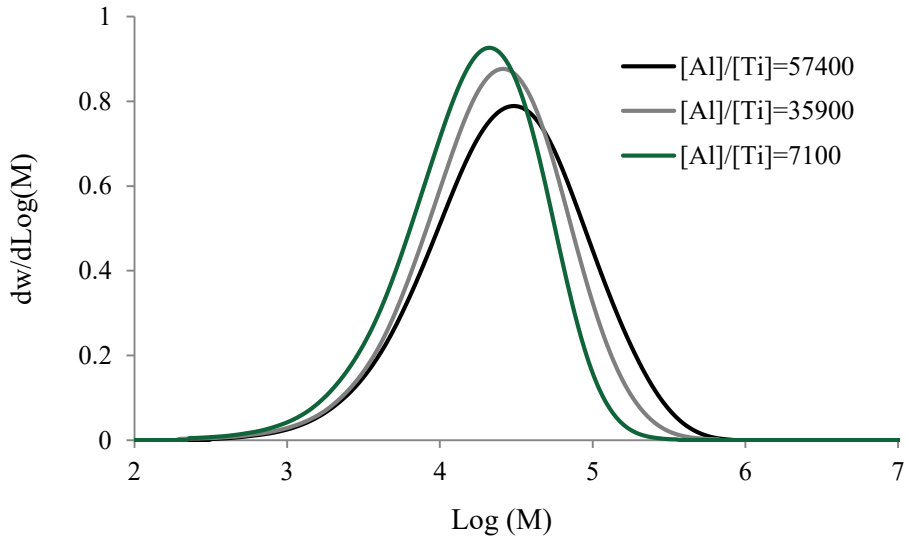

Figure 4.11 MWD for sample C/C-1, C/C-4, C/C-8 produced with different MAO concentrations.

4.2.3 Effect of Catalyst Concentration

In this section, the effect of catalyst concentration on M_n, M_w, PDI and polymer yield at the MAO concentration of 0.011 mol.L^{-1} is investigated. Seven polymerizations were performed at four different catalyst concentrations. Three of the experiments were replicated to assure reproducibility. All the variables were kept constant except catalyst concentration. Table 4.7 shows copolymerization details, GPC-IR results, and the yield of seven polymerizations.

Table 4.7 M_n, M_w, PDI and copolymerization condition at different catalyst concentrations.

Run	catalyst (µmol.L^{-1})	M_w	M_n	PDI	polymer yield (g)
C-1	0.12	39 000	12 000	3.3	2.37
C-2	0.25	38 000	12 000	3.2	5.1
C-3	0.37	39 000	12 000	3.3	7.02
C-4	0.5	37 000	12 000	3.1	10.1
C-1A	0.12	38 000	11 000	3.5	1.98
C-2A	0.25	39 000	13 000	3	5.41
C-3A	0.37	38 000	12 000	3.2	7.59

P_E = 120 psig, T = 120 °C, V_S = 160 mL, [1-H] = 0.148 mol.L^{-1}, H_2 = 0.8 mmol.

The ethylene flow rate curves increase proportionally to the catalyst concentrations, as shown in Figure 4.12. Only selected curves are plotted in this figure for easier comparison.

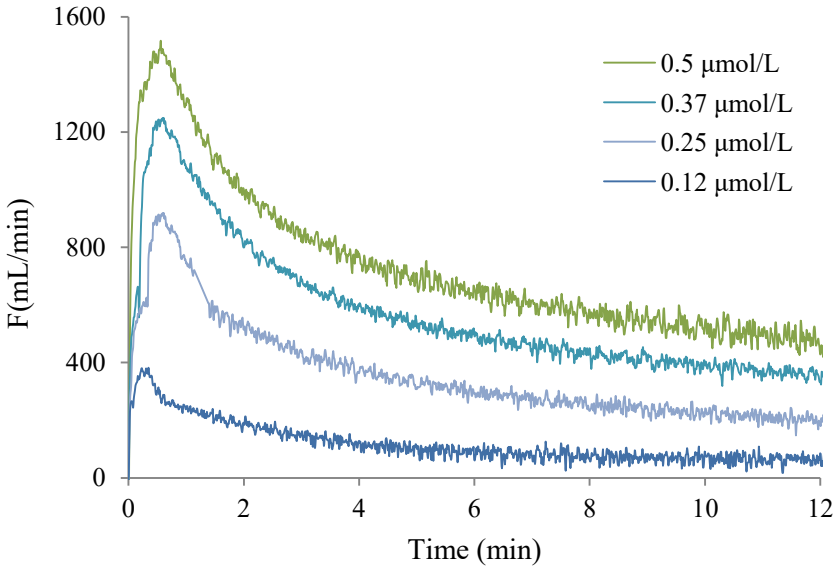

Figure 4.12 Ethylene flow rates at different CGC-Ti concentrations.

Figure 4.13 shows that polymer yield is a linear function of catalyst concentration, as expected from a first order reaction (see mechanism in Table 4.2), which further support the adequacy of our model for these copolymerizations.

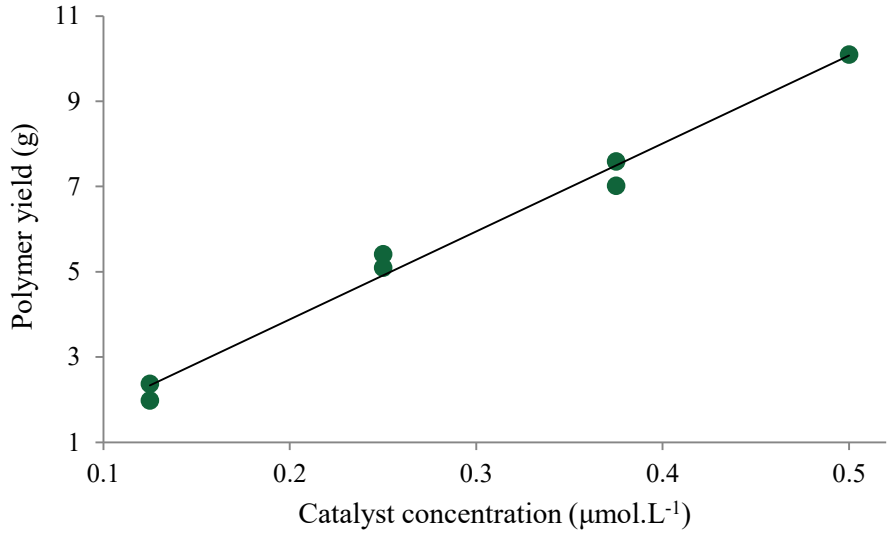

Figure 4.13 Polymer yield as a function of CGC-Ti concentration.

Figure 4.14 shows that M_n, M_w, and PDI of copolymers does not depend on catalyst concentration, which is also an expected result of this polymerization system.

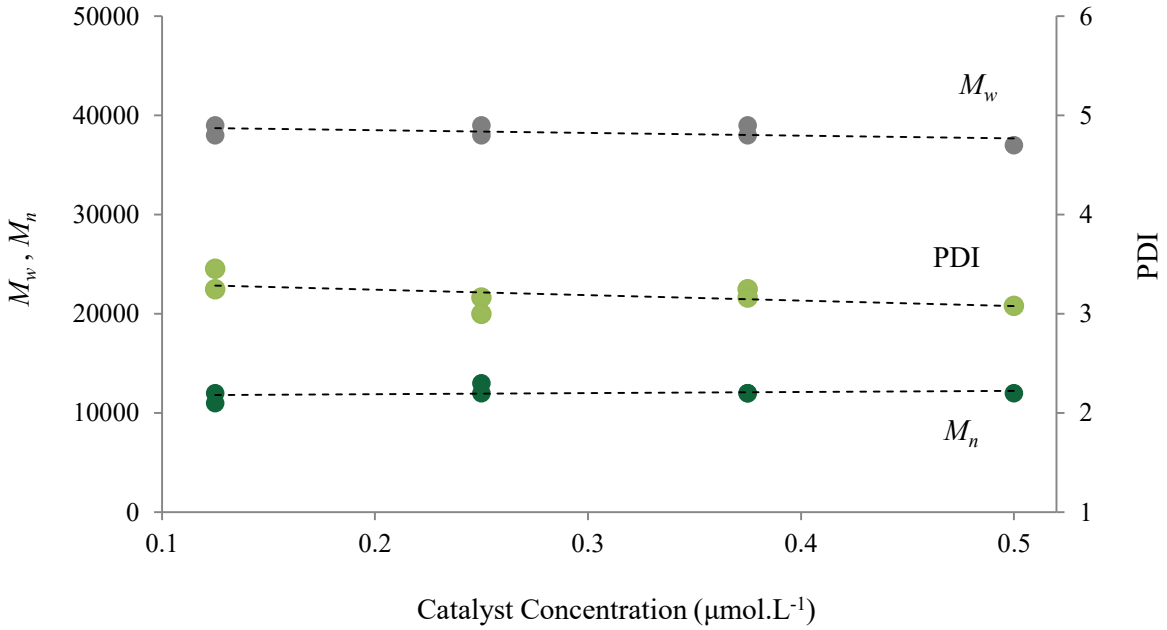

Figure 4.14 M_n, M_w, and PDI as a function of CGC-Ti concentration.

4.2.4 Effect of Ethylene/Hydrogen Ratio

Several chain transfer reactions may occur during coordination polymerization, including β-hydride elimination, transfer to monomer, transfer to cocatalyst, and transfer to hydrogen. When H_2 is present in the reactor, in most cases it becomes the dominant transfer reaction. This is why H_2 is the chain transfer of choice in the polyolefin industry. Therefore, it is important to know the hydrogen response of different catalysts.[3,56]

4.2.4.1 Effect of Hydrogen on Polymer Molecular Weight

In ethylene polymerization, in addition to decreasing polymer molecular weight, H_2 also reduces the polymerization rate. Chain transfer to hydrogen produces a metal hydride site that can be initiated via monomer insertion to grow another polymer chain. One of the mechanisms proposed to explain this phenomenon proposes that the metal hydride sites formed after transfer to H_2 are

less reactive towards ethylene insertion. Consequently, adding H_2 to the reactor makes the catalyst less active.

Ten copolymerizations were performed to evaluate the effect of H_2 on polymerization rate and polymer molecular weight. Table 4.8 lists polymerization conditions and copolymer properties. Hydrogen concentrations in toluene were estimated using the Peng-Robinson equation available in Aspen Hysys.

Table 4.8 M_n, M_w, PDI and polymerization conditions for different H_2 concentrations.

Run	H_2 (mmol.L^{-1})	M_w	M_n	PDI
H-1	0	168 000	47 000	3.6
H-2	0.146	64 000	20 000	3.1
H-3	0.174	62 000	19 000	3.2
H-4	0.276	47 000	14 000	3.3
H-5	0.368	42 000	11 000	3.7
H-6	0.454	31 000	8500	3.6
H-7	0.545	25 000	8200	3.0
H-8	0.644	17 000	5300	3.2
H-9	0.722	12 000	4000	3.0
H-10	0.895	10 500	3500	3.0

P_E = 120 psig, T = 120 °C, V_S = 160 mL, [1-*H*] = 0.148 mol.L^{-1}, [Al]/[Ti] = 28 700.

Figure 4.15 shows that ethylene uptake rates decrease monotonically as H_2 concentrations in the reactor increase.

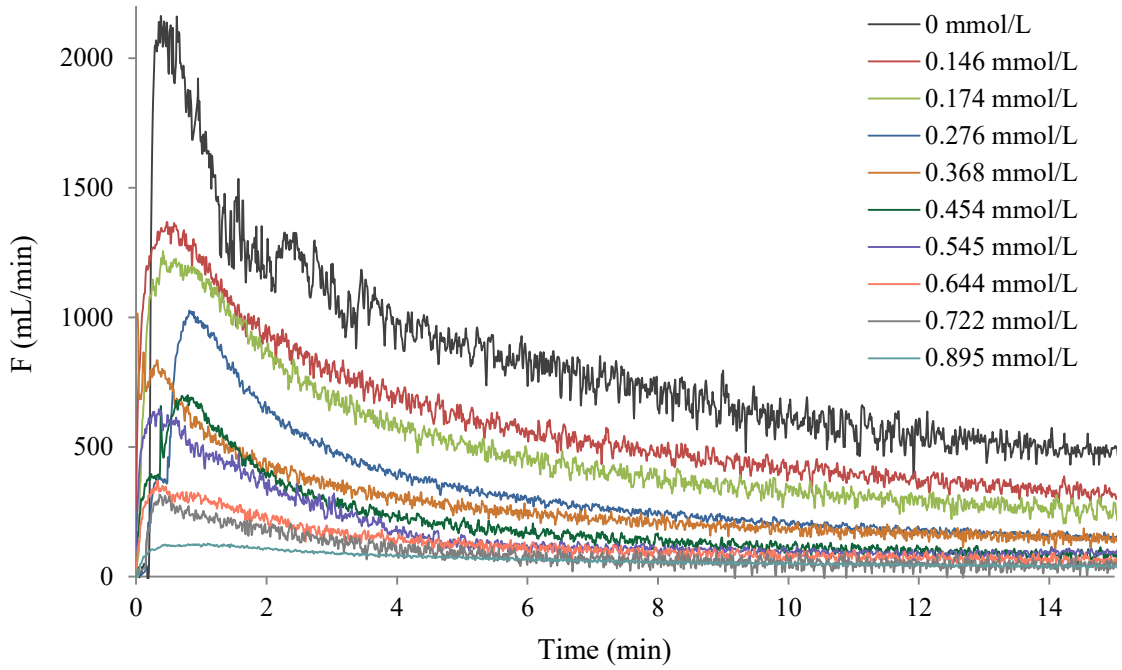

Figure 4.15 Ethylene uptake rates with CGC-Ti under different H_2 concentrations. The legends are the H_2 concentration in toluene. See Table 4.8 for other polymerization conditions.

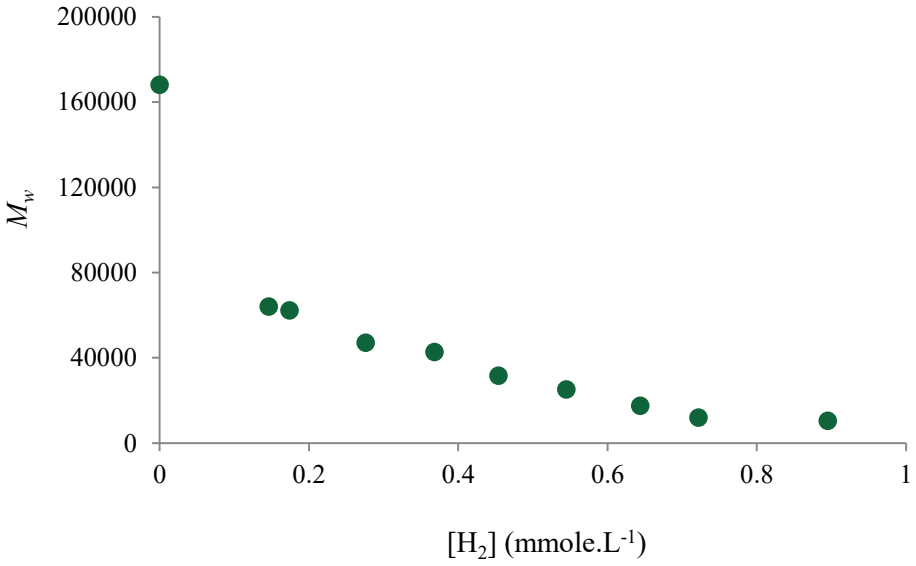

Figure 4.16 Molecular weight of copolymers made with CGC-Ti as a function of hydrogen concentration in toluene.

Figure 4.16 shows that M_w decreases with increasing H_2 concentration. Injecting even a minimum amount of H_2 into the reactor makes M_w to drop about 100,000 g/mol.

4.2.4.2 Estimation of Chain Transfer Rate Constants

During coordination polymerization, the main chain transfer reactions include transfer to H_2, monomers, cocatalyst, and β-hydride elimination. The mechanism of all these reactions is presented in Table 4.9.

Table 4.9 Chain transfer reactions for binary copolymerizations with CGC-Ti.

Transfer to hydrogen	$P_i^A + H_2 \xrightarrow{k_{tHA}} P^H + D_i$	(4.32)
	$P_i^B + H_2 \xrightarrow{k_{tHB}} P^H + D_i$	(4.33)
Initiation	$P_H + A \xrightarrow{k_{iA}} P_1^A$	(4.34)
	$P_H + B \xrightarrow{k_{iB}} P_1^B$	(4.35)
β-hydride elimination	$P_i^A \xrightarrow{k_{t\beta A}} P_H + D_i$	(4.36)
	$P_i^B \xrightarrow{k_{t\beta B}} P_H + D_i$	(4.37)
Transfer to monomer	$P_i^A + A \xrightarrow{k_{tAA}} P_1^A + D_i$	(4.38)
	$P_i^A + B \xrightarrow{k_{tAB}} P_1^A + D_i$	(4.39)
	$P_i^B + A \xrightarrow{k_{tBA}} P_1^B + D_i$	(4.40)
	$P_i^B + B \xrightarrow{k_{tBB}} P_1^A + D_i$	(4.41)
Transfer to cocatalyst	$P_i^A + Al \xrightarrow{k_{tAlA}} P^A + D_i$	(4.42)
	$P_i^B + Al \xrightarrow{k_{tAlB}} P^B + D_i$	(4.43)

The polymer number average chain length, r_n, is determined by the relative ratios of propagation to total chain transfer, as given by expression

$$\frac{1}{r_n} = \frac{R_H+R_\beta+R_M+R_{Al}}{R_P} \tag{4.44}$$

r_n can also be defined as.

$$r_n = \frac{M_n}{mw} \tag{4.45}$$

where mw is the average molar mass of repeating unit in the polymer chain as shown in Equation (4.46).

$$mw = F_B mw_B + (1 - F_B)mw_A \tag{4.46}$$

and F_B is the molar fraction of 1-hexene in the copolymer, mw_B and mw_A are the molar masses of 1-hexene and ethylene, respectively.

The propagation rate for the terminal model is given by

$$R_P = k_{PAA}[A][P^A] + k_{pAB}[B][P^A] + k_{PBA}[A][P^B] + k_{pBB}[B][P^B] \tag{4.47}$$

where P^A and P^B are the numbers of moles of growing polymer chains terminated in monomers A and B

$$P^A = \sum_1^\infty P_i^A \tag{4.48}$$

$$P^B = \sum_1^\infty P_i^B \tag{4.49}$$

and $[A]$ and $[B]$ are the concentration of monomers A and B at the active sites, respectively.

Equation (4.47) may be rewritten as

$$R_P = (k_{PAA}\phi_A f_A + k_{PAB}\phi_A f_B + k_{PBA}\phi_B f_A + k_{PBB}\phi_B f_B)[M][P] \tag{4.50}$$

where ϕ_A and ϕ_B are the molar fractions of growing polymer chains terminated in monomer *A* and *B*, respectively, [*M*] is the total concentration of monomers, and [*P*] is the total concentration of living polymer chains.

The rate of transfer to monomers is given by

$$R_M = k_{tAA}[A][P^A] + k_{tAB}[B][P^A] + k_{tBA}[A][P^B] + k_{tBB}[B][P^B] \quad (4.51)$$

In β-hydride elimination reaction, the H atom bonded to the β-carbon in the polymer chain is detached and transferred to the active site, forming a metal hydride site. The same metal hydride site is produced as a result of transfer to H_2. The rates of these reactions are given by the following expressions

$$R_\beta = k_{t\beta A}[P^A] + k_{t\beta B}[P^B] \quad (4.52)$$

$$R_H = k_{tHA}[H_2][P^A] + k_{tHB}[H_2][P^B] \quad (4.53)$$

Similarly, the rate of chain transfer to cocatalyst equals

$$R_{Al} = k_{tAlA}[Al][P^A] + k_{tAlB}[Al][P^B] \quad (4.54)$$

Substituting Equations (4.50) to (4.54) into Equation (4.44) and doing some manipulations yields

$$\frac{1}{r_n} = \frac{[H_2](k_{tHA}\phi_A + k_{tHB}\phi_B)}{\Theta[M]} + \frac{\alpha}{\Theta[M]} \quad (4.55)$$

where

$$\Theta = (k_{PAA}\phi_A f_A + k_{PAB}\phi_A f_B + k_{PBA}\phi_B f_A + k_{PBB}\phi_B f_B) \quad (4.56)$$

and

$$\alpha = (k_{t\beta A}\phi_A + k_{t\beta B}\phi_B) + (k_{tAA}\phi_A f_A + k_{tBA}\phi_B f_A + k_{tAB}\phi_A f_B + k_{tBB}\phi_B f_B)[M] + (k_{tAlA}\phi_A + k_{tAlB}\phi_B)[Al] \quad (4.57)$$

In this set of experiments, all the variables except H_2 concentration were kept constant, which means that F_B was constant. The F_B value, with injected 1-hexene concentration of 0.148 mol.L^{-1},

was calculated to be 0.028 using the same procedure in Section 4.2.1.1 (Table 4.3). According to Equation (4.46), *mw* can be calculated as:

$$mw = 0.028 \times 84.16 + (1 - 0.028) \times 28.05 = 29.6 \quad (4.58)$$

where 84.16 and 28.05 are the molar masses of 1-hexene and ethylene, respectively.

By having *mw* and the M_n values (from Table 4.8) we are able to calculate r_n. Table 4.10 reports the reciprocal of r_n values at different H_2 concentrations.

Table 4.10 Reciprocal of r_n values at different **[**H_2] concentrations in copolymerization with CGC-Ti.

Run	H_2 (mol.L^{-1})	$\frac{1}{r_n}$
H-1	0	0.0006
H-2	0.00015	0.0015
H-3	0.00017	0.0016
H-4	0.00027	0.0021
H-5	0.00037	0.003
H-6	0.00045	0.0035
H-7	0.00056	0.004
H-8	0.00064	0.006
H-9	0.00072	0.007
H-10	0.00089	0.008

Since only H_2 concentration was changed in this set of runs, all the other variables in Equation (4.55) are constants, including $\emptyset_A$, $\emptyset_B$ and the lumped parameters θ and α. Thus, by plotting $\frac{1}{r_n}$ as a function of $[H_2]$, we should be able to estimate k_{tHA} and k_{tHB} from the intercept and slope of Figure 4.17.

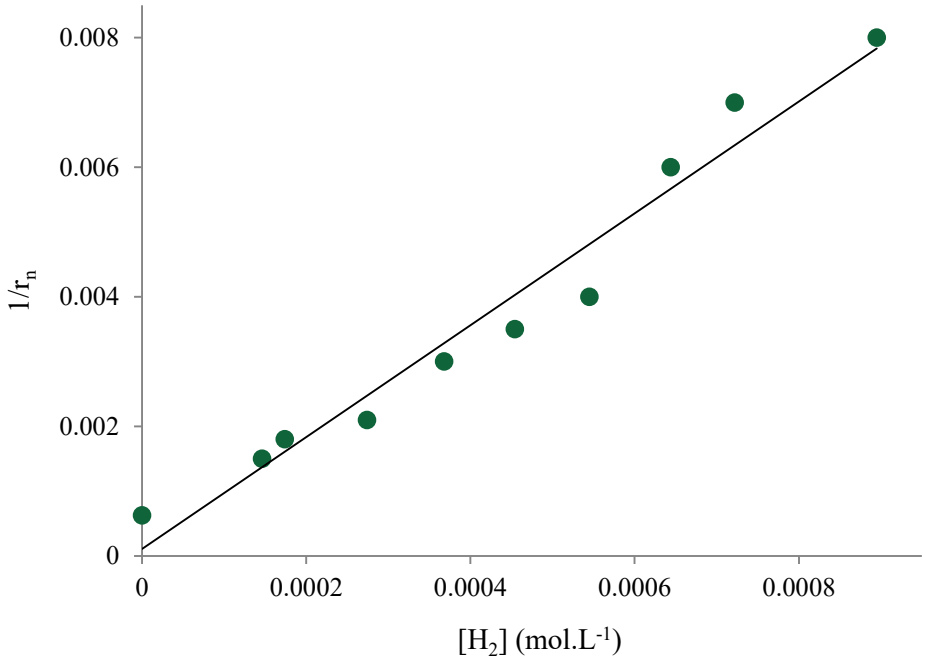

Figure 4.17 Number average chain length as a function of hydrogen concentration.

Table 4.11 shows lumped parameter constants estimated by linear regression of the data in Figure 4.17.

Table 4.11 Estimated values using linear regression.

Parameter	Estimated value using linear regression	Standard error
$\frac{(k_{tHA}\phi_A + k_{tHB}\phi_B)}{\theta[M]}$	8.6	0.6
$\frac{\alpha}{\theta[M]}$	0.0001	0.0003
SSE: 2.05×10^{-6}		

Slope value equals

$$\frac{(k_{tHA}\phi_A + k_{tHB}\phi_B)}{\theta[M]} = 8.6 \tag{4.59}$$

In Equation (4.59), the parameter $\emptyset_B$ was calculated using Equation (4.17)

$$\emptyset_B = \frac{k_{pAB} f_B}{k_{pBA}(1-f_B)+k_{pAB} f_B} \tag{4.17}$$

where k_{pAB} and k_{pBA} were estimated in Table 4.5 and f_B = 0.21 was calculated using the Peng-Robinson equation in Aspen Hysys.

The values for f_B, ϕ_B, k_{pAA}, k_{pAB}, k_{pBA}, and k_{pBB} were substituted in Equation (4.56) to calculate θ. Substituting all these values in Equation (4.59), one gets

$$k_{tHA} + (0.421)k_{tHB} = 201885.1 \tag{4.60}$$

It is possible to estimate the value of k_{tHA} and k_{tHB} by conducting complementary sets of experiments. The slope and intercept terms of Equation (4.55), for which Equation (4.60) is a particular solution, depend on the fraction of 1-hexene in the reactor, f_B. Therefore, by repeating the H_2 experiments above for other values of f_B (and consequently ϕ_B, fraction of 1-hexene in the copolymer), one can generate a family of curves such as the ones shown in Figure 4.18, which was plotted assuming initial guesses for $k_{tAA}, k_{tBA}, k_{tAB}, k_{tBB}, k_{tAlA}, k_{tAlB}, k_{tHA}$, and k_{tHB} for f_B varying from 0.2 to 0.7. It should be possible then to find the values for k_{tHA} and k_{tHB} by multivariate regression.

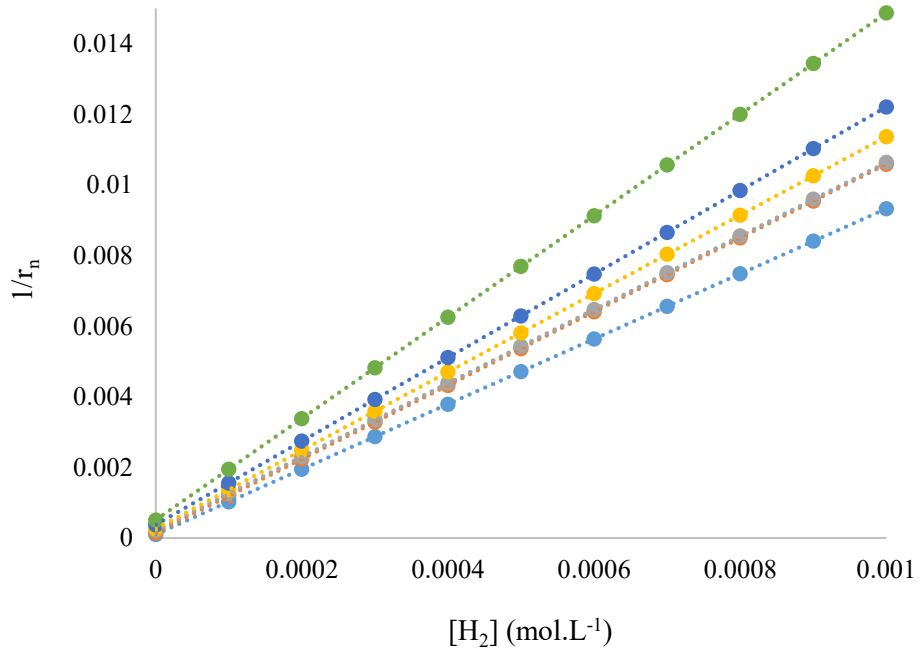

Figure 4.18 Number average chain length as a function of H_2 concentration at different f_B values where k_{tAA} = 0.0001 L.mol^{-1}.s^{-1}, k_{tBA} = 0.0002 L.mol^{-1}.s^{-1}, k_{tAB} = 0.0003 L.mol^{-1}.s^{-1}, k_{tBB} = 0.0004 L.mol^{-1}.s^{-1}, k_{tAlA} = 0.00012 L.mol^{-1}.s^{-1}, k_{tAlB} = 0.00025 L.mol^{-1}.s^{-1}, k_{tHA} = 1.7×10^5 L.mol^{-1}.s^{-1}, k_{tHB} = 8.7×10^4 L.mol^{-1}.s^{-1}.

Since this is a time-consuming step that would require several more experiments, it will be left as a recommendation for future work.

Chapter 5 : Ethylene/1-Hexene Copolymerization with Cp_2ZrCl_2

5.1 Introduction

This chapter investigates the copolymerization of ethylene and 1-hexene with Cp_2ZrCl_2 under varying ethylene/1-hexene ratio, catalyst/cocatalyst ratio, and hydrogen concentration in a semi-batch reactor. A mathematical model was proposed and applied to estimate the polymerization kinetic constants for this system.

5.2 Copolymerization with Cp_2ZrCl_2

5.2.1 Effect of Ethylene/1-Hexene Ratio

Nine copolymerizations were performed under different 1-hexene concentrations to study the effect of 1-hexene concentration on the kinetics of polymerization with Cp_2ZrCl_2. The comonomer concentration was varied from 0 to 1.19 $mol \cdot L^{-1}$ in the reactor, while all other polymerization conditions were kept constant. Three polymerizations were replicated to verify the reproducibility of the polymerizations. Table 5.1 lists the experimental conditions and M_w, M_n, and PDI of copolymers. The 1-hexene concentrations in Table 5.1 were calculated considering the number of moles injected into the reactor at room temperature; they are not the concentrations in the liquid phase when thermodynamic equilibrium is reached at the final polymerization temperature and pressure.

Table 5.1 M_n, M_w, and PDI of ethylene/1-hexene copolymers made with Cp_2ZrCl_2 at different 1-hexene concentrations.

Run	1-hexene (mol.L^{-1})	M_w	M_n	PDI
E/H-0A	0	8700	3200	2.7
E/H-2A	0.15	6400	2800	2.2
E/H-4A	0.3	6000	2600	2.3
E/H-8A	0.59	6000	2800	2.1
E/H-12A	0.89	5400	2400	2.2
E/H-16A	1.19	4400	2200	2.0
E/H-4B	0.3	6100	2600	2.3
E/H-12B	0.89	5500	2400	2.2
E/H-16B	1.19	5300	2200	2.4

P_E = 120 psig, T = 120 ˚C, V_S = 160 mL, [1-H] = 0.15 mol.L^{-1}, H_2 = 3 mmol, [Al]/[Zr] = 57 400.

Figure 5.1 plots ethylene uptake curves as a function of polymerization time. Only selected polymerizations are shown in the plot for the sake of clarity. When comparing Figure 5.1 and Figure 4.1, one notices that the catalyst deactivation profiles differ substantially. For instance, CGC-Ti deactivates faster than Cp_2ZrCl_2. In addition, increasing 1-hexene concentration in the reactor does not affect the ethylene uptake rates as significantly as for CGC-Ti, even though the same trend is observed: as 1-hexene concentration increases, the ethylene uptake rate decreases (lower polymerization rate) since 1-hexene has a lower polymerization rate than ethylene.

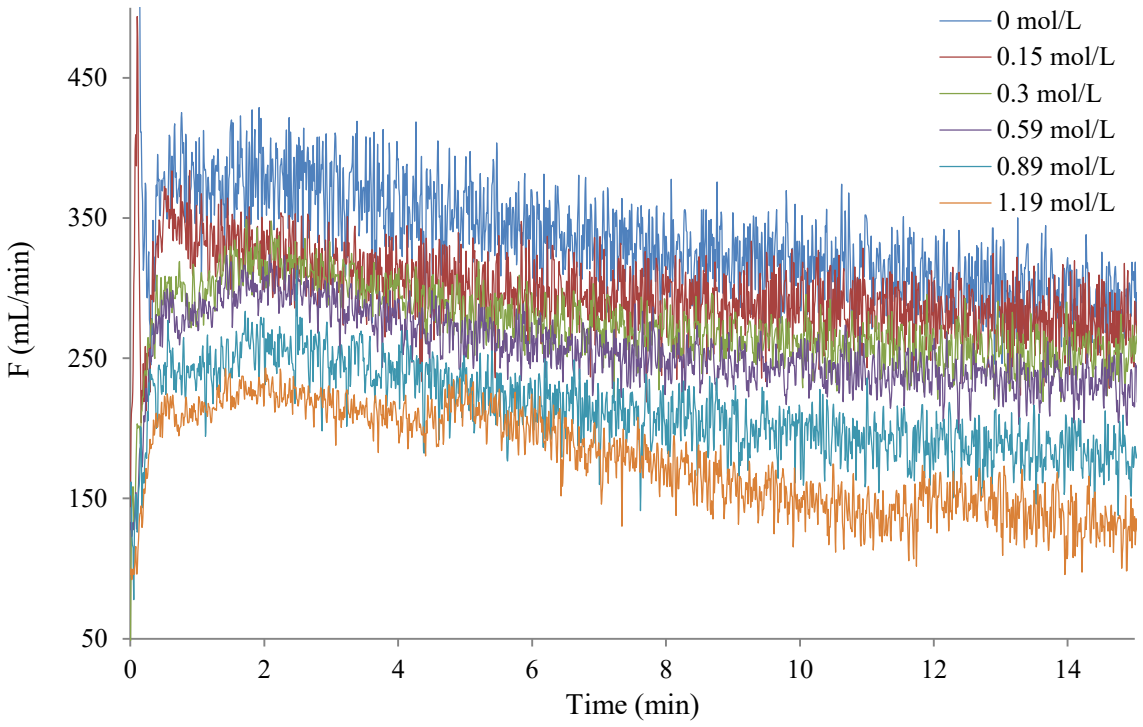

Figure 5.1 Ethylene consumption rates for different 1-hexene concentrations with Cp_2ZrCl_2 . The legends are the concentrations of 1-hexene injected into the reactor.

The proposed mechanism for ethylene/1-hexene copolymerization with Cp_2ZrCl_2/MAO is listed in Table 5.2. Ethylene and 1-hexene propagation and catalyst deactivation are considered to be first order reactions. The terminal model is used to describe the copolymerization. The activation, initiation, and propagation steps are as the same as the mechanism proposed in Table 4.2 for CGC-Ti, but based on the shapes of the ethylene uptake curves (Figure 5.1), we assumed that Cp_2ZrCl_2 deactivated following first order kinetics, see Equations (5.8) to (5.10).

Table 5.2 Copolymerization mechanism with Cp_2ZrCl_2.

Activation	$C + MAO \overset{k_a}{\rightarrow} C^*$	(5.1)
Initiation	$C^* + A \overset{k_{iA}}{\longrightarrow} P_1^A$	(5.2)
	$C^* + B \overset{k_{iB}}{\longrightarrow} P_1^B$	(5.3)
Propagation	$P_i^A + A \overset{k_{pAA}}{\longrightarrow} P_{i+1}^A$	(5.4)
	$P_i^A + B \overset{k_{pAB}}{\longrightarrow} P_{i+1}^B$	(5.5)
	$P_i^B + A \overset{k_{pBA}}{\longrightarrow} P_{i+1}^A$	(5.6)
	$P_i^B + B \overset{k_{pBB}}{\longrightarrow} P_{i+1}^B$	(5.7)
Deactivation	$P_i^A \overset{k_d}{\rightarrow} C_d + D_i$	(5.8)
	$P_i^B \overset{k_d}{\rightarrow} C_d + D_i$	(5.9)
	$C^* \overset{k_d}{\rightarrow} C_d + D_i$	(5.10)

The assumptions made in Chapter 4 for CGC-Ti were repeated for Cp_2ZrCl_2: catalyst deactivation does not depend on the type of monomer at the end of the polymer chain, and catalyst activation is instantaneous.

A similar model has been previously developed in our group.[40] After a few mathematical manipulations (see Appendix A), one can show that

$$\ln(\frac{F}{V_R}) = \ln((k_{pAA}(1-\emptyset_B) + k_{pBA}\emptyset_B)C_0^*[A]) - k_d t \tag{5.11}$$

where the molar fraction of living polymer chains terminated in monomer B is defined as

$$\emptyset_B = \frac{k_{pAB}f_B}{k_{pBA}(1-f_B)+k_{pAB}f_B} \tag{5.12}$$

Equation (5.11) predicts that ln (F/V_R) is a linear function of time, t; this is a simple way to test whether or not the model shown in Table 5.1 fits the experimental polymerization data. By performing linear regression for each polymerization, the slopes of the curves should be equal to $-k_d$ and the intercepts should be equal to $\ln((k_{pAA}(1-\emptyset_B)+k_{pBA}\emptyset_B)C_0^*[A])$. For simplicity, we may define the *apparent* propagation rate constant, $\tilde{k}_p$, as follows

$$\tilde{k}_p = (k_{pAA}(1-\emptyset_B)+k_{pBA}\emptyset_B) \tag{5.13}$$

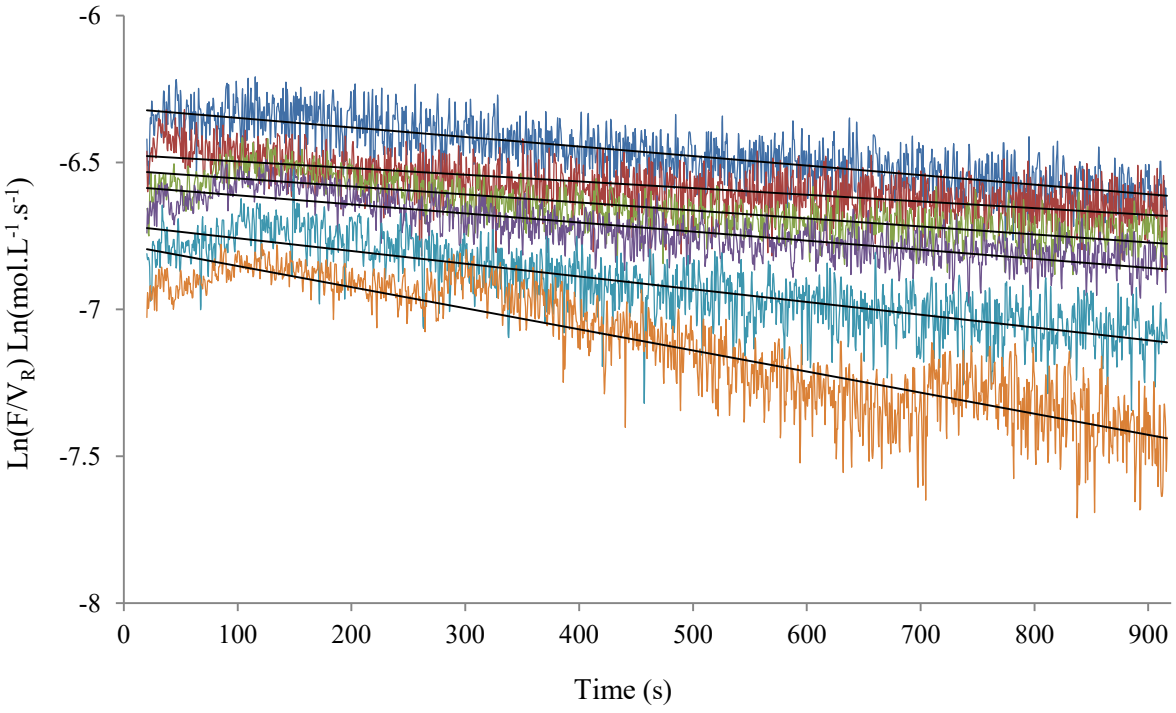

Figure 5.2 Linear regression ethylene/1-hexene copolymerizations with Cp_2ZrCl_2.

The results of the linear regression for $\tilde{k}_p$ and k_d appear in Figure 5.3.

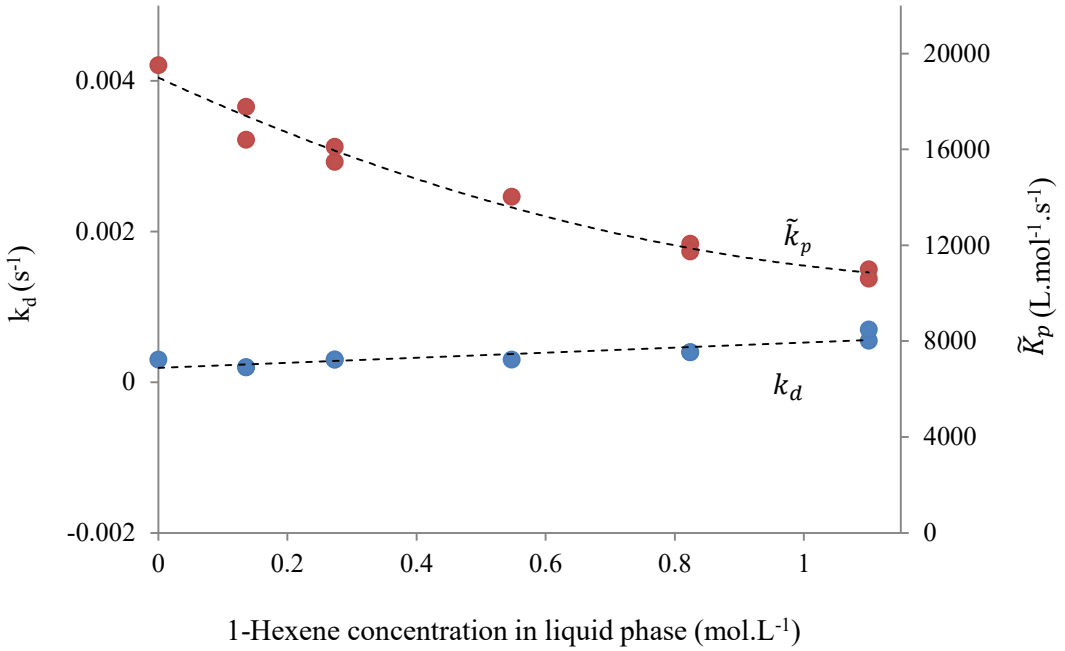

Figure 5.3 Apparent propagation rate constant and deactivation rate constant as a function of 1-hexene concentration.

The deactivation rate constant, k_d, is nearly constant (within experimental error) for all polymerization, confirming that this is a first order step that does not depend on the concentration of 1-hexene.

Since the apparent propagation rate constant depends on the molar fraction of living polymer chains terminated in monomer *B*, $\emptyset_B$ (see Equation (5.13)), it decreases as 1-hexene concentration increases.

To estimate the individual propagation rate constants, we need to substitute Equation (5.12) into Equation (5.13)

$$\tilde{k}_p = \frac{k_{pAA}k_{pBA} + f_B(-k_{pAA}k_{pBA} + k_{pAB}k_{pBA})}{k_{pBA} + f_B(k_{pAB} - k_{pBA})} \qquad (5.14)$$

The molar fraction of 1-hexene in toluene, f_B, was estimated using the Peng-Robinson equation in Aspen Hysys (the values $f_B = 1 - f_A$ are shown in Table 5.4). The three unknown constants in

Equation (5.14), k_{pAA}, k_{pBA}, and k_{pAB}, were estimated using the PSO method explained in Chapter 4.

Figure 5.4 shows how the apparent propagation rate constant varies as a function of 1-hexene molar fraction in the reactor with the nonlinear regression fit of Equation (5.14). A good fit is observed in this case.

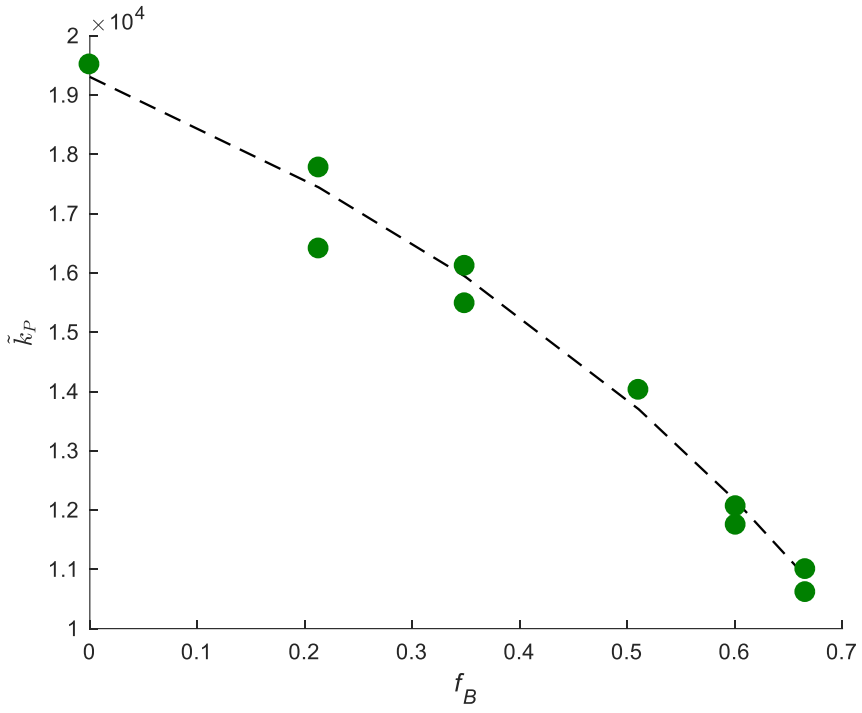

Figure 5.4 Apparent propagation rate constant versus 1-hexene molar fraction in liquid phase. The dotted line is results of the fitted Equation (5.14).

The parameter estimates obtained from the optimization are summarized in Table 5.3. To find the fourth constant, k_{pBB}, we must estimate the reactivity ratios, as shown in the following section.

Table 5.3 Propagation rate constants for ethylene/1-hexene copolymerization with Cp_2ZrCl_2.

Parameter	Estimated value
k_{pAA} (L.mol^{-1}.s^{-1})	1.9×10^4
k_{pAB} (L.mol^{-1}.s^{-1})	9.4×10^2
k_{pBA} (L.mol^{-1}.s^{-1})	2.0×10^3
SSE: 8.04×10^2	

5.2.1.1 Reactivity Ratio Estimation

The reactivity ratios were calculated following the same procedure adopted in Chapter 4, Section 4.2.1.1. The Mayo-Lewis equation, as expressed in Equation (5.15), relates the ethylene mole fraction in the copolymer to the ethylene mole fraction in the reactor.

$$F_A = \frac{r_A f_A^2 + f_A(1-f_A)}{r_A f_A^2 + 2 f_A(1-f_A) + r_B(1-f_A)^2} \tag{5.15}$$

The fraction of 1-hexene in the copolymers made with Cp_2ZrCl_2 (F_B) was determined by differential scanning calorimetry (DSC). This procedure is different from the one we adopted to measure the 1-hexene content of ethylene/1-hexene copolymers made with CGC-Ti because the molecular weight of the copolymers made with Cp_2ZrCl_2 were relatively low. In this case, when using GPC-IR the chain-end effect may makes the measurement of SCBs inaccurate because of the CH_3 groups in the chain ends.

Instead, we calibrated our DSC with five ethylene/1-hexene copolymers with known 1-hexene fractions (previously characterized with ^{13}C-NMR), and related melting temperatures to 1-hexene fractions in the copolymers. Figure 5.5 shows this calibration curve.

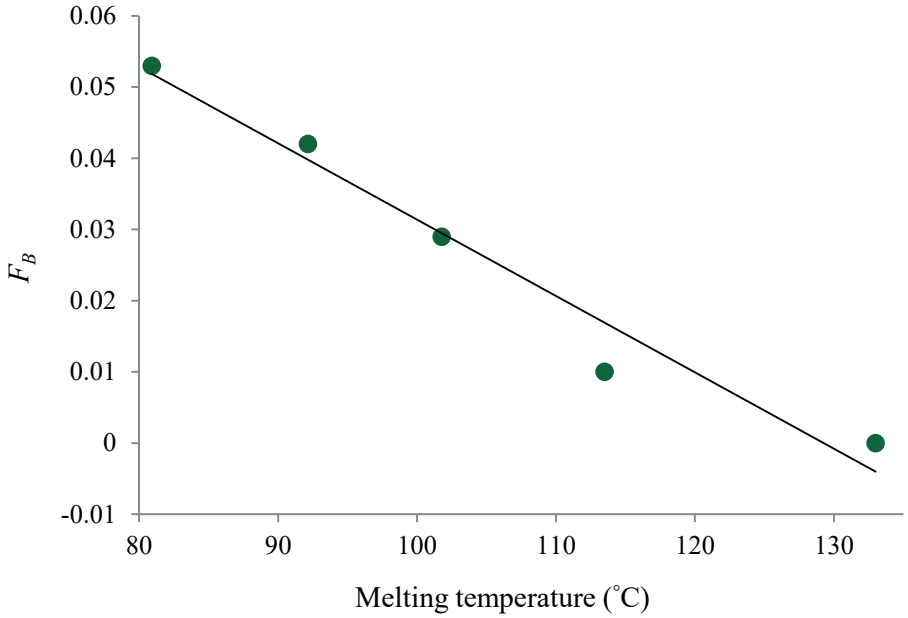

Figure 5.5 DSC calibration curve for ethylene/1-hexene copolymers.

The calibration curve from Figure 5.5 is given by the expression

$$F_B = -0.0011T_m + 0.1387 \tag{5.16}$$

The 1-hexene fraction in the copolymers was calculated using Equation (5.16). Table 5.4 summarizes the melting temperatures and the compositions of the copolymers and reactor feed. The ethylene molar fraction in the liquid phase, f_A, was estimated using the Peng-Robinson equation in Aspen Hysys.

Table 5.4 Composition of ethylene/1-hexene copolymers made with Cp_2ZrCl_2.

Run	T_m (°C)	f_A	F_B	F_A
E/H-0A	126.1	1	0	1
E/H-2A	123.8	0.786901	0.0025	0.9975
E/H-4A	121.6	0.65107	0.0049	0.9951
E/H-8A	117.6	0.489411	0.0093	0.9907
E/H-12A	113.5	0.3990	0.0137	0.9863
E/H-16A	110	0.334216	0.0177	0.9823
E/H-4B	121.5	0.65107	0.005	0.9950
E/H-12B	113.8	0.3990	0.0135	0.9865
E/H-16B	109.7	0.334216	0.018	0.982

Figure 5.6 plots the ethylene mole fraction in the copolymer as a function of ethylene molar fraction in the liquid phase. The experimental data were fitted using the Mayo-Lewis equation. The reactivity ratios were estimated in MATLAB using the Levenberg-Marquardt algorithm and least square analysis.

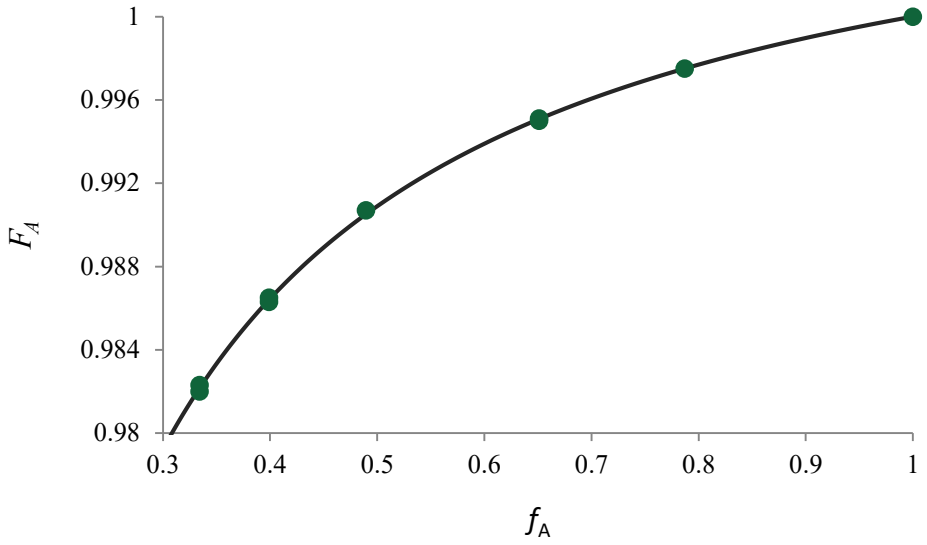

Figure 5.6 Mole fraction of ethylene in ethylene/1-hexene copolymers made with Cp_2ZrCl_2. The continuous line is the fitted Mayo-Lewis equation.

Table 5.5 lists the estimated values for the reactivity ratios obtained from curve fitting.

Table 5.5 Reactivity ratios for ethylene/1-hexene copolymerization with Cp_2ZrCl_2.

Parameter	Value	95% confidence
r_A	1.1×10^{2}	1.0×10^{2}, 1.1×10^{2}
r_B	5.6×10^{-3}	-1.6×10^{-2}, 2.7×10^{-2}
$SSE: 1.038 \times 10^{-7}$, $R^2 = 0.9997$		

The confidence interval for r_B includes zero, which calls into question the validity of this estimate. Values for r_B are notoriously hard to estimate because they tend to be relatively small, since 1-hexene in not very reactive, and the likelihood of a 1-hexene molecule adding to a chain terminated in 1-hexene (quantified by k_{pBB} in the proposed model) is quite small for most metallocenes. To obtain a narrower confidence interval, we would need to perform polymerizations with higher 1-hexene concentrations in the reactor, so that copolymers with higher F_B were produced (note that the highest F_B in Table 5.4 is F_B = 1- F_A = 1 – 0.982 =

0.018). This simply indicates that Cp_2ZrCl_2 is not a good 1-hexene incorporator, making the estimation of r_B and k_{pBB} hard to achieve. For practical purposes, we may set these values to zero. In comparison, CGC-Ti is a much better 1-hexene incorporator, reaching a maximum molar fraction of 1-hexene in the copolymer of F_B = 0.159 (see Table 4.3), which allowed us to estimate r_B adequately for that catalyst.

Thus, k_{pBB} is estimated using the reactivity ratio based on the following equation

$$k_{pBB} = r_B \times k_{pBA} \cong 0 \tag{5.17}$$

5.2.2 Effect of Cocatalyst Concentration

In this set of experiments, all variables were kept constant except the MAO concentration to investigate the effect of [Al]/[Zr] ratio on the copolymerizations. Six copolymerizations were performed at [Al]/[Zr] ratio varying from 115000 to 14000.

Figure 5.7 shows the ethylene uptake rates at different [Al]/[Zr] ratios. The results show that ethylene consumption rates are the same over the investigated range of MAO concentrations.

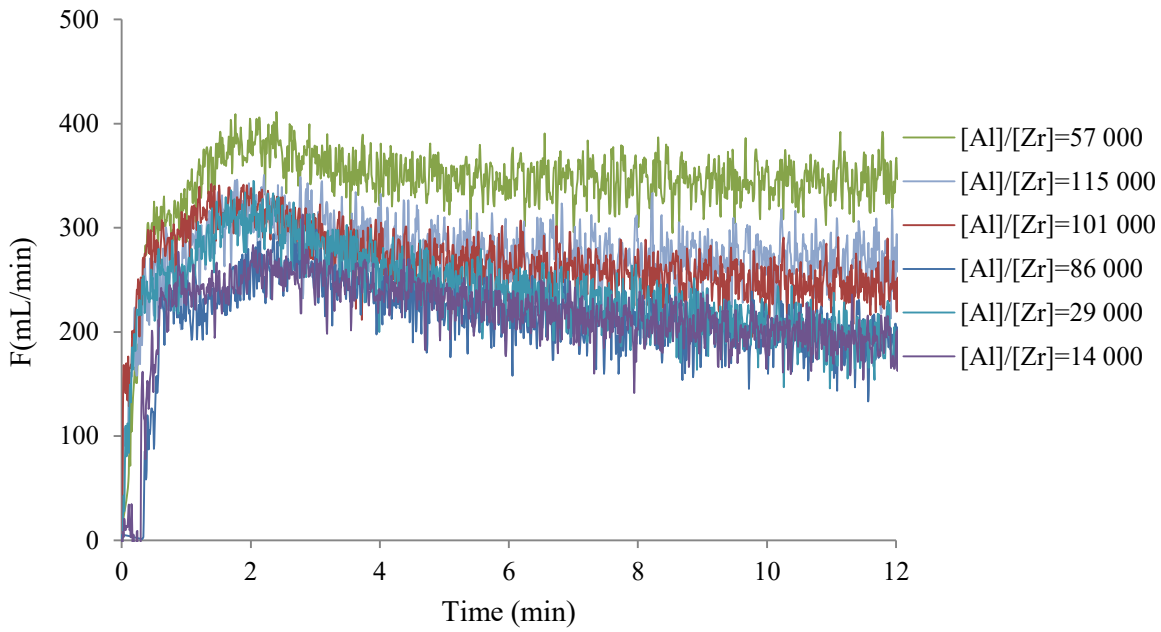

Figure 5.7 Ethylene consumption rates at different [Al]/[Zr] ratios.

Table 5.6 summarizes the polymerization conditions as well as the M_n, M_w, and PDI of the samples for these runs.

Table 5.6 Copolymerization details at different [Al]/[Zr] ratio with Cp_2ZrCl_2 catalyst.

Run	[Al]/[Zr]	M_w	M_n	PDI
C/C-1	115000	11500	5000	2.4
C/C-2	101000	11800	5000	2.4
C/C-3	86000	13000	5000	2.4
C/C-4	57000	14800	6000	2.5
C/C-5	29000	11300	5000	2.3
C/C-6	14000	12000	5000	2.3

P_E = 120 psig, T = 120 °C, V_S = 160 mL, [1-H] = 0.15 mol.L^{-1}, H_2 = 0.8 mmol.

Figure 5.8 plots M_n, M_w, and PDI as a function of [Al]/[Zr] ratio. The results show that these variables do not depend on MAO over this range of concentrations.

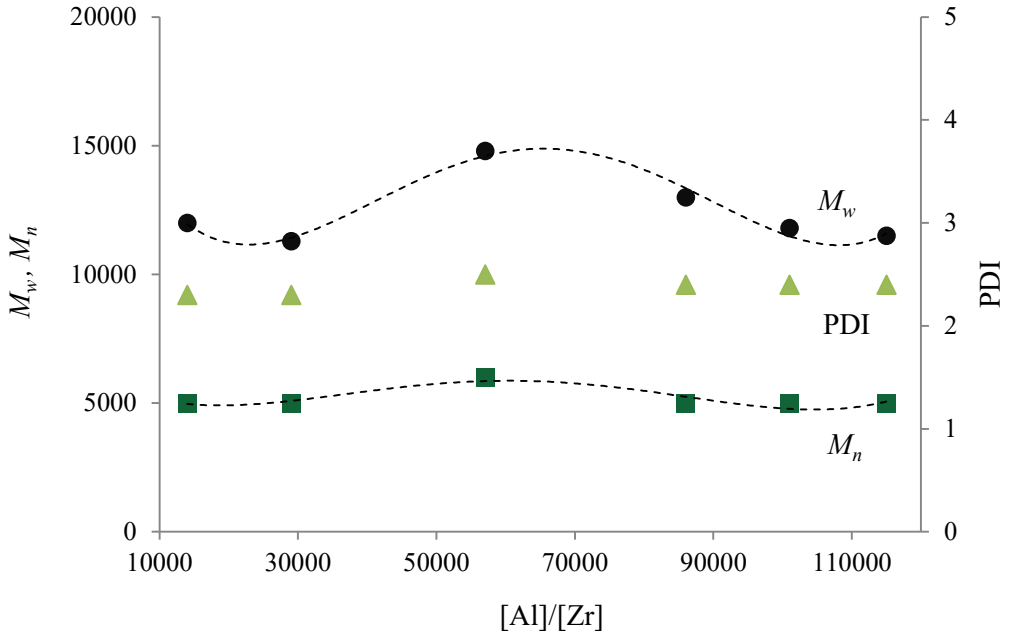

Figure 5.8 M_n, M_w, and PDI of copolymers made at different [Al]/[Zr] ratio.

5.2.3 Effect of Catalyst Concentration

The effect of varying catalyst concentration when the MAO concentration was fixed at 0.01 mol.L^{-1} was investigated to measure its influence on M_n, M_w, PDI, polymer yield, and polymerization rate. Table 5.7 summarizes the polymerization conditions, polymerization yield, M_n, M_w, and PDI.

Table 5.7 Copolymerization details at different concentration of Cp_2ZrCl_2.

Run	catalyst (µmol.L^{-1})	M_w	M_n	PDI	polymer yield (g)
C-1	0.06	14000	5600	2.5	2.5
C-2	0.12	14000	5400	2.6	4.07
C-3	0.19	15000	6000	2.5	7.76
C-4	0.25	14000	5600	2.5	10.4
C-5	0.31	14000	5800	2.4	13.67

P_E = 120 psig, T = 120 °C, V_S = 160 mL, [1-H] = 0.15 mol.L^{-1}, H_2 = 0.8 mmol.

Figure 5.9 plots the ethylene consumption rate at three different Cp_2ZrCl_2 concentrations, showing that the polymerization rate depends linearly on catalyst concentration.

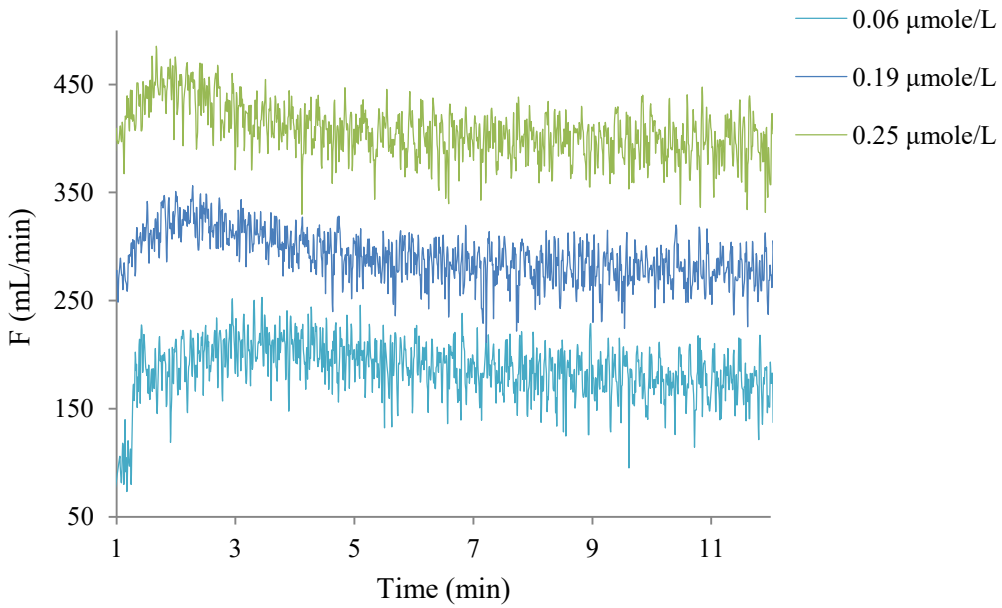

Figure 5.9 Ethylene uptake rates at different Cp_2ZrCl_2 concentrations.

Figure 5.10 shows that catalyst concentration does not influence M_n, M_w, and PDI significantly under the investigated conditions.

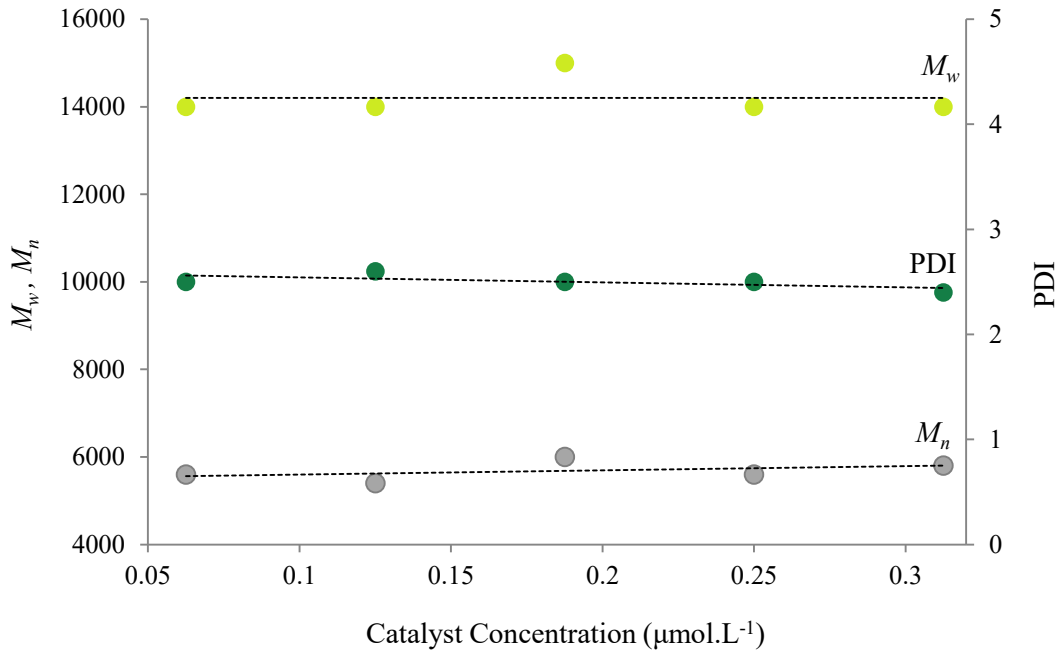

Figure 5.10 M_n, M_w, and PDI of copolymers made at different Cp_2ZrCl_2 concentrations.

Figure 5.11 shows that there is a linear relationship between the yield of polymer and catalyst concentration. Increasing the catalyst concentration would enhance the production yield proportionally, which confirms our model assumption that this system follows first order kinetics with respect to catalyst concentration.

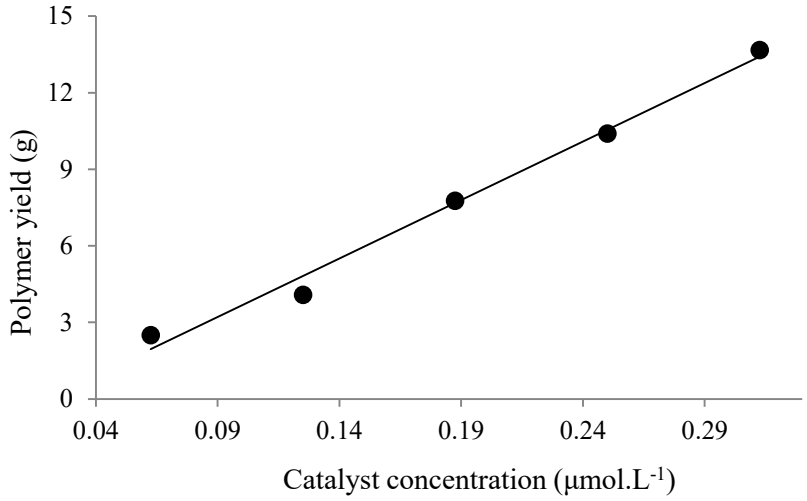

Figure 5.11 Polymer yield as a function of Cp_2ZrCl_2 concentration.

5.2.4 Effect of Ethylene/Hydrogen Ratio

Six copolymerizations at different H_2 concentrations were performed to examine its influence on the copolymerization of ethylene/1-hexene.

Table 5.8 shows the polymerization conditions and the GPC-IR results of M_w, M_n, and PDI. The H_2 concentrations in toluene at the polymerization conditions were estimated using the Peng-Robinson equation available in Aspen Hysys.

Table 5.8 Hydrogen concentrations and M_n, M_w, and PDI of copolymers made with Cp_2ZrCl_2.

Run	[H_2] (mmol.L^{-1})	M_w	M_n	PDI
H-0	0	65 000	30 200	2.1
H-1	0.17	14 000	5500	2.5
H-2	0.37	8600	3500	2.5
H-3	0.64	7700	2700	2.8
H-4	1.3	2700	1100	2.4
H-5	1.9	2400	1000	2.4

P_E = 120 psig, T = 120 °C, V_S = 160 mL, [1-H] = 0.15 mol.L^{-1}, [Al]/[Zr] = 57 400.

Figure 5.12 compares ethylene uptake curves at different H_2 concentrations. As for CGC-Ti (see Chapter 4), H_2 decreases the rate of polymerization. Interestingly, H_2 drops the overall polymerization rate, but at the same time decreases the catalyst deactivation rate.

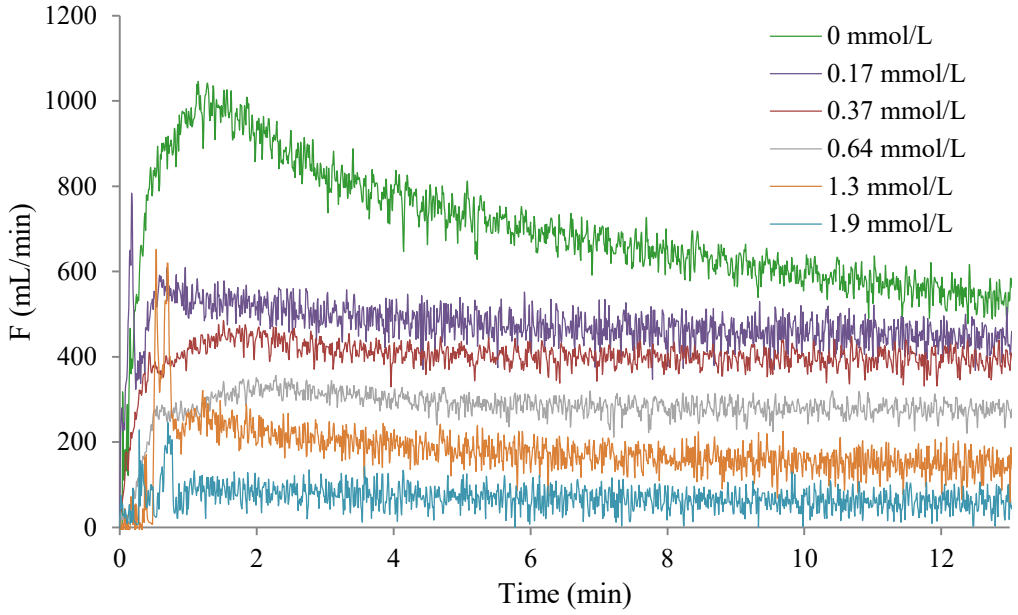

Figure 5.12 Ethylene polymerization rate at different H_2 concentration with Cp_2ZrCl_2. The legends are the concentration of H_2 in the liquid phase.

Figure 5.13 shows that the molecular weight of the copolymers decrease with increasing H_2 concentration. Similarly, to what we observed with CGC-Ti, even a small amount of H_2 will drop the polymer molecular weight substantially.

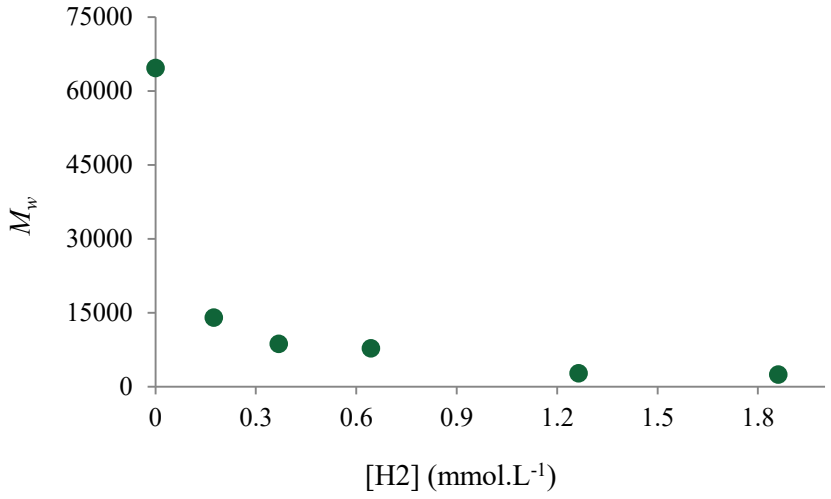

Figure 5.13 Molecular weight of copolymers made with Cp_2ZrCl_2 as a function of H_2 concentration in toluene.

5.2.4.1 Estimation of Chain Transfer Rate Constants

The procedure for estimating the value of the chain transfer rate constant to H_2 was described in Chapter 4, Section 4.2.4.2. Based on Equation (5.18), the reciprocal of number average chain length should have a linear relationship with H_2 concentration.

$$\frac{1}{r_n} = \frac{[H_2](K_{tHA}\phi_A + K_{tHB}\phi_B)}{\theta[M]} + \frac{\alpha}{\theta[M]} \tag{5.18}$$

Therefore, the plot $\frac{1}{r_n}$ versus $[H_2]$ should be linear, and its slope and intercept can be used to estimate the chain transfer to H_2 rate constant (Figure 5.14).

As per the discussion in Chapter 4, r_n is estimated using equations below.

$$r_n = \frac{M_n}{mw} \tag{5.19}$$

$$mw = F_B mw_B + (1 - F_B) mw_A \tag{5.20}$$

Considering the concentration of injected 1-hexene in this set of experiments (0.15 mol.L^{-1}), F_B equals 0.0025 (see Table 5.4). The value of mw can be calculated as the same procedure in Chapter 4.

The values of reciprocal of r_n at different H_2 concentrations are reported in Table 5.9.

Table 5.9 Reciprocal of r_n values at different [H_2] concentrations in copolymerization with Cp_2ZrCl_2.

Run	H_2 (mol.L^{-1})	$\frac{1}{r_n}$
H-0	0	0.00093
H-1	0.00017	0.0051
H-2	0.00037	0.0081
H-3	0.00064	0.01
H-4	0.0013	0.025
H-5	0.0019	0.027

Figure 5.14 plots the $1/r_n$ as a function of [H_2]. The values of slope and intercept are estimated by performing linear regression and reported in Table 5.10.

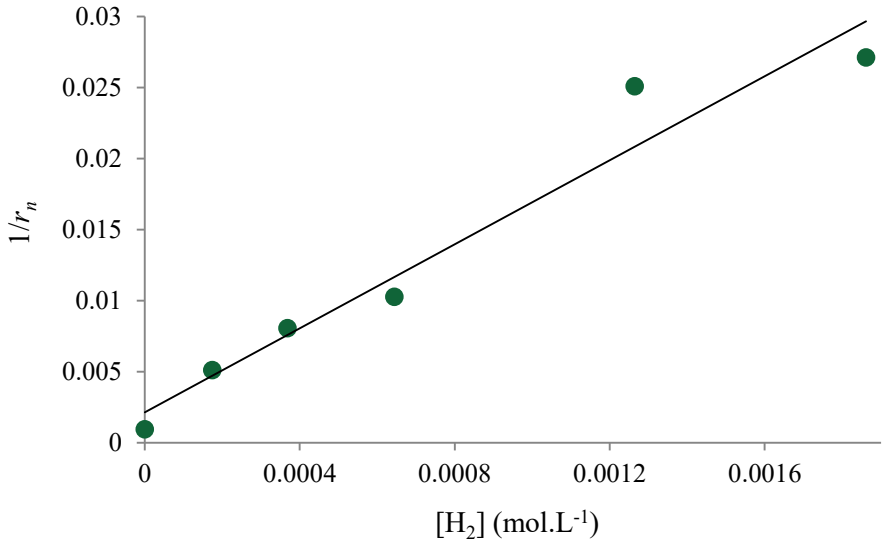

Figure 5.14 Reciprocal of r_n versus H_2 concentration for copolymerizations with Cp_2ZrCl_2.

Table 5.10 summarizes the result of this linear regression.

Table 5.10 Estimated values using linear regression.

Parameter	Estimated value	Standard error
$\frac{(k_{tHA}\phi_A + k_{tHB}\phi_B)}{\theta[M]}$	14.786	1.67
$\frac{\alpha}{\theta[M]}$	0.0021	0.0016
SSE: 2.83×10^{-5}		

The values of $\emptyset_A, \emptyset_A$, θ, and [M], where f_B equals 0.21, were calculated similarly to the procedure in Chapter 4 (see Section 4.2.4.2). By substituting all the constant parameters into the slope term, the summation of H_2 chain transfer rate constants is estimated.

$$k_{tHA} + 0.196k_{tHB} = 83778.57 \tag{5.21}$$

One can estimate the k_{tHA} and k_{tHB} individually using the method proposed in Section 4.2.4.2. Several sets of experiments at different f_B values should be performed to obtain different versions of Equation (5.21) to perform multivariate regression.

Chapter 6 : Polymerization with Cp_2ZrCl_2/CGC-Ti

6.1 Introduction

Metallocenes make polyolefins with narrow MWD and SCBD because they are single-site catalysts. Polyolefins with narrow MWD have better mechanical properties, but are harder to process than polymers with broader MWD, such as those made with Ziegler-Natta catalysts. For many applications, broader MWD and/or SCBD may be desirable. Producing polymers with tailored microstructures and enhanced properties is possible if we use two metallocenes in the same reactor. Catalysts having different reactivity ratios, chain transfer and propagation rates can then be used to make polyolefins with controlled MWD and SCBD.

In Chapter 4 and Chapter 5, we showed that CGC-Ti and Cp_2ZrCl_2 had different deactivation profiles and responded differently to changes in 1-hexene, H_2, and MAO concentrations. For instance, CGC-Ti had a higher reactivity ratio towards 1-hexene incorporation and made copolymers with higher molecular weights than Cp_2ZrCl_2.

Some industrial applications of polyolefins require properties that can only be met by using series of reactors or combining two or more metallocenes in a single reactor. For instance, to make pipes with high environmental stress crack resistance,[57] the SCB frequency must be higher for chains with higher molecular weights than for chains with lower molecular weights.[47] It is impossible to make this product with Ziegler-Natta catalysts because they make polyolefins in which the SCB frequency decreases with increasing molecular weight. For metallocenes, on the other hand, the SCB frequency is uniform and independent of polymer molecular weight.

Therefore, by taking into account the polymerization kinetics of each metallocene, it is possible to mix two catalysts so that the one that produces polymer with higher molecular weight also has a higher reactivity ratio towards comonomer incorporation. Bimodal MWDs are of the interest for many industrial applications. Bimodality broadens the MWD, which is responsible for improved processability and good mechanical properties.[58] However, not all of the combinations of metallocene catalysts lead to producing polyolefins with bimodal MWD.

In previous studies, the criterion for producing polyolefin with bimodal MWD using two single-site catalysts has been reported[58]

$$\rho_w = \frac{(M_{w1} - M_{w2})^2}{2M_{w1}M_{w2}} \quad (6.1)$$

To get a bimodal MWD, ρ_w must be equal or greater than one. However, if the molecular weight of the polymers produced with individual catalyst does not meet the criterion, the MWD of polymers with combined catalyst will be broader than for the individual catalysts, but not bimodal.

In Chapter 4 and Chapter 5 we investigated the ethylene/1-hexene copolymerization kinetics with CGC-Ti and Cp_2ZrCl_2. In the present chapter, we will test the following hypotheses:

1. Can the polymerization kinetics of the binary catalyst (CGC-Ti/Cp_2ZrCl_2) be described as a linear combination of the kinetics for Cp_2ZrCl_2 and CGC-Ti alone?
2. Can the microstructure of the polymer made with the binary catalyst be predicted as a superposition of the microstructures of the polymer made with each catalyst separately?

Fundamentally, we want to find out whether or not each active site type in the binary catalyst behave in the same way they behaved when alone in the reactor. If the answer is yes, then it becomes much easier to design products and polymerization conditions of binary catalysts from the individual behaviour of each catalyst in the mixture.

6.2 Copolymerization with Combined Cp_2ZrCl_2/CGC-Ti

6.2.1 Polymerization Rate

Ethylene/1-hexene copolymerizations with single and binary catalysts were carried out in the semi-batch solution reactor under same conditions, while keeping the cocatalyst/catalyst ratio constant. The kinetics of polymerization with binary catalysts was investigated to verify whether the individual catalysts behaved independently or interfered with each other's behaviour.

Table 6.1 lists copolymerization conditions with individual and binary metallocene catalysts. For the binary system, the overall catalyst concentration was kept the same as for the individual catalysts (0.25 μmol.L^{-1}).

While keeping the overall catalyst concentration constant, different catalysts ratios were tested for the binary system. The CGC-Ti mole fraction ($\frac{CGC-Ti}{CGC-Ti+Cp_2ZrCl_2}$) was varied from 0 to 1.

Table 6.1 Copolymerization condition for combined and individual CGC-Ti/Cp_2ZrCl_2 catalysts.

Catalysts (μmol.L^{-1})	0.25
1-Hexene (mol.L^{-1})	0.668
MAO (mol.L^{-1})	0.011
Ethylene Pressure (psig)	120
Temperature (˚C)	120
Solvent (mL)	160

Figure 6.1 shows ethylene consumption rates for the copolymerization of ethylene/1-hexene with CGC-Ti and Cp_2ZrCl_2 alone. This figure clearly illustrates the different deactivation profiles of these catalysts.

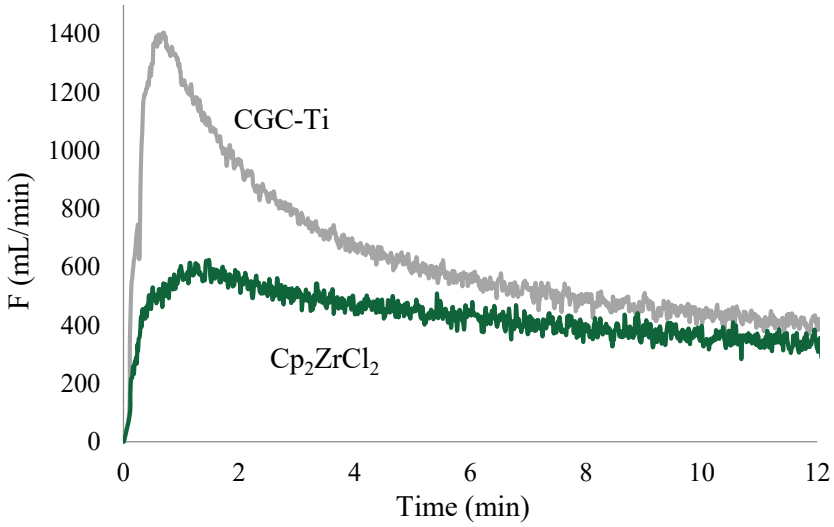

Figure 6.1 Ethylene consumption rates for ethylene/1-hexene copolymerizations with CGC-Ti and Cp_2ZrCl_2 catalysts.

To test the main hypothesis in this chapter, we performed 3 copolymerizations with binary CGC-Ti/Cp_2ZrCl_2 containing CGC-Ti mole fractions of 0.25, 0.5, and 0.75. Since all the copolymerization conditions were the same used for the individual catalysts in Figure 6.1, the rates of polymerization with the binary catalysts should fall between the rates for the individual catalysts, and be expressed as their linear combination. Therefore, for the combined catalyst, one may write

$$\overline{R_p} = x_{Ti}R_{p,Ti} + (1 - x_{Ti})R_{p,Zr} \tag{6.2}$$

where is $\overline{R_p}$ is the polymerization rate (ethylene uptake rate) of the binary catalyst, $R_{p,Ti}$ and $R_{p,Zr}$ are the rates of polymerization with only CGC-Ti and Cp_2ZrCl_2, respectively, and x_{Ti} is the molar fraction of CGC-Ti in the binary catalyst.

Figure 6.2 shows that the curves predicted with Equation (6.2) agree relatively well with the ethylene uptake rates for the three tested binary catalyst systems, with the exception of very short polymerization times, where the model tends to overpredict the rate of ethylene uptake.

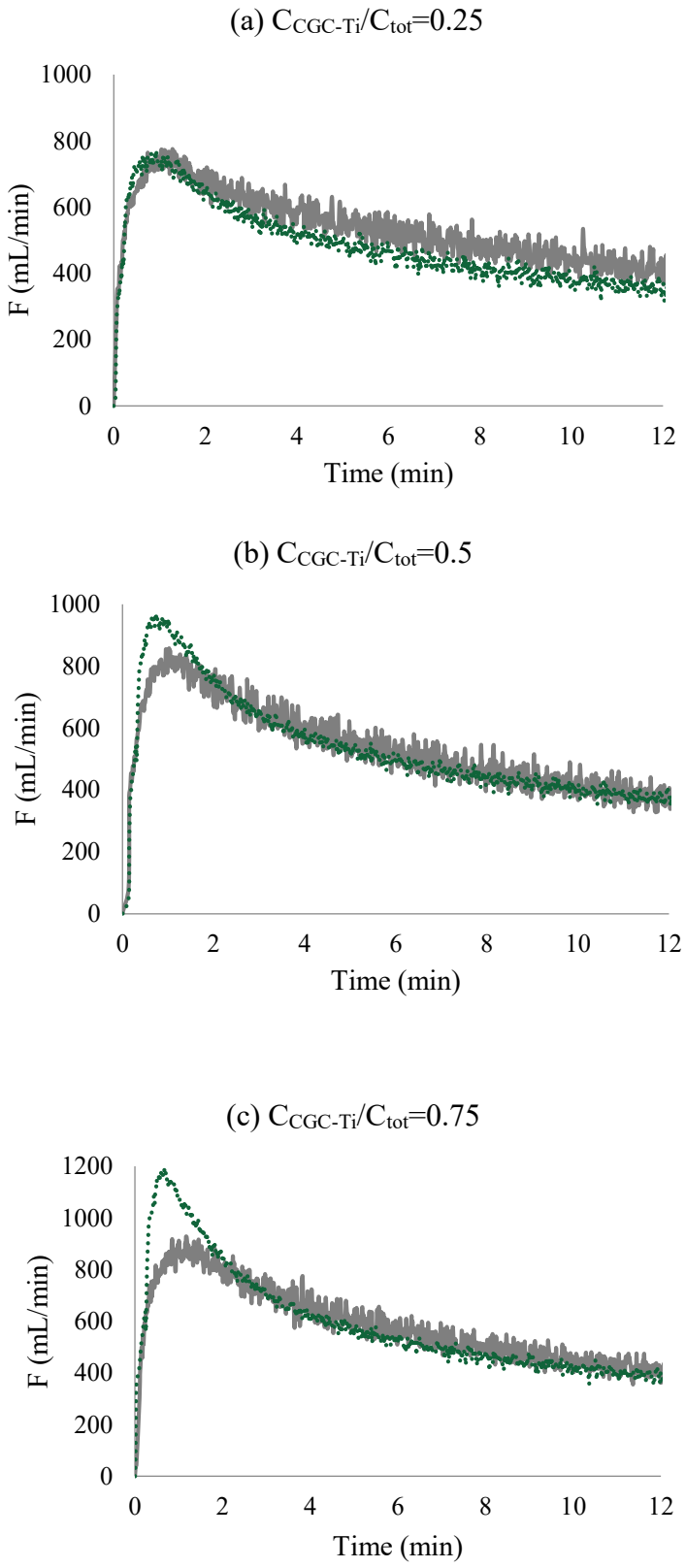

Figure 6.2 Ethylene uptake curve predictions for binary systems with different CGC-Ti/Cp_2ZrCl_2 ratios. Grey curves are for the binary catalyst, and green curves are model predictions using Equation (6.2).

For easier comparison, the ethylene uptake curves of all 5 ratios are plotted in a single graph in Figure 6.3. The ethylene uptake curves for the binary catalysts fall between the ethylene uptake curves of the individual catalysts, as expected if the metallocenes behave independently of each other.

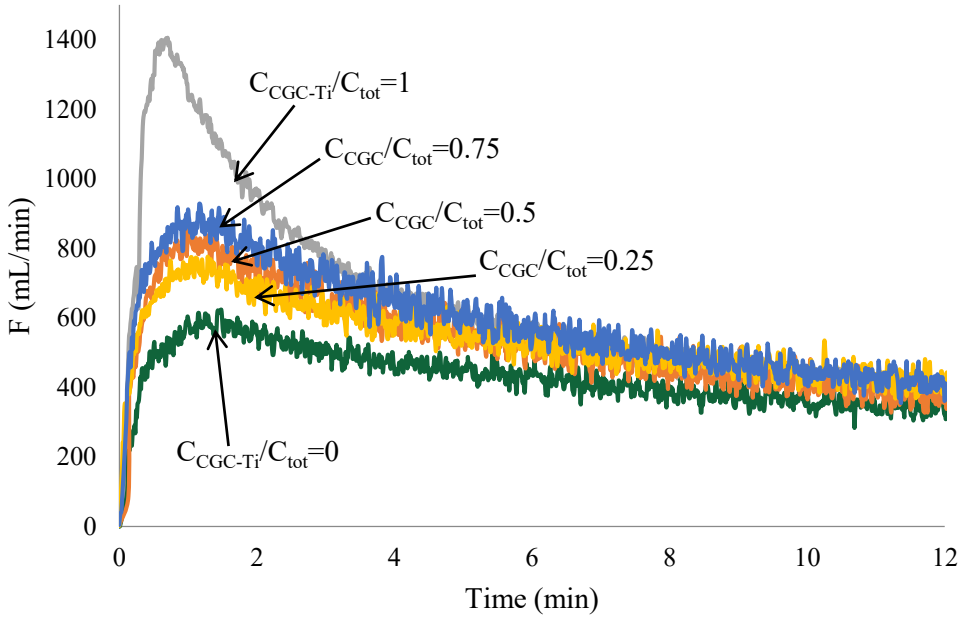

Figure 6.3 Ethylene consumption rates of binary and individual catalysts.

6.2.2 Polymer Molecular Weight Distribution

The samples made in the experiments described in Section 6.2.1 were characterized by GPC-IR to obtain their MWD and SCBD. Table 6.2 summarizes their M_n, M_w, and PDI. Sample M1, made only with CGC-Ti, has the highest molecular weight, while Cp_2ZrCl_2 produced a copolymer with lowest molecular weight. By combining the two single-site catalysts, the PDI of the copolymers increased in comparison with Samples M1 and M2, as expected.

The observed trend for the M_n and M_w, in binary systems is reasonable. Among the three binary samples, the one that was made with the highest concentration of CGC-Ti catalyst has the highest molecular weight and broadest distribution.

Table 6.2 M_n, M_w, and PDI for copolymers made with different combinations of CGC-Ti and Cp_2ZrCl_2.

Run	$C_{CGC\text{-}Ti}/C_{tot}$	M_w	M_n	PDI
M1	1	79000	25000	3.1
M2	0	44000	15800	2.8
M3	0.25	54000	17000	3.1
M4	0.5	61000	18200	3.3
M5	0.75	75000	21000	3.6

Figure 6.4 shows the MWD of sample M1 and M2 made with CGC-Ti and Cp_2ZrCl_2, respectively. The MWD of the sample made with CGC-Ti is broader than the one made with Cp_2ZrCl_2.

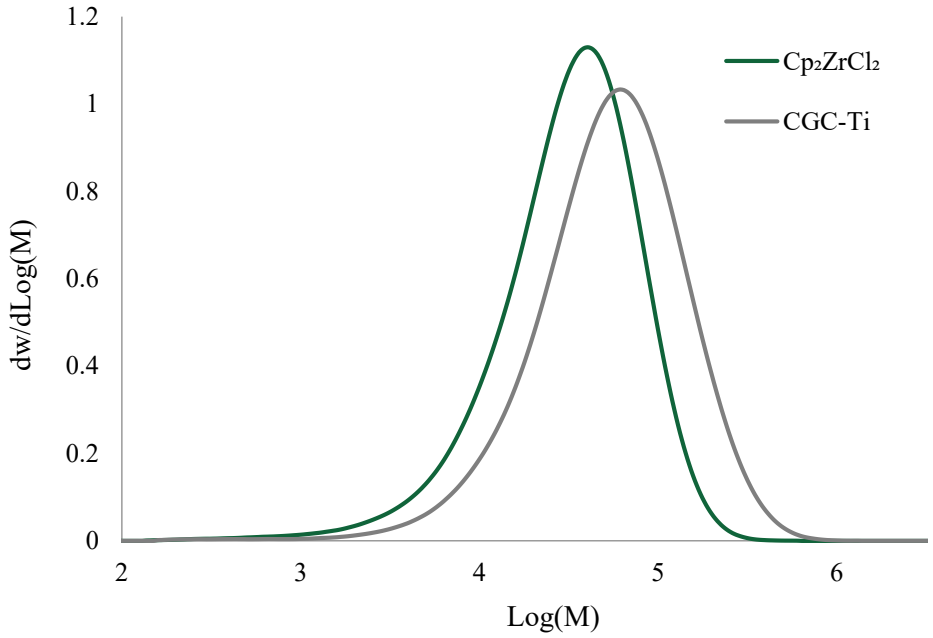

Figure 6.4 MWD of samples made with Cp_2ZrCl_2 and CGC-Ti alone.

Substituting the molecular weights of sample M1 and M2 into Equation (6.1) predicts that the MWD of polymer made with the binary catalyst would not become bimodal, since $\rho_w = 0.17 < 1.0$. The MWD of copolymers made with the 3 binary catalysts may be predicted using the MWD of polymer made on each single catalyst, assuming that these catalysts do not interact in the binary mixture. The MWD of a polymer made with two single-site catalysts can be expressed as weighted summation of two distributions.[58]

$$\overline{MW} = m_{Ti} MW_{Ti} + (1 - m_{Ti}) MW_{Zr} \tag{6.3}$$

where m_{Ti} is the mass fraction of polymer made on CGC-Ti.

Figure 6.5 compares the predicted MWD of binary samples with experimental data acquired from GPC-IR. The green dashed curves are the predicted MWD and the MWD of each catalyst are shown in blue curves.

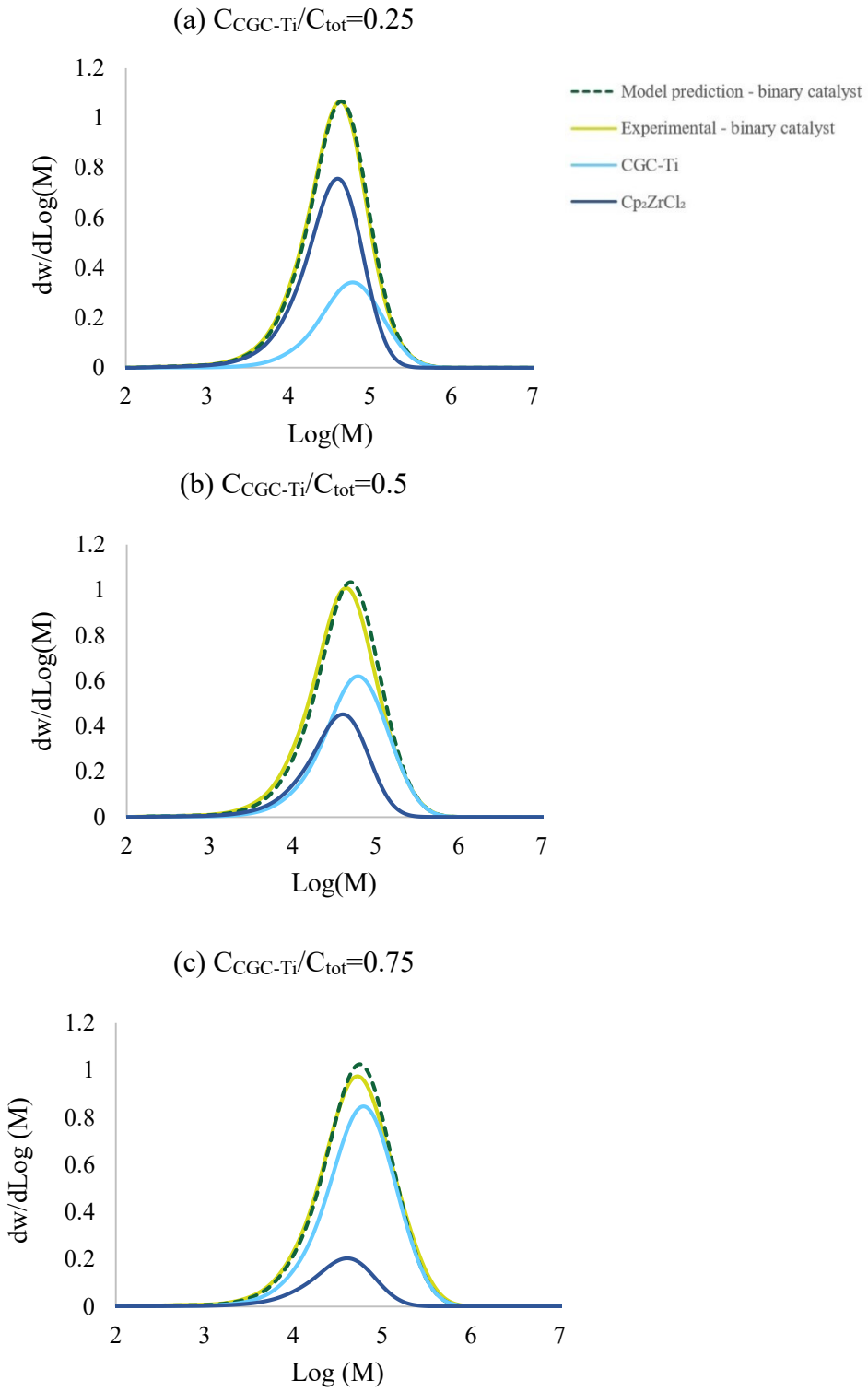

Figure 6.5 Predicted MWD in comparison with GPC-IR results. Yellow curves are for the binary catalyst, green curves are model predictions using Equation (6.3), and blue curves are the MWD of each catalyst.

The MWD prediction for polymers made with the binary catalysts agrees remarkably well with the experimental results, indicating that the catalysts do not interfere with each other when combined in the binary catalyst system.

Figure 6.6 compares the MWD of all three binary samples. The MWD of the sample made at CGC-Ti mole fraction of 0.75 is slightly broader than the other two samples.

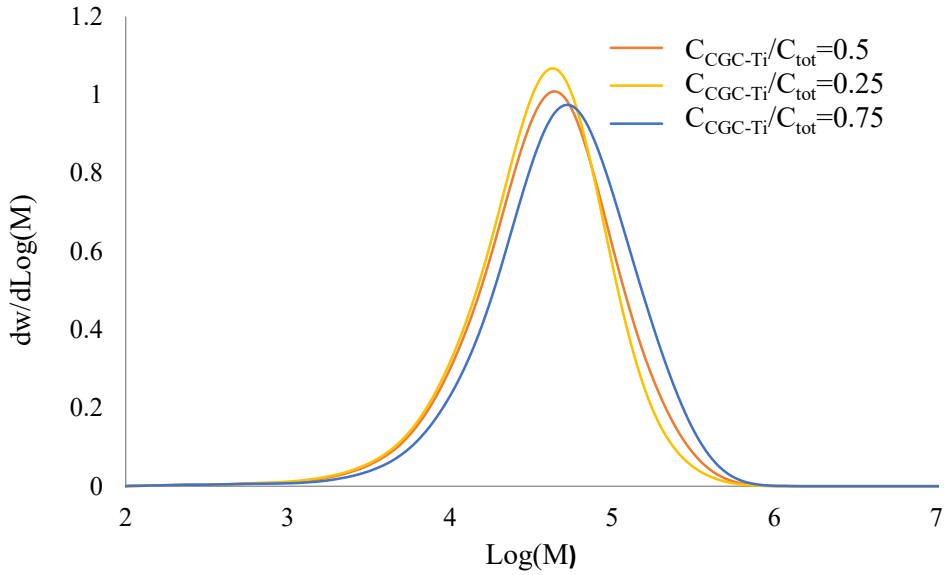

Figure 6.6 MWD of samples made with combined catalyst systems.

6.2.3 Short Chain Branch Distribution

Assuming that the metallocenes do not interact in the binary mixture, the overall SCBD may be expressed as the linear combination of the SCBDs of the copolymers made with each catalyst. Equation (6.4) describes the weighted summation of the two SCBDs

$$\overline{SCB_{MW}} = f_{Ti,MW} SCB_{Ti} + (1 - f_{Ti,MW}) SCB_{Zr} \tag{6.4}$$

where $f_{Ti,MW}$ is the total weight fraction of polymer with molecular weight MW made with the CGC-Ti in the binary system

$$f_{Ti,MW} = \frac{m_{Ti} \times w_{Ti,MW}}{m_{Ti} \times w_{Ti,MW} + m_{Zr} w_{Zr,MW}}$$

and $w_{Ti,MW}$ is the weight fraction of polymer made with CGC-Ti at a given molecular weight MW and m_{Ti} is the mass fraction of polymer made with CGC-Ti in the binary system.

Figure 6.7 compares model predictions and experimental results of SCBD across the molecular weight distributions. Predicted and experimental SCB frequencies increase with molecular weight, but the predictions deviate substantially from the experimental data, especially for low molecular weights of polymer made with binary catalysts with higher CGC-Ti mole fraction. Considering that the 'site independency' assumption worked well to describe the polymerization kinetic curves and MWD of the binary metallocenes, this is an unexpected result that may be related to accuracy limitations of the GPC-IR measurements. More experiments, as part of a future research work, may tell if this is indeed the case.

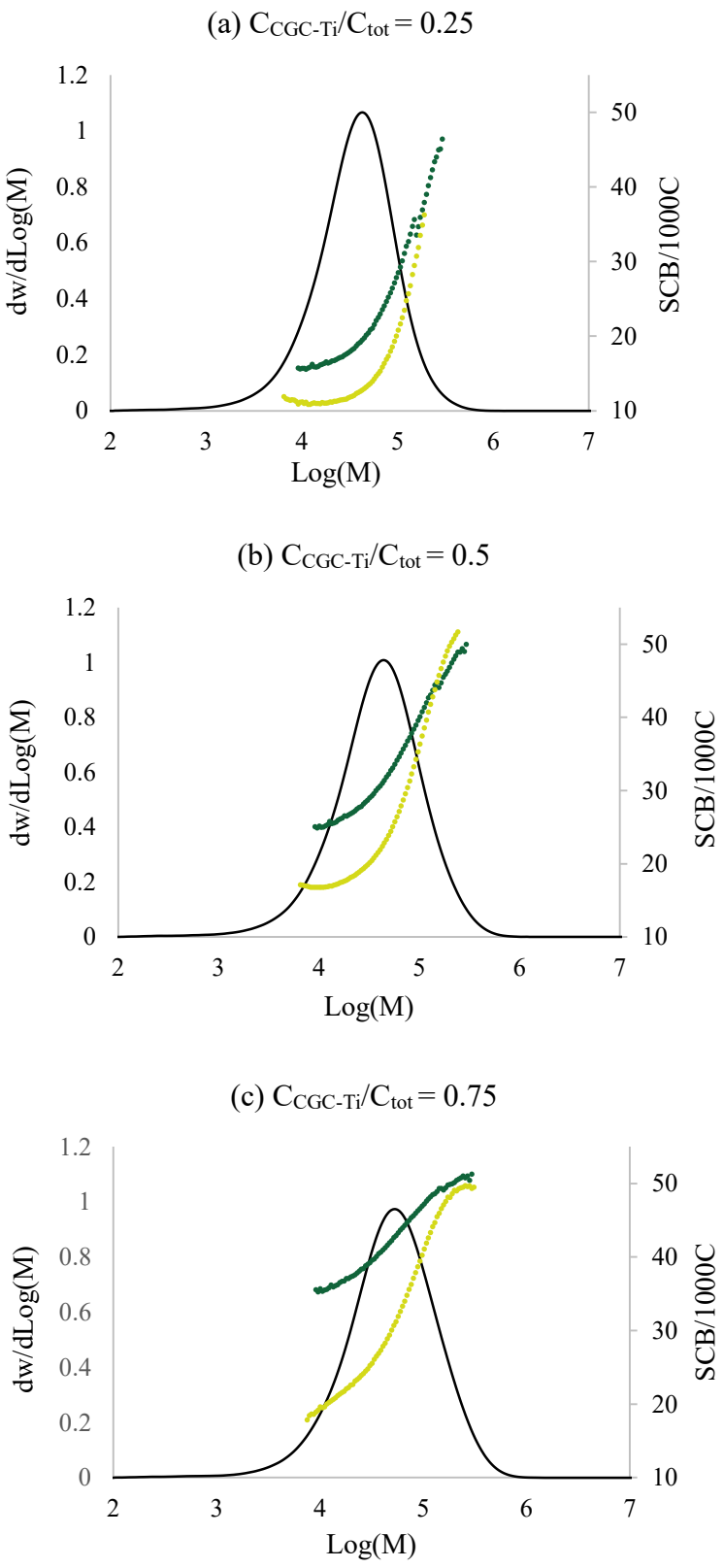

Figure 6.7 Predicted SCBD in comparison with GPC-IR results. Yellow curves are for the binary catalyst and green curves are model predictions using Equation (6.4).

Figure 6.8 shows the GPC-IR results for all samples.

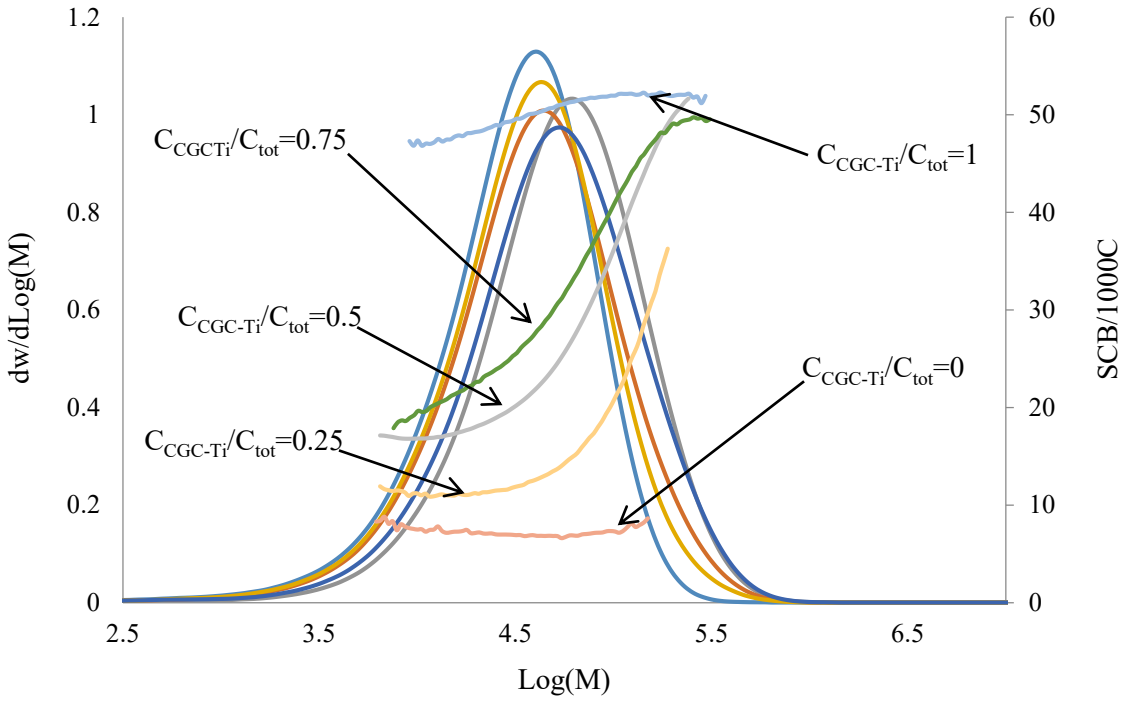

Figure 6.8 GPC-IR results for the SCBD across the MWD for the single and binary systems.

The plot clearly shows that the SCBDs of polymers made with the single metallocenes do not depend strongly on polymer molecular weight, but the SCBs of copolymers made with catalyst mixture increases with molecular weight.

In conclusion, evidence from polymerization kinetics and MWD seems to support the hypothesis that Cp_2ZrCl_2 and CGC-Ti behave independently of each other under the conditions investigated in this thesis. The overall increasing trend of SCBs with increasing molecular weight supports this hypothesis, but less persuasively, since it captured only the correct trends, but not values. Therefore, the prediction of SCBD of polymers made with binary systems and/or designing a product based on the individual catalyst knowledge, must be done carefully with regard to the variation of SCBs between model and experimental. Therefore, using models and/or experimental data for each catalyst, it is possible to design recipes to synthesize tailor-made polyolefins using the combined CGC-Ti/Cp_2ZrCl_2 system in terms of polymerization rate and MWD, but not necessarily SCBD.

Chapter 7 : Conclusions and Future Work

7.1 Conclusions

This dissertation investigated the copolymerization of ethylene and 1-hexene with two different metallocenes, CGC-Ti and Cp_2ZrCl_2, either alone or in binary mixtures, under different polymerization conditions. Models were developed to describe the polymerization kinetics with these catalysts, and the leading model parameters were estimated using a rigorous non-linear particle swarm optimization procedure.

The main objectives of this investigations were:

1. To develop mathematical models for the copolymerization kinetics of ethylene and 1-hexene with CGC-Ti and Cp_2ZrCl_2.
2. To estimate the main polymerization kinetic constants for these models.
3. To assess whether the behaviour of binary CGC-Ti/Cp_2ZrCl_2 mixtures could be predicted from the polymerization kinetics of the individual catalysts.
4. To assess whether the microstructure of ethylene/1-hexene copolymers made with binary CGC-Ti/Cp_2ZrCl_2 mixtures could be predicted from the microstructures of the copolymers made with each catalyst alone.

Ethylene/1-hexene copolymerization with Cp_2ZrCl_2 follows a 'standard' copolymerization model that obeys first order kinetics for the propagation of ethylene and 1-hexene, and also for catalysts deactivation. Unlike Cp_2ZrCl_2, CGC-Ti does not follow first order catalyst decay kinetics. A reversible catalyst site deactivation/activation step promoted by MAO was proposed to describe copolymerizations with CGC-Ti. CGC-Ti does, however, follow first order kinetics for the propagation of ethylene and 1-hexene over the range of conditions tested in this thesis. Both catalysts follow first order kinetics with respect to catalysts concentration. The results discussed in Chapter 4 and Chapter 5 demonstrate that the proposed models described the polymerization kinetics with CGC-Ti and Cp_2ZrCl_2 adequately.

Particle swarm optimization was used to estimate leading polymerization kinetic constants, such as propagation rates (Terminal model), catalysts deactivation rates, and combined transfer to H_2.

Reactivity ratios for these catalysts have also been estimated using the Mayo-Lewis equation successfully.

The results presented in Chapter 6 confirm that it is possible to predict the polymerization kinetics and copolymer microstructure for binary mixtures of CGC-Ti and Cp_2ZrCl_2 using the mathematical models developed for each catalyst alone. This is a very powerful conclusion because it allows us to design polyolefins with controlled microstructures using binary catalysts from the knowledge of each catalyst added to the system. This permits a considerable reduction in the number of experiments required to make copolymers with tailor-made properties, such as those required in pipe applications where the SCB frequency should increase with increasing polymer molecular weight.

7.2 Recommendations

Several important parameters need to be estimated for a more complete understanding of these catalysts:

1. Perform the experiments suggested at the end of Chapter 4 and Chapter 5 to estimate the individual H_2 chain transfer constants, k_{tHA} and k_{tHB}.
2. Augment the experimental design to estimate other chain transfer constants, such as $k_{t\beta}$, k_{tA}, k_{tAl}.
3. Perform more experiments under wider range of conditions to investigate whether the SCBD results support the hypothesis that Cp_2ZrCl_2 and CGC-Ti behave independently in binary mixtures.
4. Repeat these experiments at different polymerization temperatures to estimate activation energies and pre-exponential constants for the different polymerization rate constants using the Arrhenius law.
5. Repeat this investigation with the same metallocene catalysts supported on SiO_2 and investigate how this procedure affects polymerization kinetics. Most commercial polyolefin processes use supported catalysts, so this study would have significant practical interest.

6. Link copolymer microstructure to polymer physical properties using empirical or semi-empirical models. This would permit the prediction of polymer properties (such as environmental stress crack resistance) directly from the knowledge of polymerization kinetics and conditions.
7. MAO and H_2 have a clear effect on polymerization rates that need to be quantified with models that correct for the values of the propagation rate constants.

References

1. PlasticsEurope. Plastics - the Facts 2016. 38 (2016). Available at: http://www.plasticseurope.es/Document/plastics---the-facts-2016-15787.aspx?FolID=2. (Accessed: 15th September 2017)

2. World Plastics Production 1950 – 2015. Available at: https://committee.iso.org/files/live/sites/tc61/files/The Plastic Industry Berlin Aug 2016 - Copy.pdf. (Accessed: 15th September 2017)

3. Soares, J. B. P. & McKenna, T. F. L. *Polyolefin Reaction Engineering*. (WILEY-VCH Verlag GmbH & Co. KGaA, 2012).

4. Asua, J. M. *Polymer Reaction Engineering*. (Oxford: Wiley-Blackwell, 2007).

5. Bovey, F. A. & Schilling, F. C. Short-Chain and Long-chain Branching in Low-Density Polyethylene. **535,** 76–80 (1975).

6. Charles E. Carraher, J. *Carraher's Polymer Chemistry*. (CRC Press, 2011).

7. Mortimer, G. A. & Hamner, W. F. Density of polyethylene. *J. Polym. Sci. Part A Gen. Pap.* **2,** 1301–1309 (1964).

8. Norio Kashiwa. The Discovery and Progress of MgCl 2 -Supported TiCl 4 Catalysts. *J. Polym. Sci. Part A Polym. Chem.* **42,** 1–8 (2004).

9. Cossee, P. Ziegler-Natta catalysis I. Mechanism of polymerization of α-olefins with Ziegler-Natta catalysts. *J. Catal.* **3,** 80–88 (1964).

10. Natta, G. & Pasquon, I. The Kinetics of the Stereospecific Polymerization of α-Olefins. in 1–66 (1959). doi:10.1016/S0360-0564(08)60416-2

11. Sinn, H. & Kaminsky, W. *Advances in organometallic chemistry*. **18,** (ACADEMIC PRESS, 1980).

12. Meyer, T. & Keurentjes, J. T. F. *Handbook of Polymer Reaction Engineering*. (WILEY-VCH Verlag GmbH & Co. KGaA, Weinheim, 2005).

13. Braca, G. *et al.* Supported transition metal complexes for ethylene polymerization. *J. Mol. Catal. A Chem.* **107,** 113–121 (1996).

14. Kaminsky, W. The discovery of metallocene catalysts and their present state of the art. *J. Polym. Sci. Part A Polym. Chem.* **42,** 3911–3921 (2004).

15. Odian, G. *Principles of Polymerization* (4th ed.). (Hoboken, N.J.: Wiley-Interscience, 2004).

16. Schneider, M. J. & Mülhaupt, R. Influence of indenyl ligand substitution pattern on metallocene-catalyzed propene copolymerization with 1-octene. *Macromol. Chem. Phys.* **198,** 1121–1129 (1997).

17. Kaminsky, W. Highly active metallocene catalysts for olefin polymerization. *J. Chem. Soc. Dalt. Trans.* 1413–1418 (1998). doi:10.1039/a800056e

18. Cano, J. & Kunz, K. How to synthesize a constrained geometry catalyst (CGC) - A survey. *J. Organomet. Chem.* **692,** 4411–4423 (2007).

19. Claverie, J. P. *et al.* Catalytic polymerization of olefins in emulsion. *Abstr. Pap. 221st ACS Natl. Meet. San Diego, CA, United States, April 1-5, 2001* PMSE-187 (2001). doi:10.1021/ma0017135

20. Rieger, B., Baugh, L. S., Kacker, S. & Eds, S. S. *Late Transition Metal Polymerization Catalysts*. (WILEY-VCH Verlag GmbH & Co. KGaA, Weinheim, 2003).

21. Xie, T., McAuley, K. B., Hsu, J. C. C. & Bacon, D. W. Gas Phase Ethylene Polymerization: Production Processes, Polymer Properties, and Reactor Modeling. *Ind. Eng. Chem. Res.* **33,** 449–479 (1994).

22. Mehdiabadi, S., Soares, B. P., Bilbao, D. & Brinen, J. L. A Polymerization Kinetics Comparison between a Metallocene Catalyst Activated by Tetrakis (pentafluorophenyl) Borate and MAO for the Polymerization of Ethylene in a Semi-batch Solution Reactor. *Macromol. React. Eng.* 418–430 (2011). doi:10.1002/mren.201100015

23. Choi, Y. Polymerization of Ethylene with Supported Early and Late Transition Metal Catalysts. (University of Waterloo, 2011).

24. Negureanu, L., Hall, R. W., Butler, L. G. & Simeral, L. A. Methyaluminoxane (MAO) polymerization mechanism and kinetic model from ab initio molecular dynamics and electronic structure calculations. **128,** 16816–16826 (2006).

25. Babushkin, D. E. *et al.* Multinuclear NMR investigation of methylaluminoxane. *Macromol. Chem. Phys.* **198,** 3845–3854 (1997).

26. Xu, Z. G., Chakravarti, S. & Harmon Ray, W. Kinetic study of olefin polymerization with a supported metallocene catalyst. I.Ethylene/Propylene copolymerization in gas phase. *J. Appl. Polym. Sci.* **81,** 2901–2917 (2001).

27. Touloupidis, V. Catalytic Olefin Polymerization Process Modeling: Multi-Scale Approach and Modeling Guidelines for Micro-Scale/Kinetic Modeling. *Macromol. React. Eng.* **8,** 508–527 (2014).

28. Matos, V. *et al.* Method for Quantitative Evaluation of Kinetic Constants in Olefin Polymerizations, 3. *Macromol. React. Eng.* **1,** 137–159 (2007).

29. Embirucu, M., Prata, D. M., Lima, E. L. & Pinto, C. Continuous Soluble Ziegler-Natta Ethylene Polymerizations in Reactor Trains , 2 – Estimation of Kinetic Parameters from

Industrial Data. *Macromol. React. Eng.* 142–160 (2008). doi:10.1002/mren.200700046

30. Sirohi, a & Choi, K. Y. On-Line Parameter Estimation in a Continuous Polymerization Process. *Ind. Eng. Chem. Res.* **35,** 1332–1343 (1996).

31. Kou, B., McAuley, K. B., Hsu, C. C., Bacon, D. W. & Yao, K. Z. Mathematical model and parameter estimation for gas-phase ethylene homopolymerization with supported metallocene catalyst. *Ind. Eng. Chem. Res.* **44,** 2428–2442 (2005).

32. Kou, B., McAuley, K. B., Hsu, J. C. C. & Bacon, D. W. Mathematical model and parameter estimation for gas-phase ethylene/hexene copolymerization with metallocene catalyst. *Macromol. Mater. Eng.* **290,** 537–557 (2005).

33. Yao, K. Z., Shaw, B. M., Kou, B., McAuley, K. B. & Bacon, D. W. Modeling Ethylene/Butene Copolymerization with Multi-site Catalysts: Parameter Estimability and Experimental Design. *Polym. React. Eng.* **11,** 563–588 (2003).

34. Stewart, W. E. GREG: A Fortran Subroutine for Nonlinear Regression and Experimental Design, User's Manual. (1995).

35. Mehdiabadi, S. & Soares, J. B. P. Ethylene homopolymerization kinetics with a constrained geometry catalyst in a solution reactor. *Macromolecules* **45,** 1777–1791 (2012).

36. Neeraj P. Khare *et al.* Steady-State and Dynamic Modeling of Commercial Slurry High-Density Polyethylene (HDPE) Processes. *Ind. Eng. Chem. Res.* **41,** 5601–5618 (2002).

37. Khare, N. P. *et al.* Steady-State and Dynamic Modeling of Gas-Phase Polypropylene Processes Using Stirred-Bed Reactors. *Ind. Eng. Chem. Res.* **43,** 884–900 (2004).

38. Zhang, C., Shao, Z., Chen, X., Yao, Z., Gu, X., & Biegler, L. T. Kinetic Parameter Estimation of HDPE Slurry Process from Molecular Weight Distribution: Estimability

Analysis and Multistep Methodology. *AIChE J.* 3442–3459 (2014). doi:10.1002/aic.14527

39. Andersson, N. *et al.* Parameter Selection in the Parameter Estimation of Grade Transitions in a Polyethylene Plant. *Stud. Eng. Technol.* **3,** 1 (2015).

40. Mehdiabadi, S. & Soares, J. B. P. Quantifying the Copolymerization Kinetics of Ethylene and 1-Octene Catalyzed with rac-Et(Ind)2ZrCl2 in a Solution Reactor. *Macromolecules* **49,** 2448–2457 (2016).

41. Mueller, P. A., Richards, J. R. & Congalidis, J. P. Polymerization reactor modeling in industry. *Macromol. React. Eng.* **5,** 261–277 (2011).

42. Fineman, M. & Ross, S. D. Linear Method for Determining Monomer Reactivity Ratios in Copolymeization. *J. Polym. Sci.* **V,** 259–265 (1950).

43. Habibi, A., Vasheghani-Farahani, E., Semsarzadeh, M. a. & Sadaghiani, K. A Generalized Least Square Model for the Determination of Monomer Reactivity Ratios in Free Radical Copolymerization Systems. *Macromol. Theory Simulations* **12,** 184–195 (2003).

44. Galland, G. B., Quijada, P., Mauler, R. S. & al., et. Determination of reactivity ratios for ethylene/alpha-olefin copolymerization catalysed by the $C_2H_4[Ind]_2ZrCl_2$/methylaluminoxane system. *Macromol. Rapid Commun.* **613,** 607–613 (1996).

45. Al-Saleh, M. A., Soares, J. B. P. & Duever, T. A. The integrated deconvolution estimation model: A parameter estimation method for ethylene/α-Olefin Copolymers Made with Multiple-Site Catalysts. *Macromol. React. Eng.* **4,** 578–590 (2010).

46. Roedel, M. J. The Molecular Structure of Polyethylene. I. Chain Branching in Polyethylene during Polymerization1. *J. Am. Chem. Soc.* **75,** 6110–6112 (1953).

47. DesLauriers, P. J., Rohlfing, D. C. & Hsieh, E. T. Quantifying short chain branching

microstructures in ethylene 1-olefin copolymers using size exclusion chromatography and fourier transform infrared spectroscopy (SEC-FTIR). *Polymer (Guildf).* **43,** 159–170 (2001).

48. Tribe, K., Saunders, G. & Meißner, R. Characterization of branched polyolefins by high temperature GPC utilizing function specific detectors. *Macromol. Symp.* **236,** 228–234 (2006).

49. Mehdiabadi, S. Synthesis, Characterization and Polymerization Kinetic Study of Long Chain Branched Polyolefins Made with Two Single-Site Catalysts. (University of Waterloo, 2011).

50. De Pooter, M. *et al.* Determination of the composition of common linear low density polyethylene copolymers by 13C-NMR spectroscopy. *J. Appl. Polym. Sci.* **42,** 399–408 (1991).

51. Standard Test Method for Determination of Linear Low Density Polyethylene (LLDPE) Composition by Carbon-13 Nuclear Magnetic Resonance 1. *ASTM International* (2009). doi:10.1520/D5017-96R09E01.2

52. The MathWorks, I. Data Analysis. (2017).

53. Eberhart, R. & Kennedy, J. A new optimizer using particle swarm theory. *Proc. Sixth Int. Symp. Micro Mach. Hum. Sci.* 39–43 (1995). doi:10.1109/MHS.1995.494215

54. Lazinica, A. *Particle swarm optimization*. *Computer and Information Science* (In-Tech, 2009).

55. Kasiri, S., Ulrich, A. & Prasad, V. Kinetic modeling and optimization of carbon dioxide fixation using microalgae cultivated in oil-sands process water. *Chem. Eng. Sci.* **137,** 697–711 (2015).

56. Kissin, Y. V., Rishina, L. A. & Vizen, E. I. Hydrogen effects in propylene polymerization reactions with titanium-based Ziegler-Natta catalysts. II. Mechanism of the chain-transfer reaction. *J. Polym. Sci. Part A Polym. Chem.* **40,** 1899–1911 (2002).

57. Mehdiabadi, S., Choi, Y. & Soares, J. B. P. Synthesis of polyolefins with combined single-site catalysts. *Macromol. Symp.* **313–314,** 8–18 (2012).

58. Soares, J. B. P. & Kim, J. D. Copolymerization of ethylene and α-olefins with combined metallocene catalysts. I. A formal criterion for molecular weight bimodality. *J. Polym. Sci. Part A Polym. Chem.* **38,** 1408–1416 (2000).

Appendix A

Ethylene Uptake Rate Equations for Ethylene/1-Hexene Copolymerizations with Cp_2ZrCl_2

The molar balance of living polymer chains is expressed as

$$\frac{\mathrm{d}[P]}{\mathrm{d}t} = k_i'[M][C^*] - k_d[P] \tag{A.1}$$

where k_i' is defined as

$$k_i' = (k_{iA}f_A + k_{iB}f_B) \tag{A.2}$$

In a similar way, the molar balance for the active catalyst sites is defined as

$$\frac{\mathrm{d}[C^*]}{\mathrm{d}t} = -k_d[C^*] - k_{iA}[A][C^*] - k_{iB}[B][C^*] \tag{A.3}$$

or

$$\frac{\mathrm{d}[C^*]}{\mathrm{d}t} = -k_d[C^*] - k_i'[M][C^*] \tag{A.4}$$

Taking Laplace transform of Equation (A.1) and (A.4) with $[C^*] = [C_0^*]$, $[P] = 0$, and $[C_d] = 0$ as initial conditions yields Equation (A.5) and Equation (A.6), respectively.

$$P(s) = \frac{C^*(s)k_i'[M]}{S+k_d} \tag{A.5}$$

and

$$C^*(s) = \frac{C_0^*}{S+k_i'[M]+k_d} \tag{A.6}$$

Substituting Equation (A.6) into Equation (A.5) yields

$$P(s) = \frac{C_0^*k_i'[M]}{(S+k_d)(S+k_i'[M]+k_d)} \tag{A.7}$$

Taking the inverse Laplace transform of Equation (A.7) results in Equation (A.8).

$$[P] = C_0^*(e^{-k_dt} - e^{(-k_d-k_i'[M])t}) \tag{A.8}$$

Since the term $k_i'[M]$ is very large, we neglected the second exponential term. Then Equation (A.8) simplifies to

$$[P] = C_0^*(e^{-k_d t}) \tag{A.9}$$

The molar balance for ethylene concentration in the reactor is

$$\frac{\mathrm{d}[A]}{\mathrm{d}t} = \frac{F}{V_R} - \left(k_{pAA}[P_A] + k_{pBA}[P_B]\right)[A] \tag{A.10}$$

Since the concentration of ethylene is kept constant during the polymerization, the ethylene flow rate can be written as

$$F = \left(k_{pAA}\emptyset_A + k_{pBA}\emptyset_B\right)[P][A]V_R \tag{A.11}$$

where $\emptyset_A$ and $\emptyset_B$ are the molar fractions of living polymer chains terminated in monomer *A* and *B*, respectively.

By substituting Equation (A.9) into Equation (A.11) and doing some mathematical manipulations, we get

$$\ln(\frac{F}{V_R}) = \ln((k_{pAA}(1-\emptyset_B) + k_{pBA}\emptyset_B)C_0^*[A]) - k_d t \tag{A.12}$$

Equation (A.12) shows that ethylene flow rate has a linear relationship with time.

Appendix B

Model Equations for Ethylene/1-Hexene Copolymerization with CGC-Ti

The molar balance for living polymer chains is given by

$$\frac{\mathrm{d}[P]}{\mathrm{d}t} = k_{iA}[A][C^*] + k_{iB}[B][C^*] - k_d[P][MAO] \tag{B.1}$$

Since the MAO/CGC-Ti ratio is high ([*Al*]/[*Ti*]=28700) the product $k_d[MAO]$ may be considered constant and equal to k'_d.

Equation (B.1) can then be rewritten as

$$\frac{\mathrm{d}[P]}{\mathrm{d}t} = (k_{iA}f_A + k_{iB}f_B)[M][C^*] - k'_d[P] \tag{B.2}$$

or

$$\frac{\mathrm{d}[P]}{\mathrm{d}t} = k'_i[M][C^*] - k'_d[P] \tag{B.3}$$

where k'_i is defined as

$$k'_i = (k_{iA}f_A + k_{iB}f_B) \tag{B.4}$$

f_A and f_B are the molar fractions of monomer *A* and *B* in the liquid phase, respectively, and [*M*] is the total concentration of comonomers in the reactor.

The molar balance for active sites is given by the equation

$$\frac{\mathrm{d}[C^*]}{\mathrm{d}t} = k_a[C_d][MAO] - k_{iA}[A][C^*] - k_{iB}[B][C^*] \tag{B.5}$$

Since MAO is present in large excess, we may also assume the product $K_a[MAO]$ to be constant and equal to k'_a. Also, by defining the pseudo initiation constant as k'_i, Equation (B.5) becomes

$$\frac{\mathrm{d}[C^*]}{\mathrm{d}t} = k'_a[C_d] - k'_i[M][C^*] \tag{B.6}$$

Similarly, the molar balance for deactivated sites is defined as

$$\frac{\mathrm{d}[C_d]}{\mathrm{d}t} = k_d[P][MAO] - k_a[C_d][MAO] \tag{B.7}$$

which can also be represented more simply as

$$\frac{\mathrm{d}[C_d]}{\mathrm{d}t} = k'_d[P] - k'_a[C_d] \tag{B.8}$$

Equations (B.3), (B.6) and (B.8) can be solved using Laplace transforms considering $[C^*] = [C_0^*]$, $[P] = 0$, and $[C_d] = 0$ as initial conditions.

Taking the Laplace transform of Equation (B.3) yields

$$SP(s) - p(0) = k'_i[M]C^*(s) - k'_d P(s) \tag{B.9}$$

Solving for $P(s)$

$$P(s) = \frac{C^*(s)k'_i[M]}{S+k'_d} \tag{B.10}$$

Taking the Laplace transform of Equation (B.6) leads to

$$SC^*(s) - C_0^* = k'_a C_d(s) - k'_i[M]C^*(s) \tag{B.11}$$

Solving for $C^*(s)$

$$C^*(s) = \frac{k'_a C_d(s)+C_0^*}{S+k'_i[M]} \tag{B.12}$$

Finally, taking the Laplace transform of Equation (B.8)

$$SC_d(s) - C_d(o) = k'_d P(s) - k'_a C_d(s) \tag{B.13}$$

Solving for $C_d(s)$

$$C_d(s) = \frac{k'_d P(s)}{S+k'_a} \tag{B.14}$$

Substituting Equation (B.14) into (B.12), we get expression

$$C^*(s) = \frac{\left(k'_a k'_d P(s) \big/ S+k'_a\right)+C_0^*}{S+k'_i[M]} \tag{B.15}$$

Similarly, substituting Equation (B.15) into (B.10) yields

$$P(s) = \left[\frac{k'_a k'_d P(s) / S+k'_a + C_0^*}{S+k'_i[M]}\right]\left[\frac{k'_i[M]}{S+k'_d}\right] \tag{B.16}$$

Equation (B.16) can also be written as

$$P(s) = \frac{k'_i[M]C_0^*(S+k'_a)}{S^2(S+k'_a)+S(k'_i[M]+k'_i[M]k'_a+k'_d+k'_d k'_a)+k'_i[M]k'_d} \tag{B.17}$$

which can be expressed in a more compact way as

$$P(s) = k'_i[M]C_0^* \frac{S+k'_a}{S(S-S_1)(S-S_2)} \tag{B.18}$$

where

$$S_1 = \frac{-A-\sqrt{A^2-4B}}{2} \tag{B.19}$$

$$S_2 = \frac{-A+\sqrt{A^2-4B}}{2} \tag{B.20}$$

$$A = k'_i[M] + k'_a + k'_d \tag{B.21}$$

$$B = k'_i[M]k'_d + k'_i[M]k'_a + k'_a k'_d \tag{B.22}$$

Finally, Equation (B.18) can be split into simpler fractions using partial fraction expansion, which is a more convenient form to calculate inverse Laplace transforms

$$P(s) = k'_i[M]C_0^*\left[\frac{k'_a}{S_1 S_2 S} + \frac{S_1+k'_a}{S_1(S_1-S_2)(S-S_1)} + \frac{S_2+k'_a}{S_2(S_2-S_1)(S-S_2)}\right] \tag{B.23}$$

Taking the inverse Laplace transform of Equation (B.23) yields

$$P(t) = k'_i[M]C_0^*[\frac{k'_a}{S_1 S_2} + (\frac{S_1+k'_a}{S_1(S_1-S_2)})e^{S_1 t} + (\frac{S_2+k'_a}{S_2(S_2-S_1)})e^{S_2 t}] \tag{B.24}$$

Equation (B.24) shows the instantaneous concentration of the living polymer chains during polymerization time.